DOE/NASA/20370-79/17
NASA TM-79202

SOME TECHNIQUES FOR REDUCING THE TOWER SHADOW OF THE DOE/NASA MOD-0 WIND TURBINE TOWER

Richard R. Burley, Joseph M. Savino,
Lee H. Wagner, and James H. Diedrich
National Aeronautics and Space Administration
Lewis Research Center

September 1979

Prepared for
U.S. DEPARTMENT OF ENERGY
Energy Technology
Distributed Solar Technology Division

NOTICE

DOE/NASA/20370-79/17
NASA TM-79202

SOME TECHNIQUES FOR REDUCING THE TOWER SHADOW OF THE DOE/NASA MOD-0 WIND TURBINE TOWER

Richard R. Burley, Joseph M. Savino,
Lee H. Wagner, and James H. Diedrich
National Aeronautics and Space Administration
Lewis Research Center
Cleveland, Ohio 44135

September 1979

Work performed for
U. S. DEPARTMENT OF ENERGY
Energy Technology
Distributed Solar Technology Division
Washington, D. C. 20545
Under Interagency Agreement DE-AB29-76ET20370

SUMMARY

The DOE*/NASA Mod-0-wind turbine tower is fabricated of pipe columns with channels as horizontal members and back-to-back angles as diagonals. In an attempt to reduce tower shadow, wind tunnel tests were conducted on modifications of scale models of the tower and tower components. Removal of all panel blockage was simulated by deleting panel diagonals. This provided an optimum target shadow value for this type of tower configuration and was used as a reference configuration for comparative purposes in evaluating the following shadow abatement techniques.

1. Small diameter tension rods as diagonal members.
2. Round cross-section pipe as diagonal and horizontal members.
3. Ellipses installed on horizontal members.
4. Airfoils installed on vertical members.
5. Surface roughness applied to vertical members.

All techniques offered some reduction in tower shadow at all wind directions. Small diameter tension rods employed as tower diagonals resulted in the greatest increase in tower wake velocity, up to approximately 90 percent of the free stream value. The tower shadow abatement gained from the installation of tension rods, ellipses, weathervaning airfoils, and/or surface roughness must be further evaluated on a case-by-case basis for their structural characteristics and cost-effectiveness.

E-087

INTRODUCTION

The Mod-0 wind turbine is a two-bladed propeller type rotor designed to operate on the downwind side of the open truss support tower (ref. 1). During operation, each blade must pass through the wake of the tower where the wind speeds are always lower than the surrounding unobstructed free wind. Some of the early Mod-0 test results showed that the blade root stresses were about 60 percent higher than the expected design values because the wind speed reduction in the wake, the tower shadow, was greater than originally estimated. In an effort to reduce the blade stresses, methods of increasing the wind speed in the wake of the DOE/NASA Mod-0 wind turbine tower were evaluated using scale models in a wind tunnel.

An experimental investigation was conducted on scale models of the Mod-0 tower to accurately determine its tower shadow (ref. 2). This investigation determined the tower shadow for a scale model of the Mod-0 tower, the tower with stairway and elevator rails removed (base tower), and a base tower of all

*Formerly the Energy Research and Development Administration (ERDA).

tubular construction without gusset plate joints. The results confirmed that the Mod-0 tower shadow was considerably larger than originally estimated and that:

1. The presence of the stairs and equipment elevator rails caused very large reductions in wind speed in the wake of the tower.
2. Towers constructed of all tubular members offer less wind resistance that those made with noncircular members.
3. Average wind speed in the wake of the baseline tower is nearly independent of wind direction and independent of elevation.
4. Wake wind speed reduction is largely determined by the tower blockage (solidity) upstream.

In an effort to further identify and quantify techniques to reduce the tower shadow, tests were conducted on modifications of a 1/25 scale model of the open truss Mod-0 tower in a low speed wind tunnel. The tower structure of the Mod-0 wind turbine utilizes standard 8" pipe for the four column legs, back-to-back channels for the horizontal members, and back-to-back angles for the diagonals with gusset-plate attachments. On the scale model of the Mod-0 base tower the "baseline" tower, square cross section members were used to simulate the horizontal and diagonal members.

Based on the conclusions and recommendations of the previous investigation (ref. 2), the following tower modifications seemed to merit further study:

1. Diagonal members of small diameter wires to simulate tension rods.
2. Round horizontal and diagonal members.
3. Ellipses on the horizontal members.
4. Airfoils on the vertical members.

In addition, tests were conducted on isolated circular vertical cylinders to determine the effect of surface roughness variations. The effects of wind direction and tower elevation on tower shadow were also determined for each modification.

The purpose of this report is to present the results of the tests conducted on the above modifications.

SYMBOLS

c	chord length of airfoil
C_D	drag coefficient
D	diameter
k	diameter of surface roughness elements

k/D	degree of surface roughness
p	total pressure
p_w	wall static pressure
R_e	Reynolds number
t	maximum thickness of airfoil
V	velocity
V/V_o	velocity ratio
w	local projected width of the tower into a plane normal to oncoming undisturbed wind
W	reference tower width at elevation 19 7/16" on 1/25 scale model
θ	wind direction
Δ	width of wake
Δ/w	wake-to-tower width ratio
Δp	differential pressure
x	axial distance from downstream face of tower to downstream pressure probe

Subscripts:

avg	average
℄	centerline
min	minimum
o	free-stream

APPARATUS AND PROCEDURE

Test Facility

Test evaluations of Mod-0 tower modifications were conducted in the Lewis Research Center (LeRC) icing tunnel. A schematic view of this single-return, closed-throat tunnel is shown in figure 1. The test section is rectangular in shape, 9 ft wide, 5 ft high, and 20 ft long. Windows are provided on both sides and on the roof of the tunnel test section to allow observation of the model during testing. Tests were conducted at tunnel airspeeds of 64 and 100 mph, at ambient air temperature, and near atmospheric pressure. The Reynolds numbers based on the diameter of the legs were approximately 17,000 and 27,000.

Instrumentation and Data Reduction

The instrumentation consisted of a traversing total pressure probe, a tunnel total pressure probe, and a tunnel wall static pressure sensor. The traversing total pressure probe was located downstream of the tower as illustrated in figure 2. Another view of the tunnel arrangement is shown in figure 3.

The difference between the local total pressure (p) downstream of the tower and the wall static pressure (p_w) was measured by a differential pressure (Δp) transducer. The tunnel total pressure probe was located upstream of the tower. The difference between the free stream total pressure (p_o) and the wall static pressure, the velocity head, was measured by a second Δp transducer. The output of the Δp transducers and an analog module (fig. 4), were used to calculate the local values of the air velocity ratio V/V_o which were plotted on an X-Y plotter.

Procedure

Tests on tower configurations were conducted at a nominal free stream velocity of 100 mph, ambient air temperature, and near atmospheric pressure. Continuous profiles of V/V_o were measured at a variety of elevations for wind approach angles measured relative to a line perpendicular to a typical face of the tower of 0^o, 10^o, 35^o, and 40^o as defined in figure 5. These profiles were obtained as a continuous plot on the X-Y recorder.

Velocity ratios were obtained downstream of panels 3 and 4 (fig. 3), where the tower shadow has the greatest effect on the outer 50 percent of the rotor blade length.

The tower shadow was characterised by the wake width and the average wind speed in the wake. Wake width was determined as the distance between the points nears the outer boundaries of each profile where $V/V_o = 0.99$. This wake measurement was plotted as the wake to tower width ratio, Δ/w, variation with elevation. The average velocity ratio, V_{avg}/V_o was determined by integrating each profile across the wake. The projected local tower width, w, was calculated from geometric features of panels 3 and 4 and the wind approach angle θ.

TOWER MODEL CONFIGURATIONS TESTED

Baseline Tower

A 1/25 scale model of the Mod-0 wind turbine tower was chosen as the baseline tower (figs. 3 and 6). Scaled gusset-plates were used to attach the diagonals to the model tower.

Diagonals Removed

To determine the amount of shadow improvement obtainable by reducing or eliminating panel blockage as suggested in the previous investigation, first all diagonals were removed from each side of panels 3 and 4, and then one diagonal was replaced on each face (figs. 7 and 8).

Removing all diagonals in panels 3 and 4 left only the vertical framework and horizontals between panels and thus eliminated all other blockage at that elevation. This was a reference case that was used to determine the minimum tower shadow on a tower model having only round vertical legs and square horizontal members, an admittedly impractical design.

Tension Rods

One method of providing adequate strength in a tower while minimizing blockage is to use diagonal tension rods in place of angles. All of the square diagonals were removed from panels 3 and 4 and were replaced with small diameter rods (figs. 9 and 10).

All-pipe Tower

A variation of a tower design that uses tension rods is one that is made of all tubular members, a modification reommended in the previous investigation. A model of two panels of such a tower was fabricated and tested (figs. 11 and 12). As with the model using simulated tension rods, a definite spacing was provided between diagonal and horizontal members to minimize blockage at panel corners. For ease in mounting the model in the wind tunnel, the bottom horizontal members were fabricated of a square cross section shape.

Ellipses and Airfoils

A basic method of reducing the wake size and drag coefficient of an object is to provide a more efficient aerodynamic shape. Therefore, it was decided to determine the effectiveness of airfoil and elliptical shaped shrouds on the round vertical legs and the square horizontal sections, respectively, on a tower model with the diagonal members removed. The purpose of these tests was to determine the lowest achievable tower shadow, recognizing that the use of airfoils on the vertical legs is probably not a cost-effective method for reducing the shadow. This tower configuration is shown in figure 13. Dimensions of the ellipses and airfoils are presented in figure 14.

Full Scale Airfoils

Because the effectiveness of airfoils is dependent on Reynolds number R_e, tests were run using airfoils that were much larger than those used on the tower model. Two in-line airfoils having the same thickness-to-chord ratio as the scale model airfoils were installed in the LeRC icing tunnel in the orientation shown in figure 15. The downstream probe location was chosen to provide the same size and distance relationship for both the full scale tower and the scale model tower. Velocity ratios profiles were obtained only at the midpoint horizontal plane of the airfoils.

Surface Roughness

Another method of reducing the wake behind a round cross-section vertical member is to roughen the surface. Tests were conducted on roughened circular cylinders installed in the tunnel in the orientation shown in figure 16. The rough surface was obtained by carefully wrapping a 3-inch diameter cylinder with various grades of garnet paper. These tests were conducted at a free stream velocity of 64 mph, which for this modification provides a Reynolds number comparable to the full scale design. As with the isolated, full scale airfoil tests, velocity ratios were obtained at the midpoint horizontal plane of the vertical cylinder.

RESULTS AND DISCUSSION

The amount of wake wind speed data acquired in these tests is considerable and although much of it is included as plots in this report for the purpose of documenting it, only a portion of the data will be referred to explicitly. This data is presented as plots of:

1. Horizontal profiles of V/V_o at selected elevations (appendix A).
2. Vertical profiles of V/V_o, $V_{\text{¢}}/V_o$, V_{min}/V_o, and V_{avg}/V_o down wind of the tower model centerline (appendix B).
3. Vertical profiles of Δ/w (appendix C).
4. V_{avg}/V_o versus wind approach angle θ (appendix D).
5. Wake characteristics of Ellipses, Airfoils, and Roughened Cylinders (appendix E).

From these plots were derived the tower shadow characteristics for each configuration and panels 3 and 4, and comparisons were made to determine the relative effectiveness of each configuration in reducing the tower shadow. The results and conclusions derived from the analysis of this data are discussed below.

TOWER SHADOW CHARACTERISTICS

The tower shadow at each elevation is characterized by several features derived from the velocity profiles in the wake at that elevation. These are the dimensionless values of (1) the minimum velocity, V_{min}/V_o, (2) the average velocity, V_{avg}/V_o, and (3) the wake width, Δ/w, at each elevation, where V_o = the undisturbed free stream velocity and w = the projected width of the tower on a plane perpendicular to V_o.

The value of V_{min}/V_o provides a crude measure of the "badness" of the shadow, and also provides information on the structural and geometric features of the tower that cause the wind speed to be the low.

The characteristics that have the major impact on the wind turbine blades are the average velocity, V_{avg}, and the width Δ. The blade stresses are dependent on the difference $(V_o - V_{avg})$, the average velocity deficit, and the deficit width Δ. In this report, it was decided to present the data as V_{avg}/V_o and Δ/w.

Local Velocity Profile Characteristics

Every horizontal and vertical profile of V/V_o contains local peaks and valleys, as is illustrated in the figures of appendices A and B. The peaks occur downstream of those regions of the tower where the solidity is the lowest (that is where little or no blockage exists) such as the triangular region between the diagonals, the vertical legs, and the horizontal members for a wind approach angle of 0^o (figs. 6, 10, and 12).

The valleys, on the other hand, occur directly downwind of a member, a group of members that are more or less in line one behind the other, and members that converge at a joint. The depth of the valley tends to increase with increasing upstream blockage and increasing departure from a streamline cross-section shape. Shapes such as squares, angles, channels, I beams, etc., are aerodynamically less efficient than cylinders, ellipsoids, and airfoils in that they, for the same projected width, produce wakes that are wider and persist for a greater distance downstream, and as a result have a much higher drag coefficient (refs. 3 and 4).

Our analysis of the data revealed that the valleys are generally deepest in the wake of members that have the largest projected solidity, such as the vertical legs, horizontal members, and joints, and the highest drag coefficient, such as the square diagonals and horizontals and the joints. This is clearly seen in many of the figures in appendices A and B.

To reduce the tower shadow (i.e., increase V_{avg}/V_o), it was apparent that the values of V/V_o in the wake, especially those of the valleys, would have to be

raised. This could be accomplished by a one or more of the following changes without drastically changing the basic tower configuration: (1) reduce the projected widths and number of diagonal members, and (2) use members with more efficient (lower drag) aerodynamic shapes. The size and spacing of the horizontal members were fixed, but not their shape. However, the size, number, and shape of the diagonals could be changed. Within these restrictions, changes were made to panels 3 and 4 and tested and found to produce higher V/V_o values in the wake than for the baseline tower which led to higher V_{avg}/V_o values.

Effect of Various Modifications on V_{avg}/V_o and Δ/w

Of the three shadow characteristics V_{min}/V_o, V_{avg}/V_o, and Δ/w, those most affected by the amount of blockage and the shape of the members are V_{min}/V_o and V_{avg}/V_o. A review of the horizontal profiles in appendix A shows that all the modifications tested on panels 3 and 4, or on the all pipe model, generally produced higher values of V/V_o than the baseline tower. Changes in the diagonal elements alone produced much higher values of V/V_o and V_{avg}/V_o almost everywhere in their wake except behind the vertical legs and the horizontal members. Removal of one or both diagonals from each face of a panel reduced the blockage. Small diameter tension rods also reduced the blockage, but, in addition, they were aerodynamically more efficient than the square diagonals they replaced. In the all pipe tower model, the round diagonals were of comparable width to the square ones. This improved aerodynamic shape produced higher V/V_o and V_{avg}/V_o values with a negligible change in solidity.

On the other hand, the airfoils on the vertical legs, ellipsoidal horizontal members, and the roughened cylindrical legs (without diagonals) each produced improved characteristics in their wake without increasing the solidity (appendices A and B). It is believed that similar improvements would result if they were employed with diagonals present.

The second most important wake characteristic is the wake width Δ. The magnitude of Δ is primarily determined by the local projected width w at each elevation. The blockage and the shape of the vertical legs have a second order effect on the ratio Δ/w. Since w is dependent on the wind approach angle, Δ is likewise dependent on this angle. These conclusions are illustrated in appendix C where are shown plots of Δ/w versus height for various wind approach angles. These figures show that Δ/w increases slightly with height. This is partly due to an increase in solidity and partly due to the increased distance between the tower and the measurement plane (a wake width continuously increases as it moves downstream). More importantly, the figures in appendix C show that the effect of reducing the tower solidity does indeed produce only a second order change in the Δ/w.

Effect of Wind Approach Direction

The wind direction primarily influenced the wake width Δ for reasons mentioned above, and the V_{min}/V_o and V_{avg}/V_o were influenced only to a minor extent. In appendix D are presented plots of V_{avg}/V_o as a function of the wind approach angle for selected representative elevations. In figure 17 is a plot of (V_{avg}/V_o) avg. versus the wind direction θ for both panels 3 and 4. This average (V_{avg}/V_o) avg., is an arithmetic average of all the (V_{avg}/V_o) that was calculated for each θ and each panel. Figure 17 summarizes the effects of the various modifications on the important tower shadow characteristic (V_{avg}/V_o) avg. It is clearly seen that reduction of the solidity by reducing the size and number of the diagonal members and that the improved aerodynamic shapes lead to increased wind speed in the tower wake.

SUMMARY OF RESULTS AND CONCLUSIONS

Six tower shadow abatement techniques were investigated at various wind directions that permitted full spectrum evaluation. All of the tested modifications provided reductions in tower shadow at all wind directions. In all cases, optimum performance was obtained at an approach angle of about 40^o because of improved relative orientation to the air stream.

As expected, the lowest tower shadow was obtained for the tower with all diagonals removed, a reference case, since this eliminated all panel interference and blockage. Since it is not considered probable that wind turbine towers will be fabricated without diagonal structural members, the shadow reduction performance of this configuration was used as the comparative goal for all other techniques. The major results of the investigation of the other tower shadow abatement techniques are summarized below:

1. Tension rod tower

At a wind direction of 0^o, replacing the square cross-section diagonal members with small diameter tension rods increased the minimum wind speed in the wake of the intersection from 71 to 87 percent of the free stream value; the average wind speed behind the tower at the elevation of this intersection increased from 83 to 88 percent. Since horizontal members remained the same, there was no appreciable effect on tower shadow downstream of the horizontals. The overall effect of the tension rod diagonals for all wind directions was to increase the average of the average velocity ratio through both of the test panels (panels 3 and 4) from approximately 78 percent of the free stream velocity to approximately 85 percent, as shown in figure 49.

2. All-pipe tower

Replacing the original square cross-section diagonal and horizontal members with round members retains the wake flow advantages of a round diagonal, as for the tension rods. This resulted in increasing the average velocity downstream of the diagonal intersection from 83 percent of the free stream value to 88 percent, identical to the improvement for the tower with tension rods. In the wake of the horizontal member, however, the average velocity ratio of the configurations with round cross-section members was not significantly different from that of the configuration with square cross-section members. In addition, the average effect of the all-pipe tower at wind approach directions other than 0^{o} was to provide less shadow reduction than the tower with tension rod diagonals. This is shown clearly in figure 49.

3. Installation of ellipses

In an attempt to determine a method of reducing shadow behind the horizontal members which had a square cross-section, ellipses were attached to the vertical faces of these members at one elevation. The wind speeds in the wake of these members between the verticals increased from 62 to 90 percent of the free stream value; average wind speed behind the tower at this elevation increased from 81 to 89 percent. This is equivalent to shadow improvement experienced at the diagonal intersection for both the tension rod and all-pipe tower configurations. Figure 49 illustrates, however, that the average of the velocity ratio for both panels 3 and 4, and over the entire wind spectrum, showed considerable increase in downstream velocity over both the tension rod and all-pipe tower configurations.

4. Attaching airfoils

No improvement of tower shadow downstream of the circular vertical member was apparent from any of the above techniques except at the joints where the horizontal and diagonal members meet the verticals. Since the actual tower has round cross-section verticals, airfoils were attached to these members. Average air speed in the wake of these members was increased from 78 to 95 percent of the free stream value for all wind directions. If airfoils are weathervaned, a very low tower shadow downstream of the vertical members would be realized.

5. Surface roughness

Another potentially less expensive technique for reducing tower shadow is the application of a rough surface to round cross-section members. This technique proved to be as effective as airfoils in improving velocity in the wake of vertical members. Furthermore, the effectiveness of a roughened vertical member is independent of wind direction. However, a particular surface roughness is effective only over a very narrow range of wind velocities.

From the above tests, it was learned that the following alternatives should be considered in wind turbine tower design to increase the wind flow through the tower:

1. Use small diameter tension rods or pipe as structural diagonals.
2. Round cross-section (pipe) or elliptical members may provide a slight advantage as horizontal structural members.

Other localized techniques have undetermined practically and cost effectiveness.

REFERENCES

1. Puthoff, Richard L.; and Sirocky, Paul J.: Preliminary Design of a 100 kW Wind Turbine Generator. NASA TM X-71585, 1974.

2. Savino, Joseph M.; and Wagner, Lee H.: Wind Tunnel Measurements of the Tower Shadow on Models of the ERDA/NASA 100 kW Wind Turbine Tower. NASA TM X-73548, 1976.

3. Schlichting, Hermann (J. Kestin, transl.): Boundary Layer Theory. Sixth ed. McGraw-Hill, 1968.

4. Hoerner, Sighard F.: Fluid-Dynamic Drag. Second ed. S. F. Hoerner, Midland Park, New Jersey, 1958.

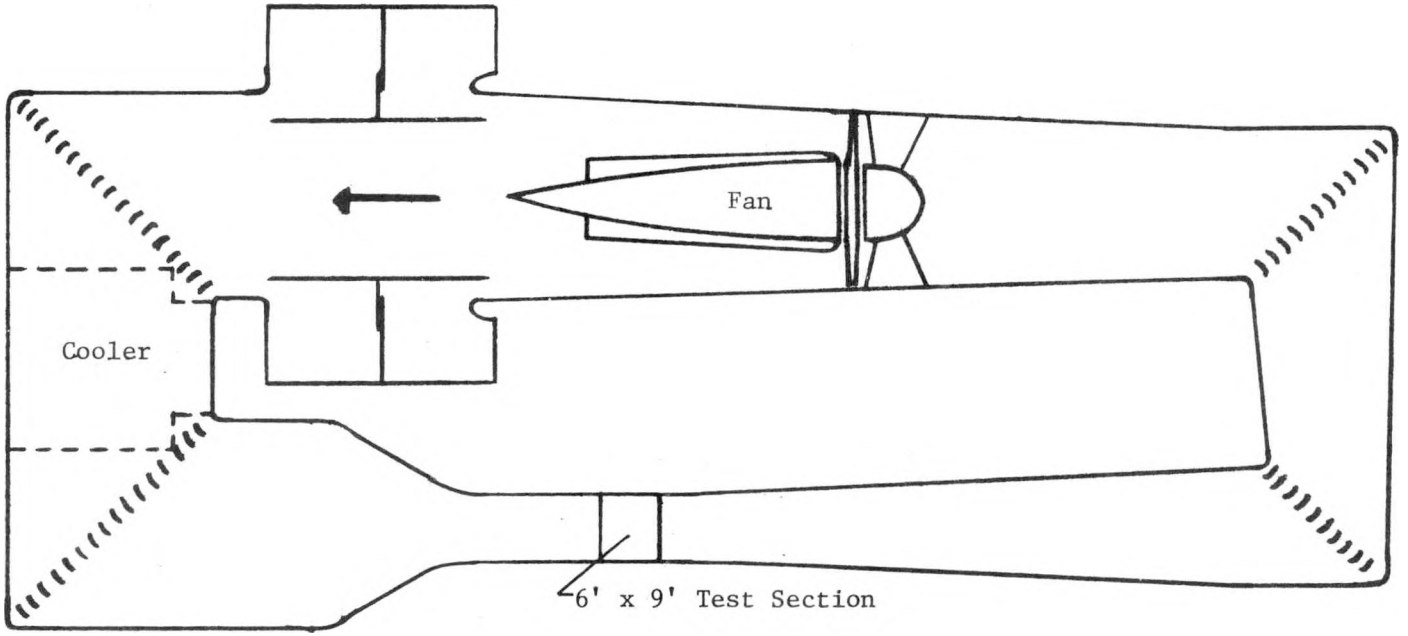

FIGURE 1 - Schematic of Lewis Research Center Icing Tunnel

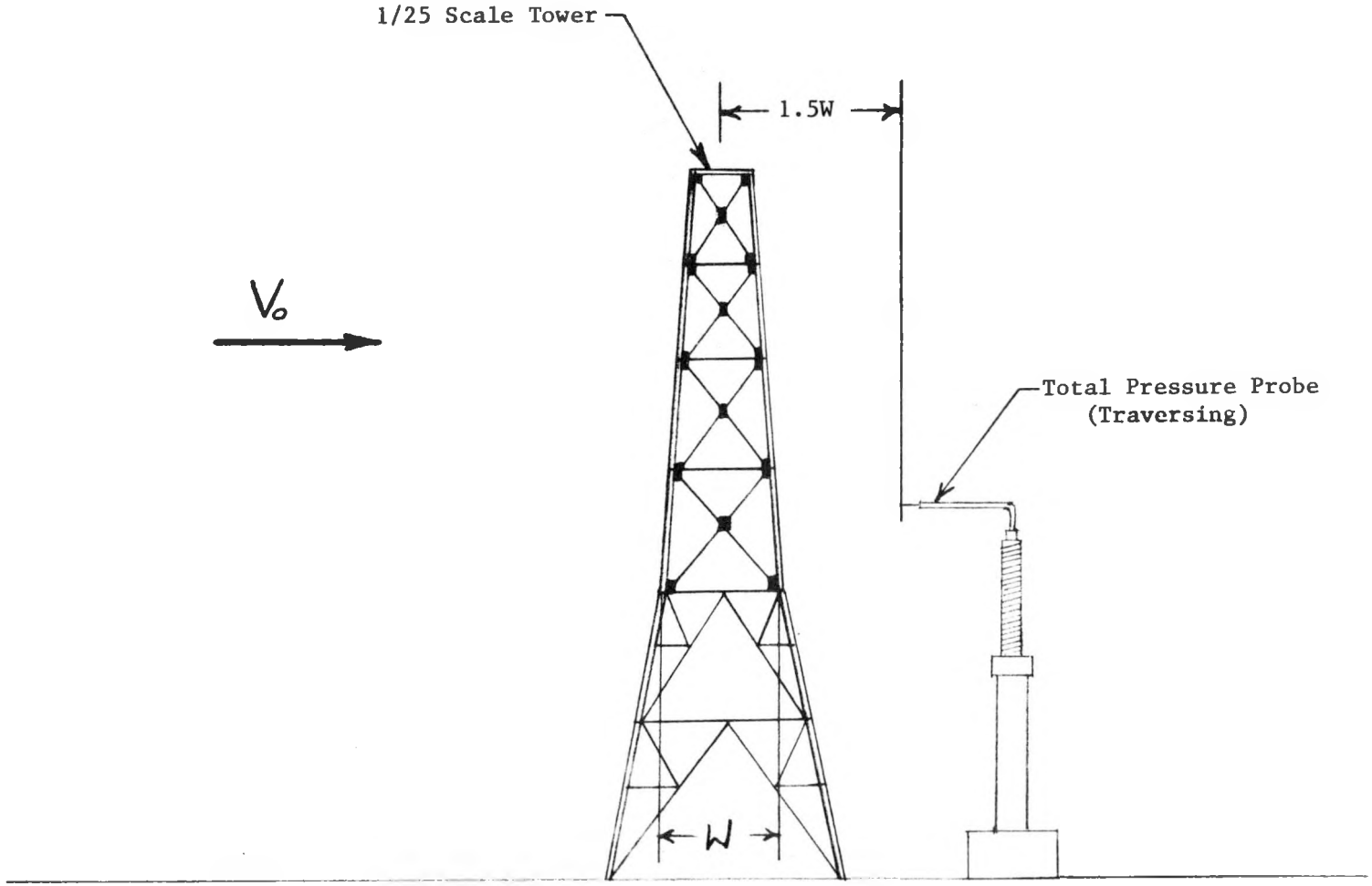

FIGURE 2. Orientation of Downstream Pressure Probe

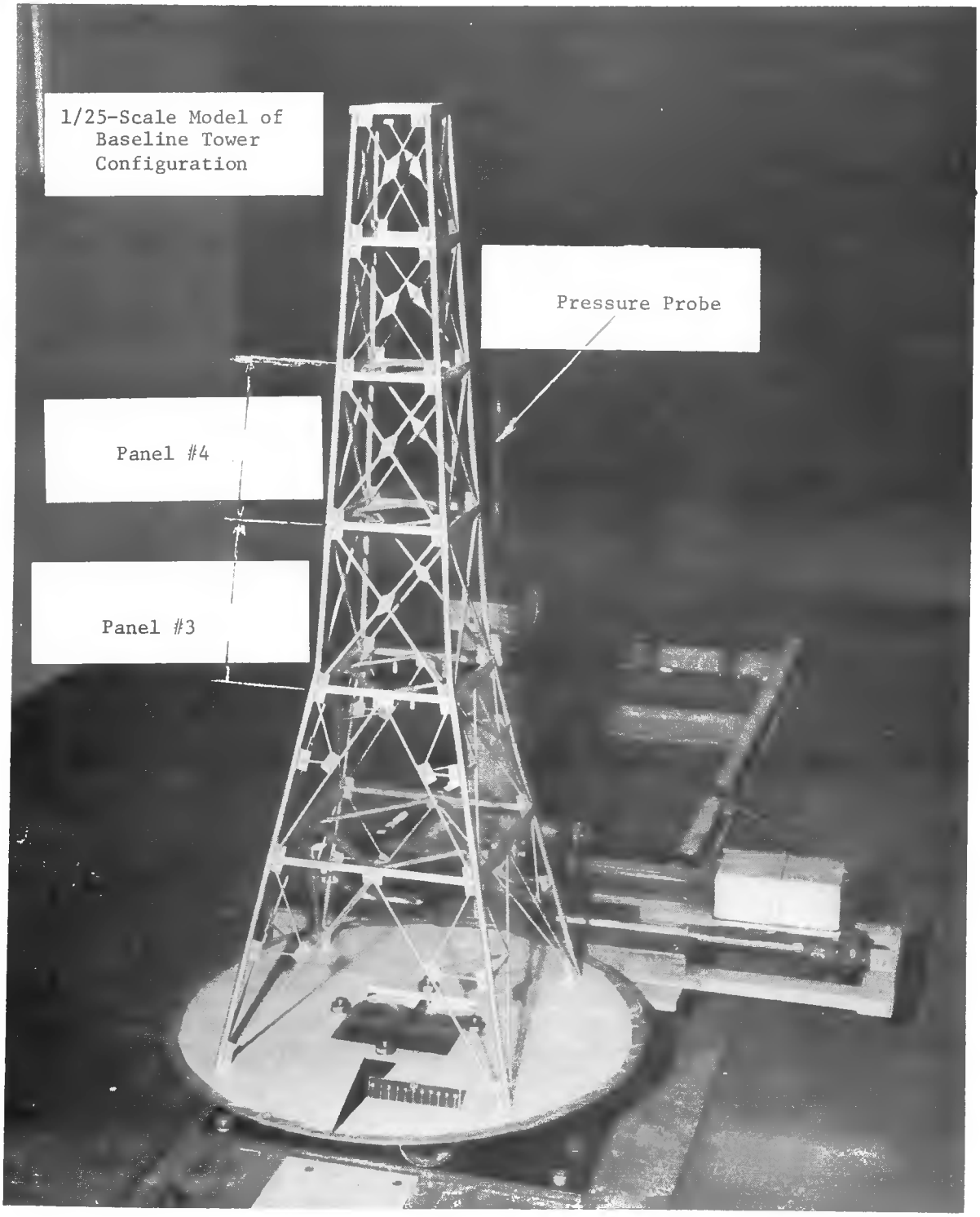

FIGURE 3 - Tunnel Test Arrangement

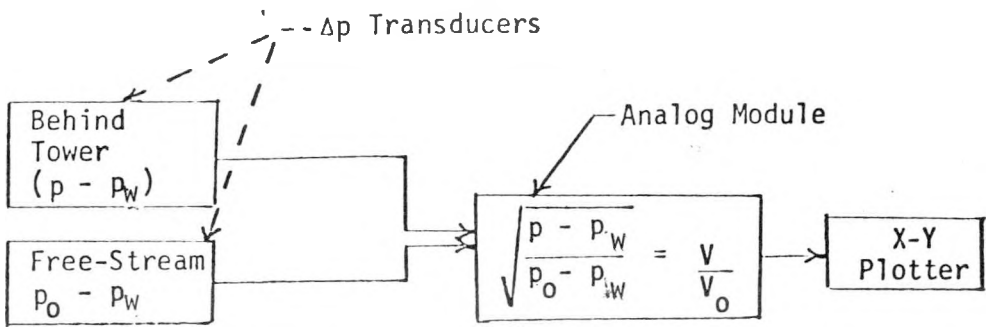

FIGURE 4 - Schematic of Velocity Profile Ratio Determination

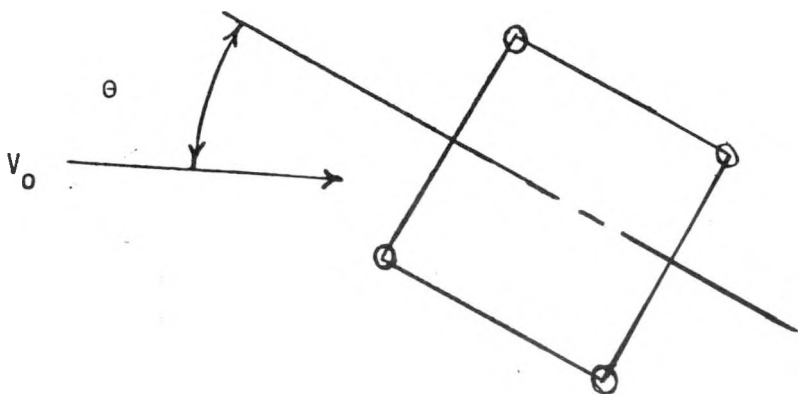

FIGURE 5 - Definition of Wind Direction

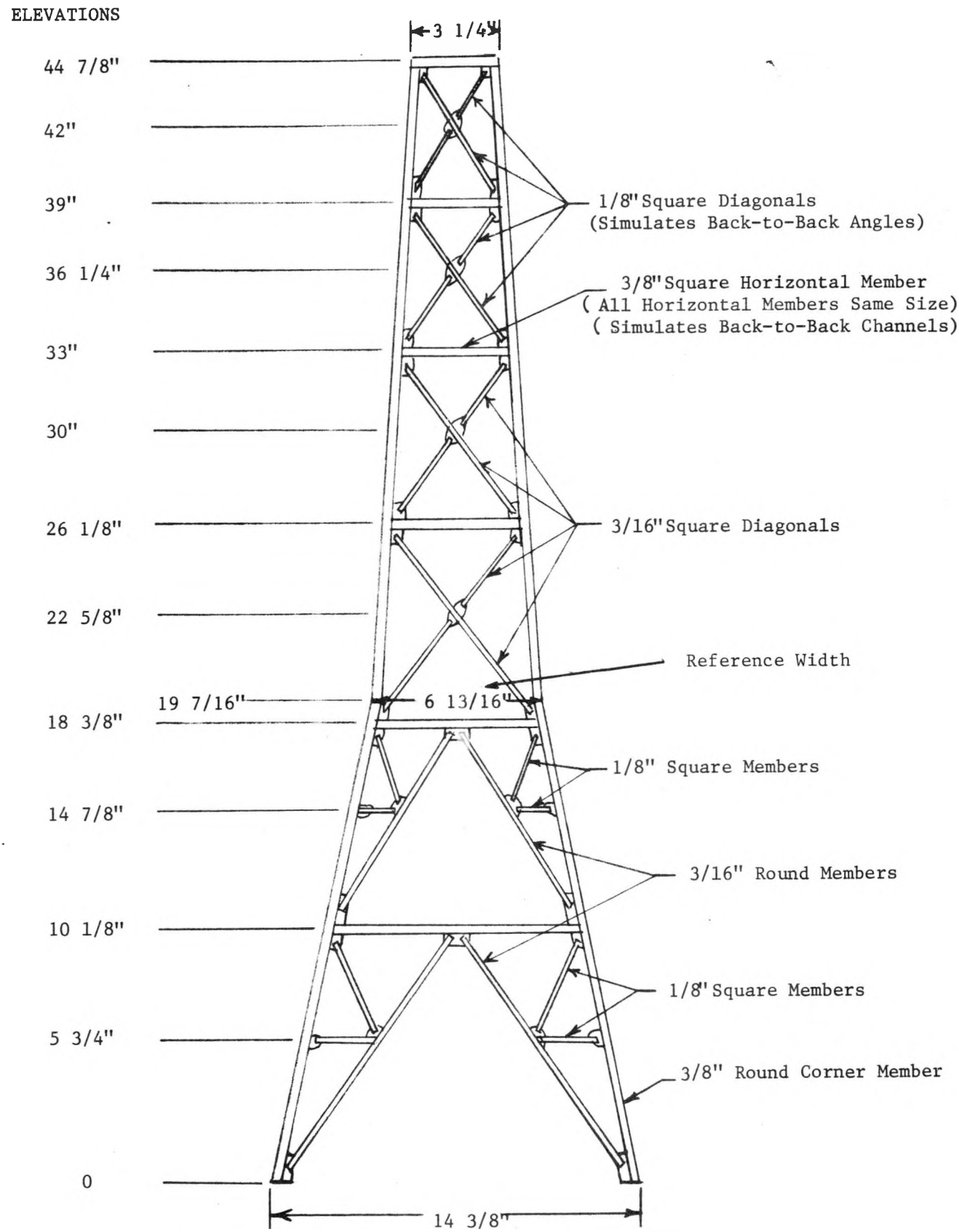

FIGURE 6 - Baseline Tower Dimensions

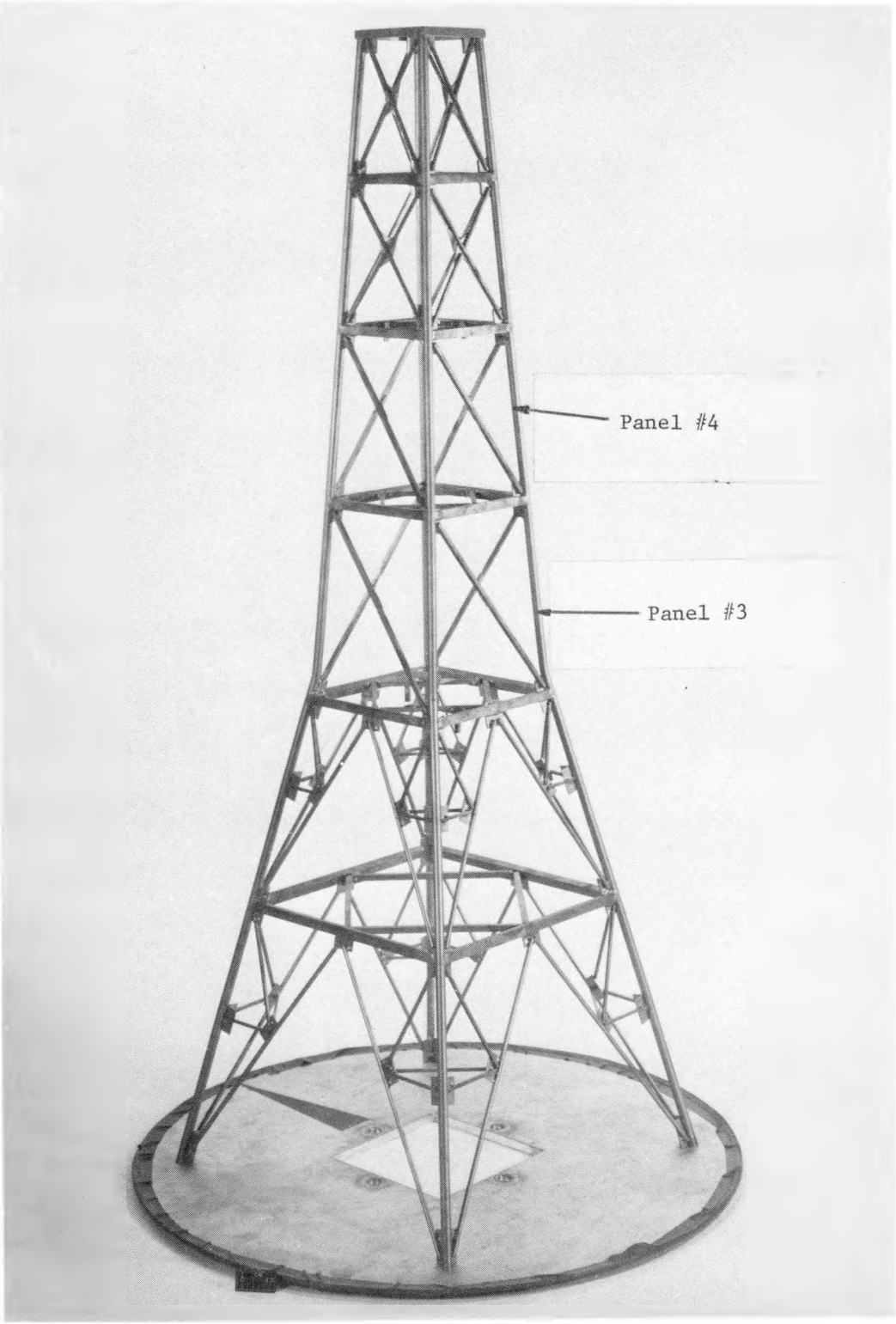

FIGURE 7 - Tower Configuration With One Diagonal Removed
From Each Side of Panels 3 and 4

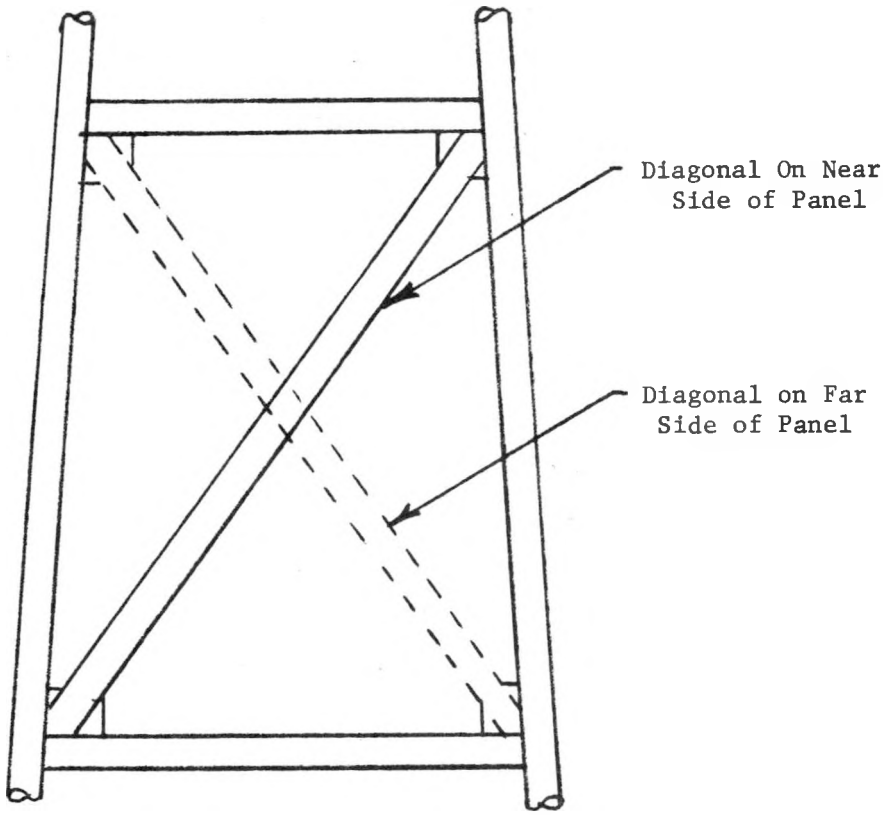

FIGURE 8 - Schematic View of One Diagonal Removed From Each Side of Tower

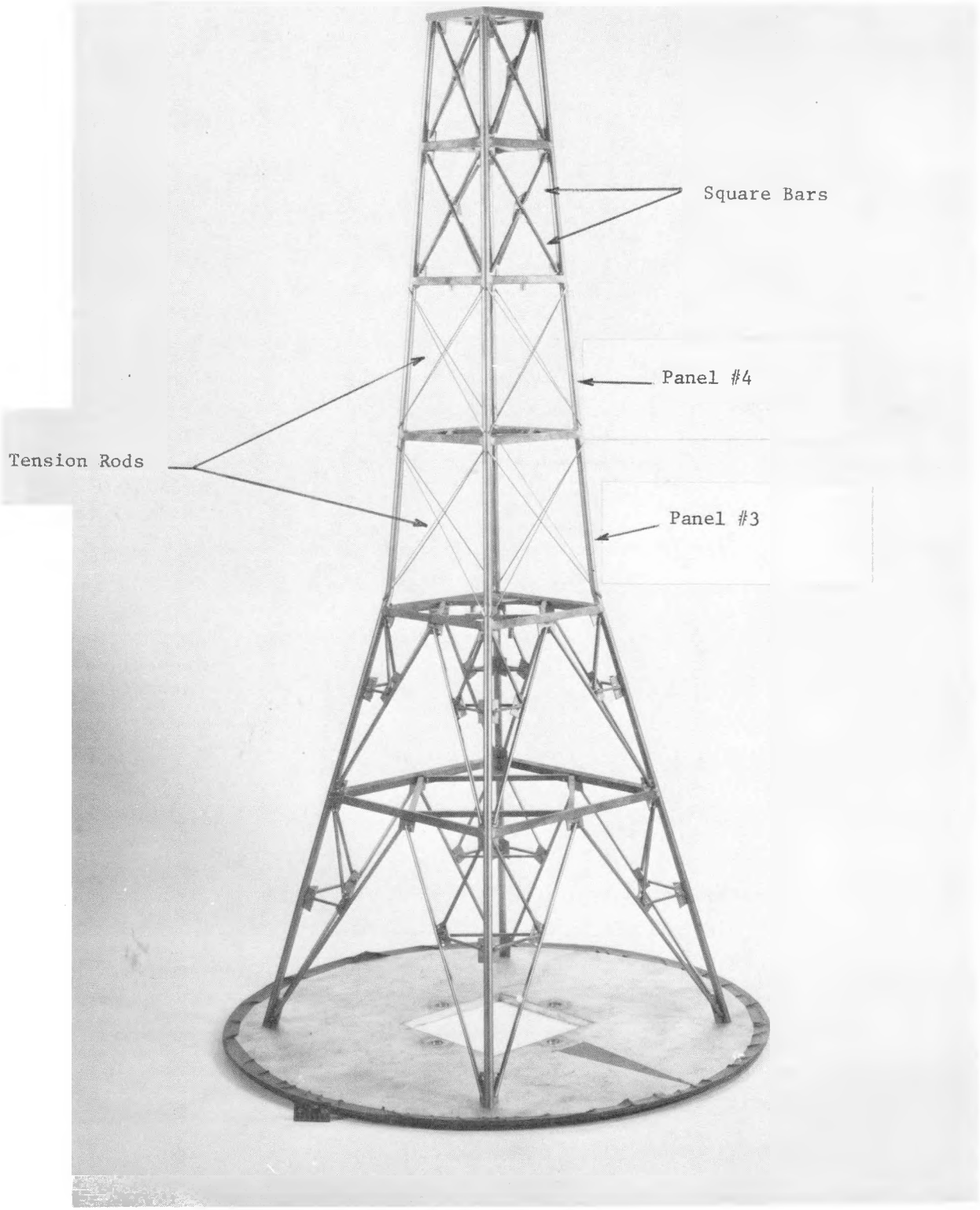

FIGURE 9 - Tower Configuration With Tension Rods Installed as Diagonals in Panels 3 and 4

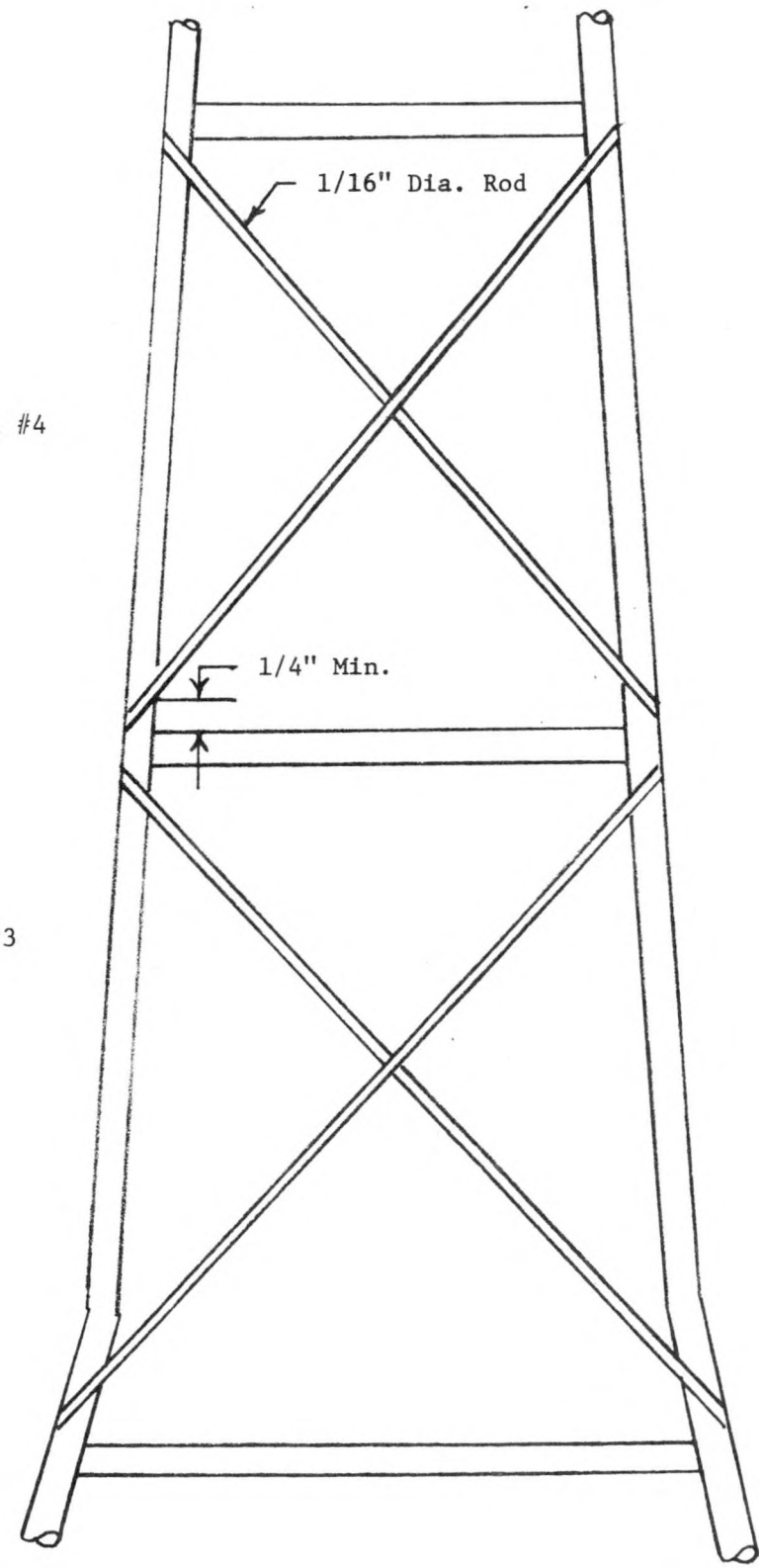

FIGURE 10 - Tension Rod Positioning

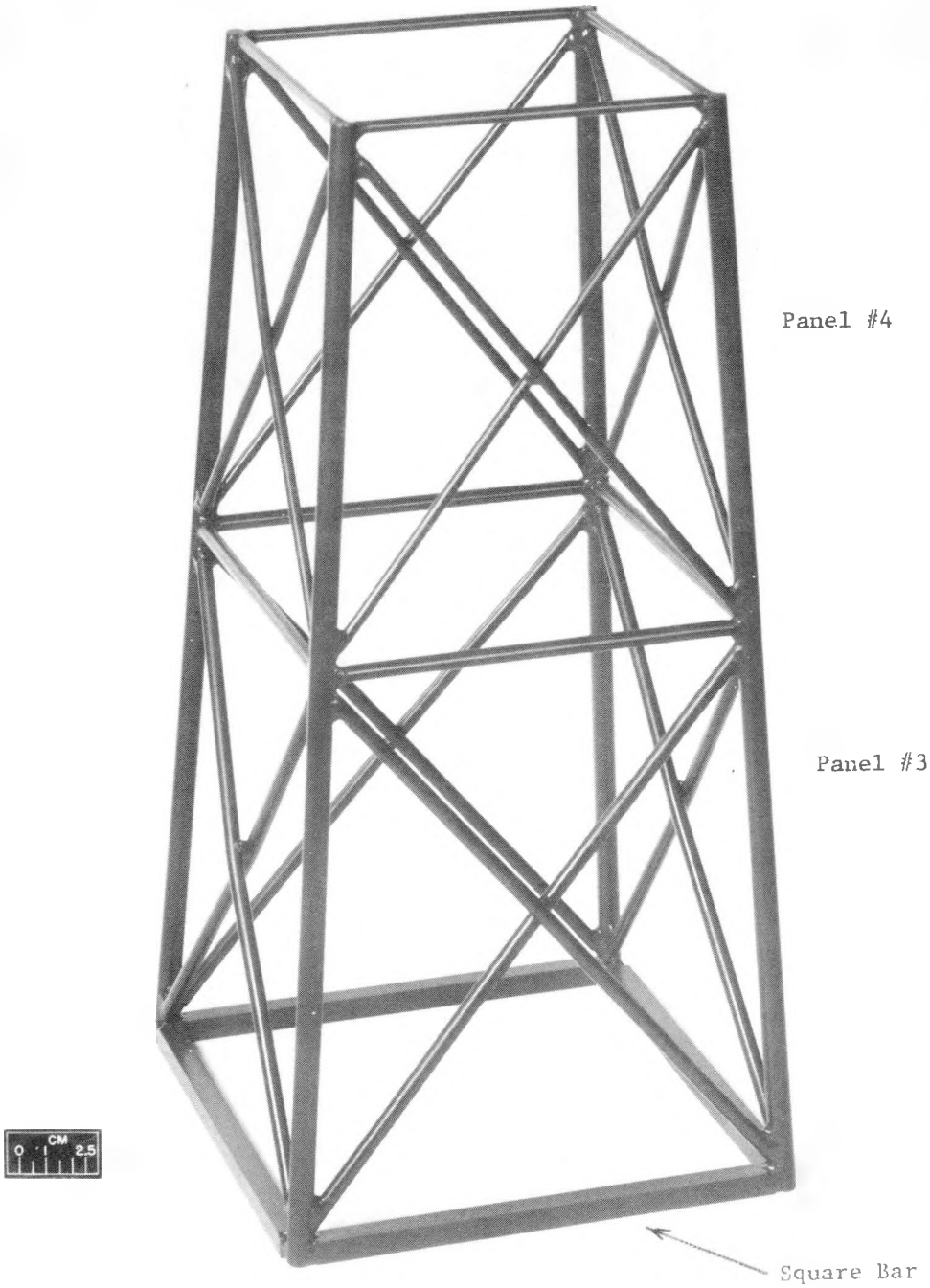

FIGURE 11 - Model of Two All-Pipe Tower Panels

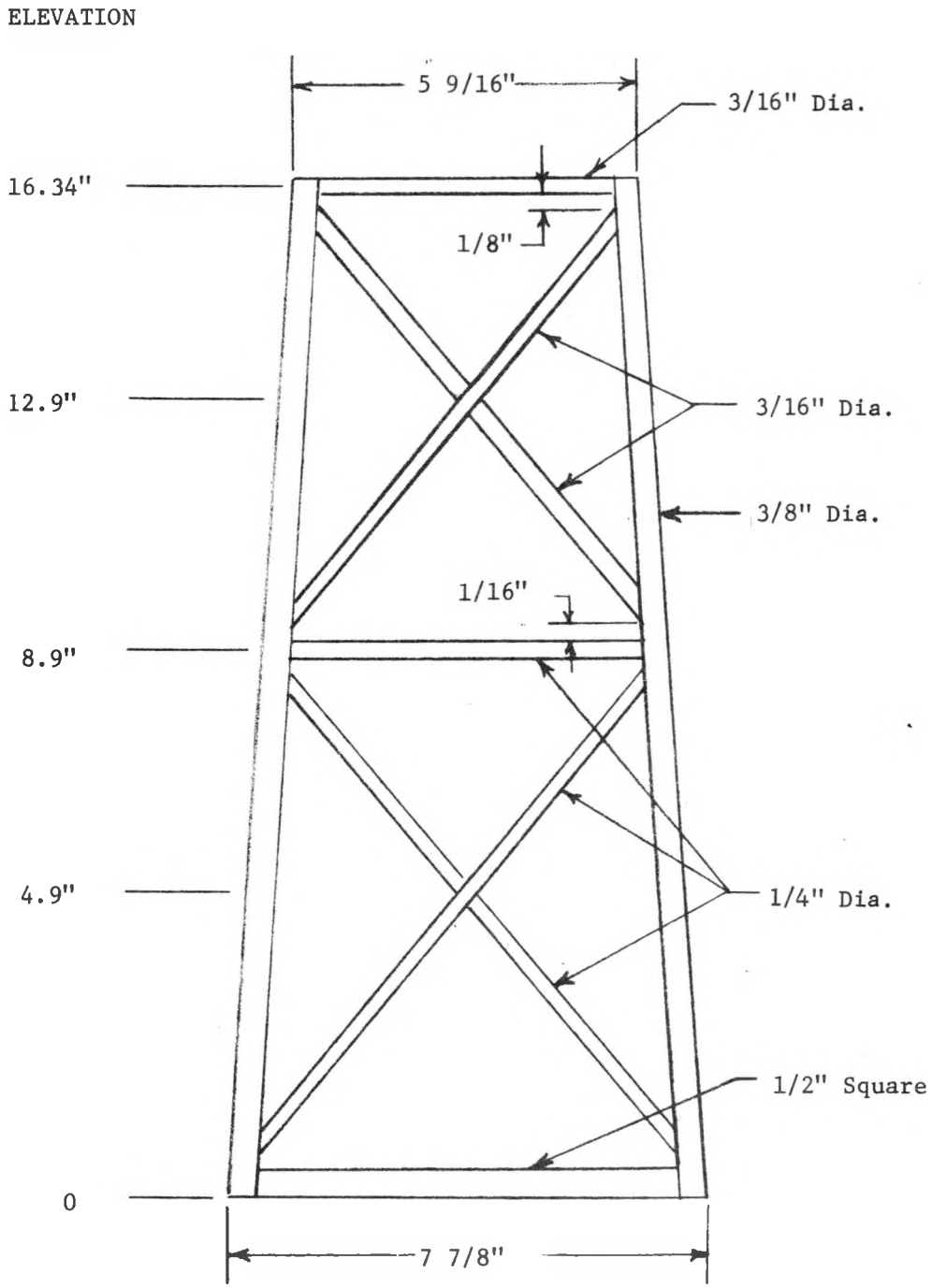

FIGURE 12 - All-Pipe Tower Model Dimensions

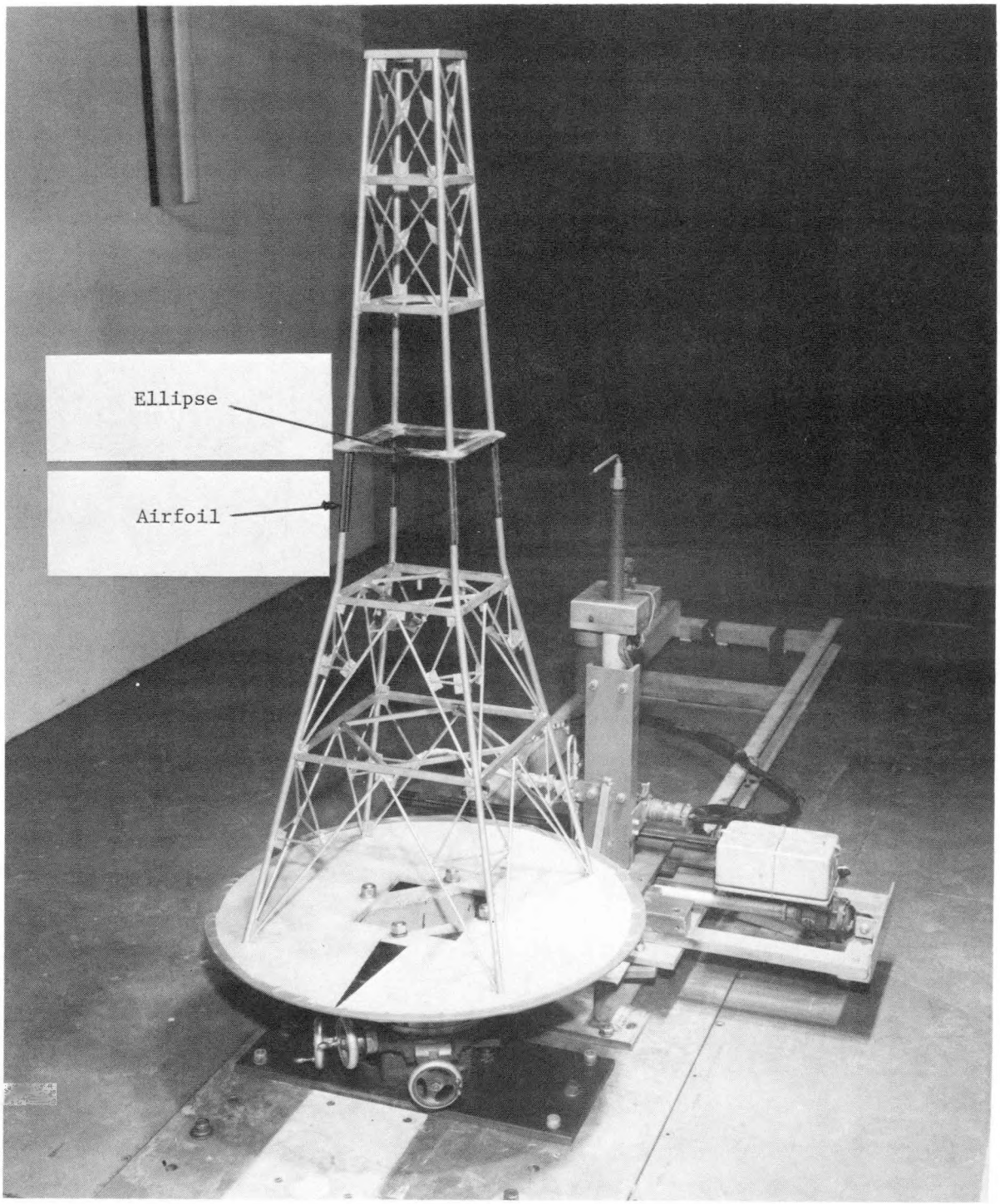

FIGURE 13 - Tower Configuration With Ellipses and Airfoils Installed

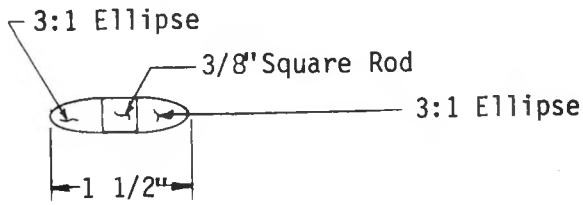

Ellipse on Horizontal Members

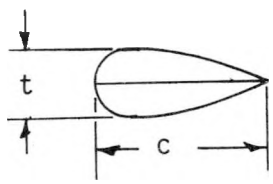

t	c
.375"	.938"

Airfoils on Vertical Members

FIGURE 14 - Ellipse and Airfoil Dimensional Characteristics

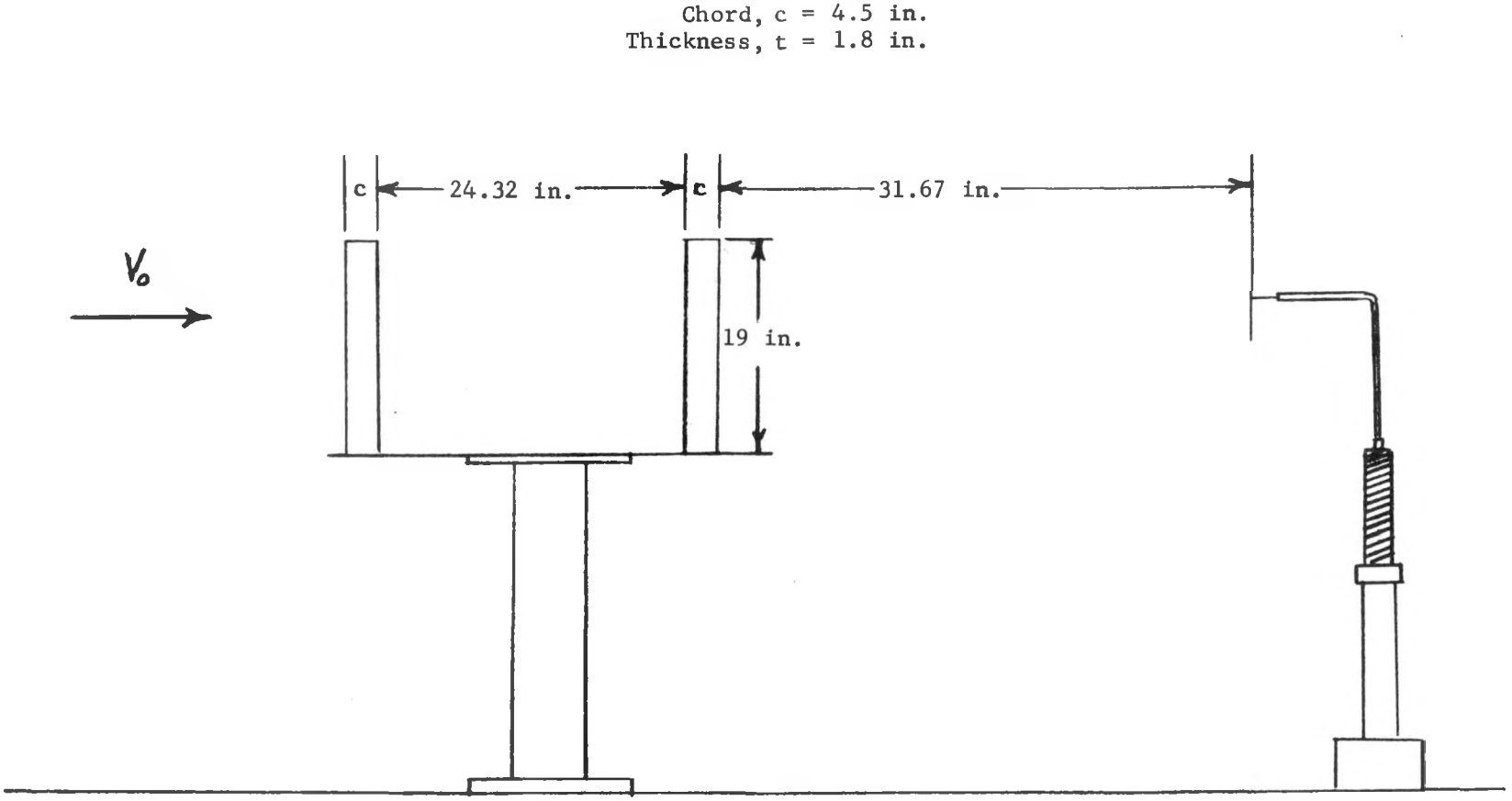

FIGURE 15 - Velocity Profile Measurement Downstream of Isolated, Full-Scale Airfoils

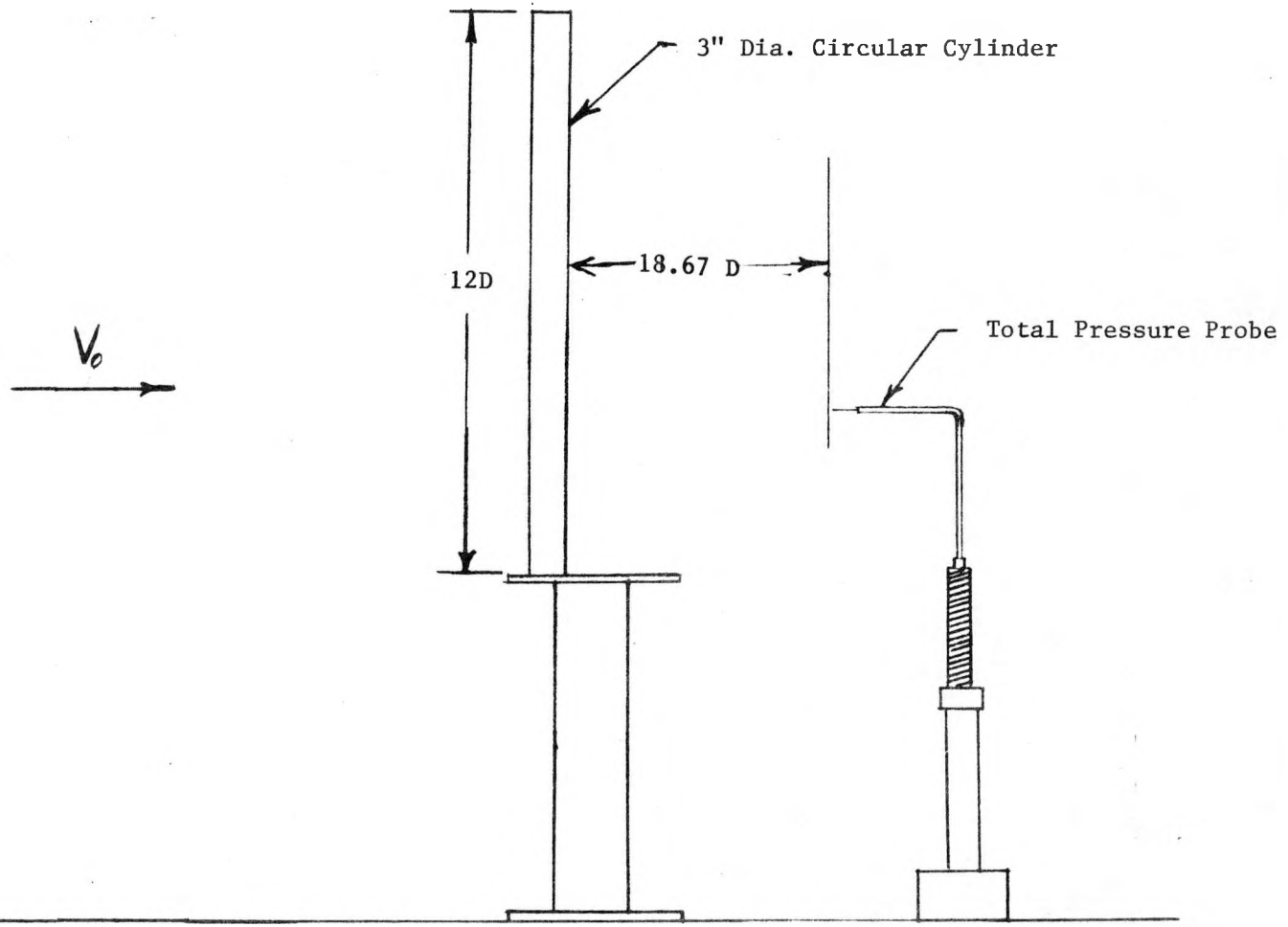

FIGURE 16 - Velocity Profile Measurement Downstream of Vertical Members of Various Surface Roughness

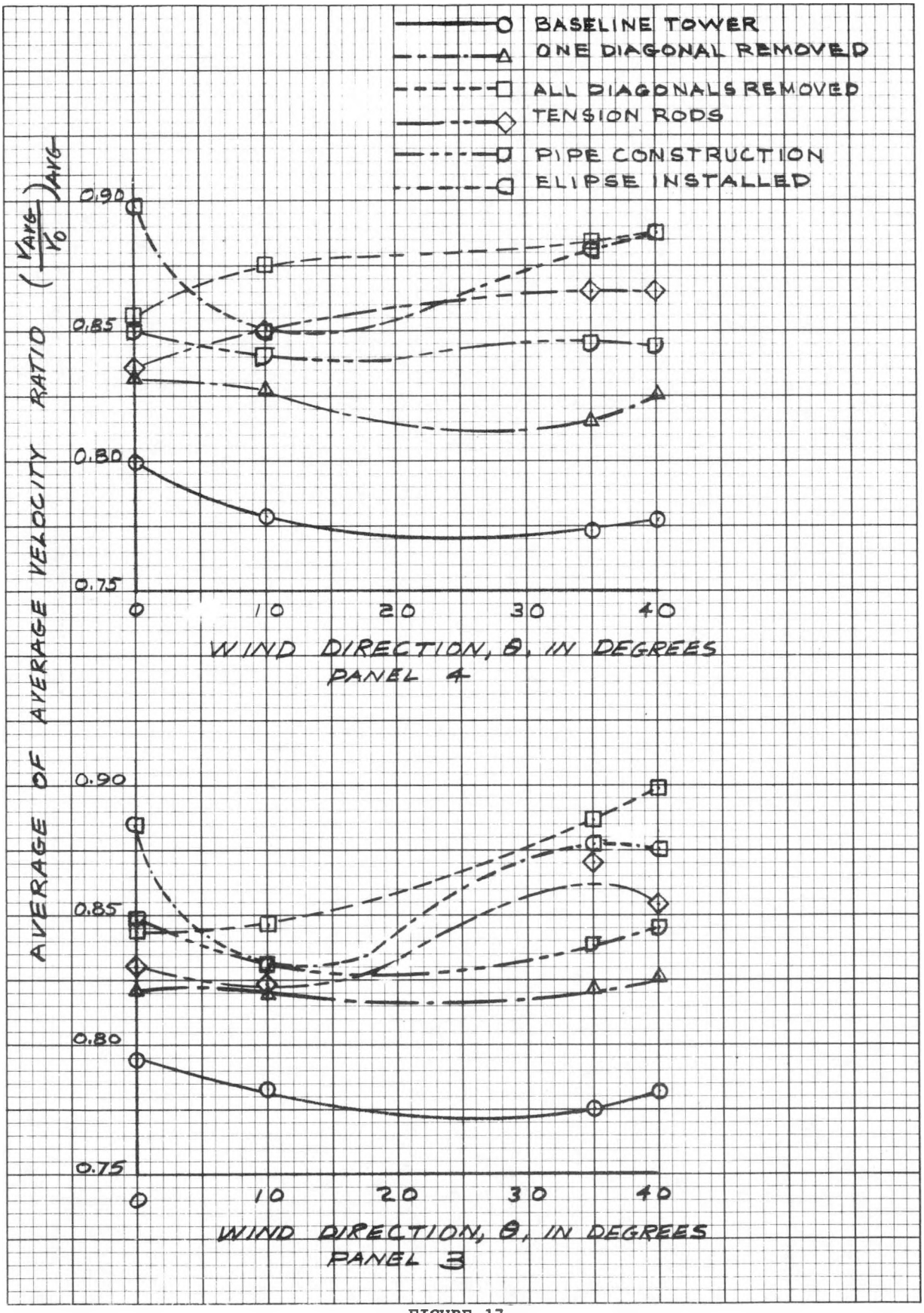

FIGURE 17
Comparison of Effect of Wind Direction on the Average of Average Velocity Ratio by Panels for all Scale Model Towers

APPENDIX A

Velocity Ratio Profiles at Selected Elevations for Wind Directions of 0^{o}, 10^{o}, 35^{o}, 40^{o}; All Tower Configurations

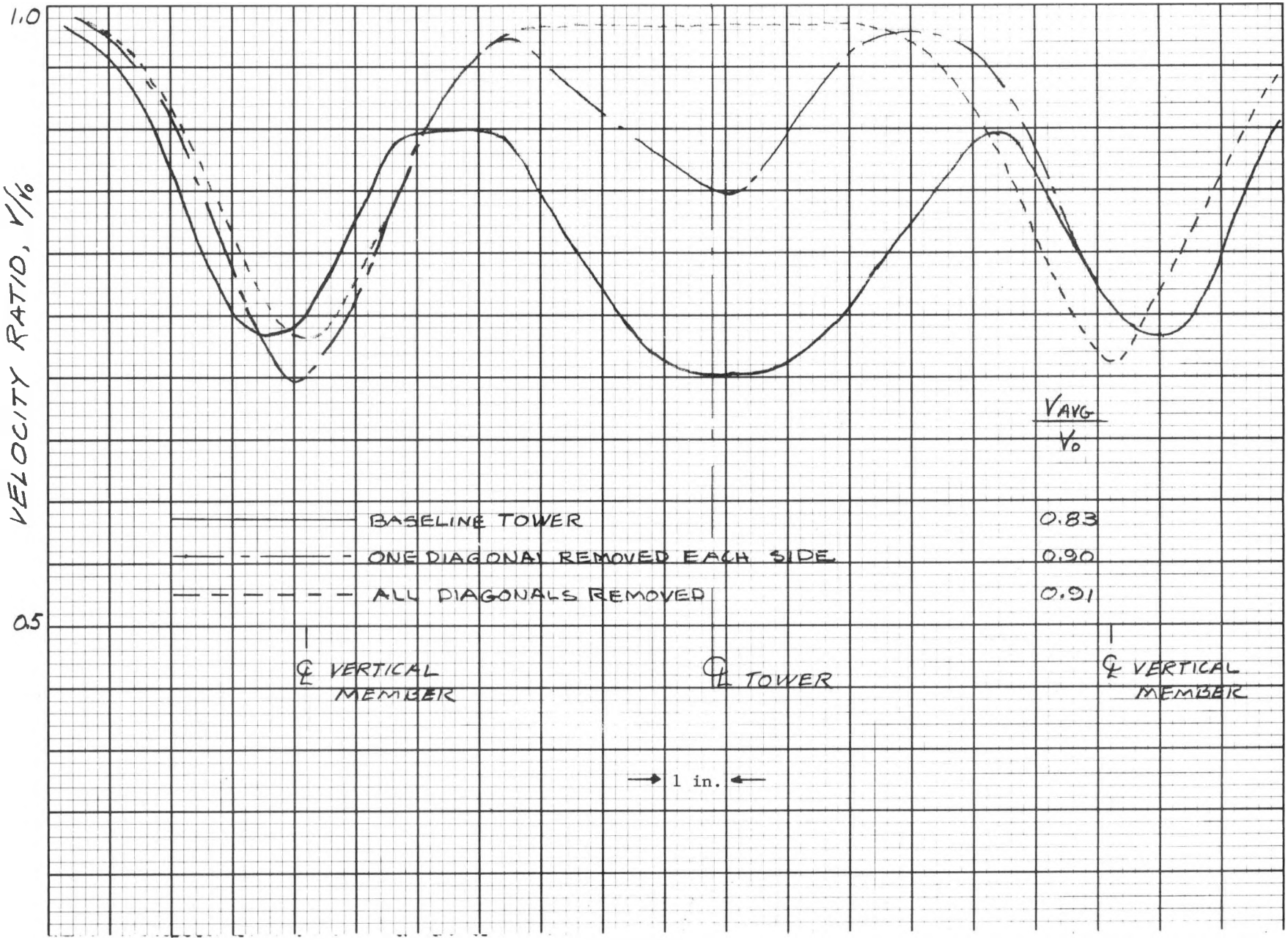

FIGURE 18a
Comparison of Velocity Ratio Profiles at Elevation of 22.7 Inches for Baseline Tower and Tower with Diagonals Removed (Wind Direction 0^{o})

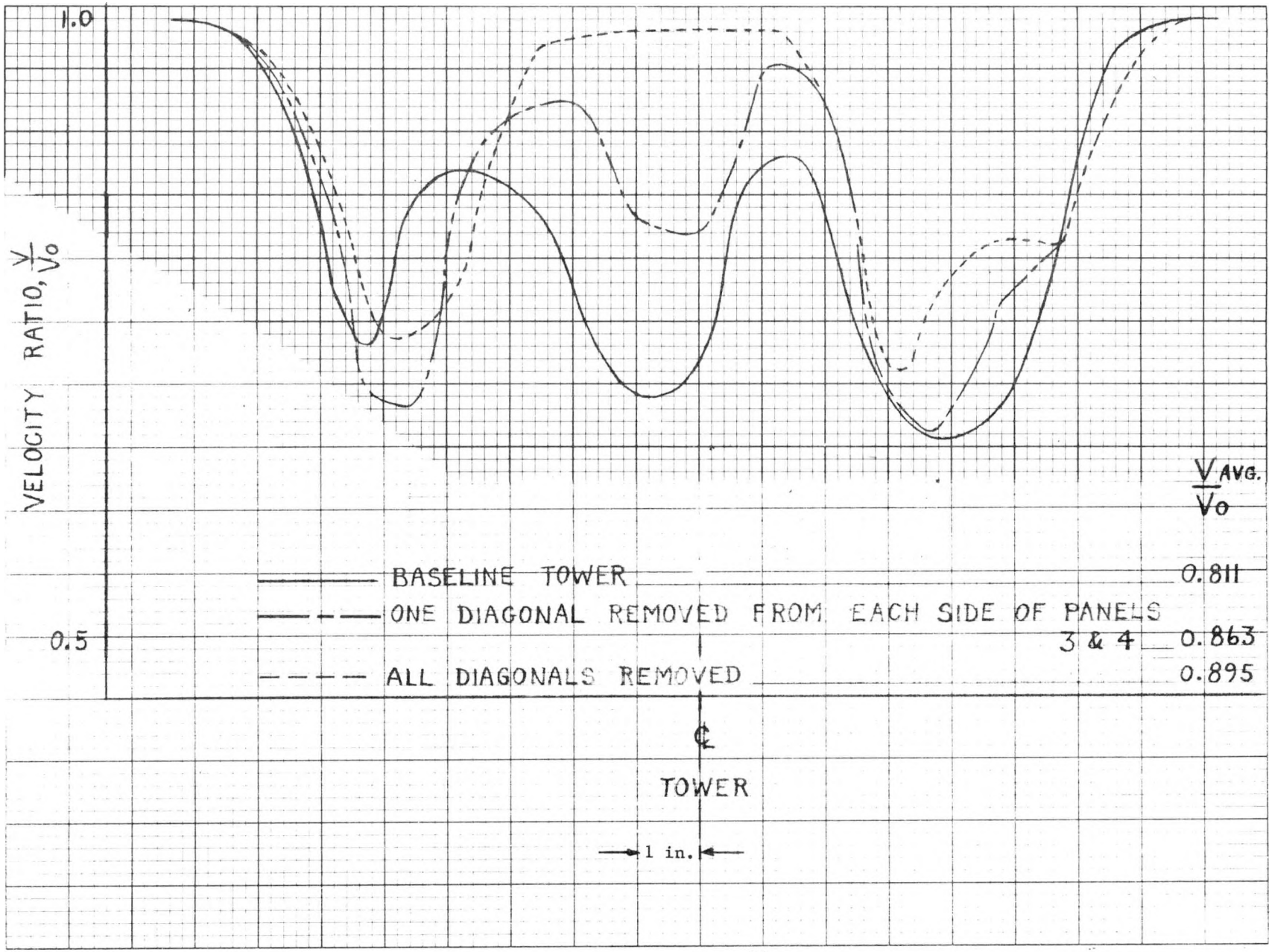

FIGURE 18b
Comparison of Velocity Ratio Profiles for Baseline Tower and Tower with Diagonals Removed at Elevation of 22.7 inches (Wind Direction of 10°)

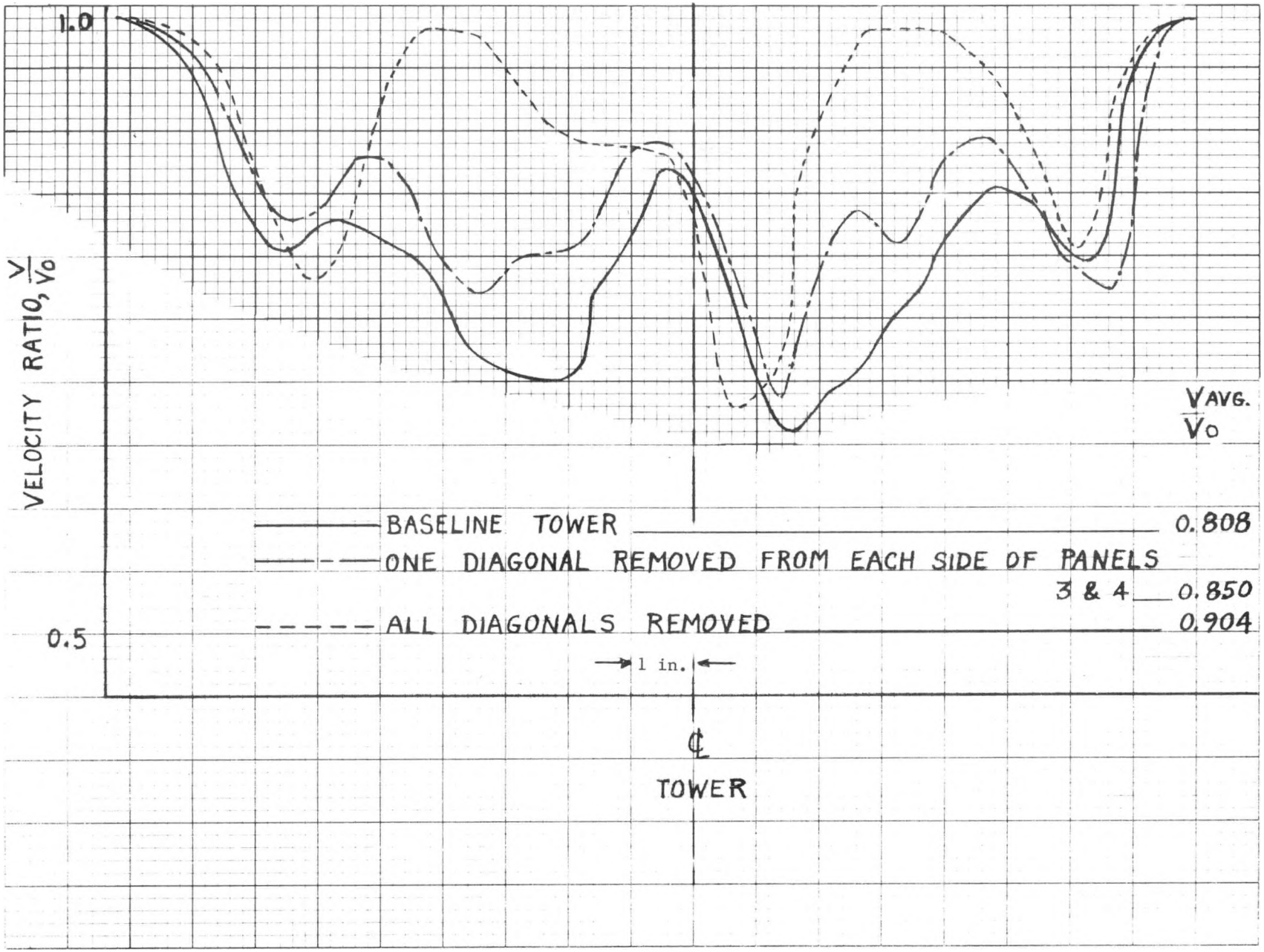

FIGURE 18c
Comparison of Velocity Ratio Profiles for Baseline Tower and Tower with Diagonals Removed at Elevation of 22.7 inches (Wind Direction of 35°)

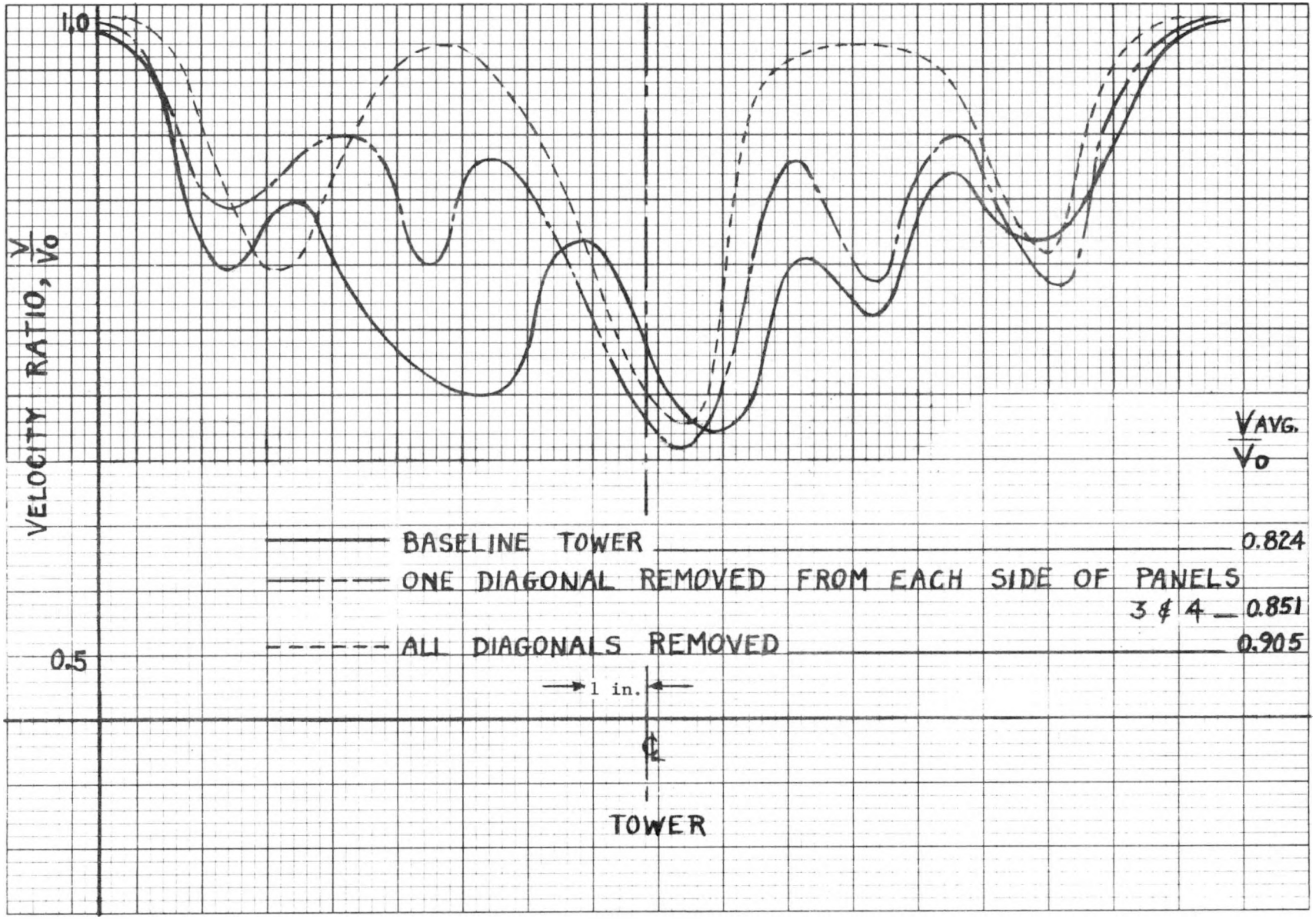

FIGURE 18d
Comparison of Velocity Ratio Profiles for Baseline Tower and Tower with Diagonals Removed at Elevation of 22.7 inches (Wind Direction of 40°)

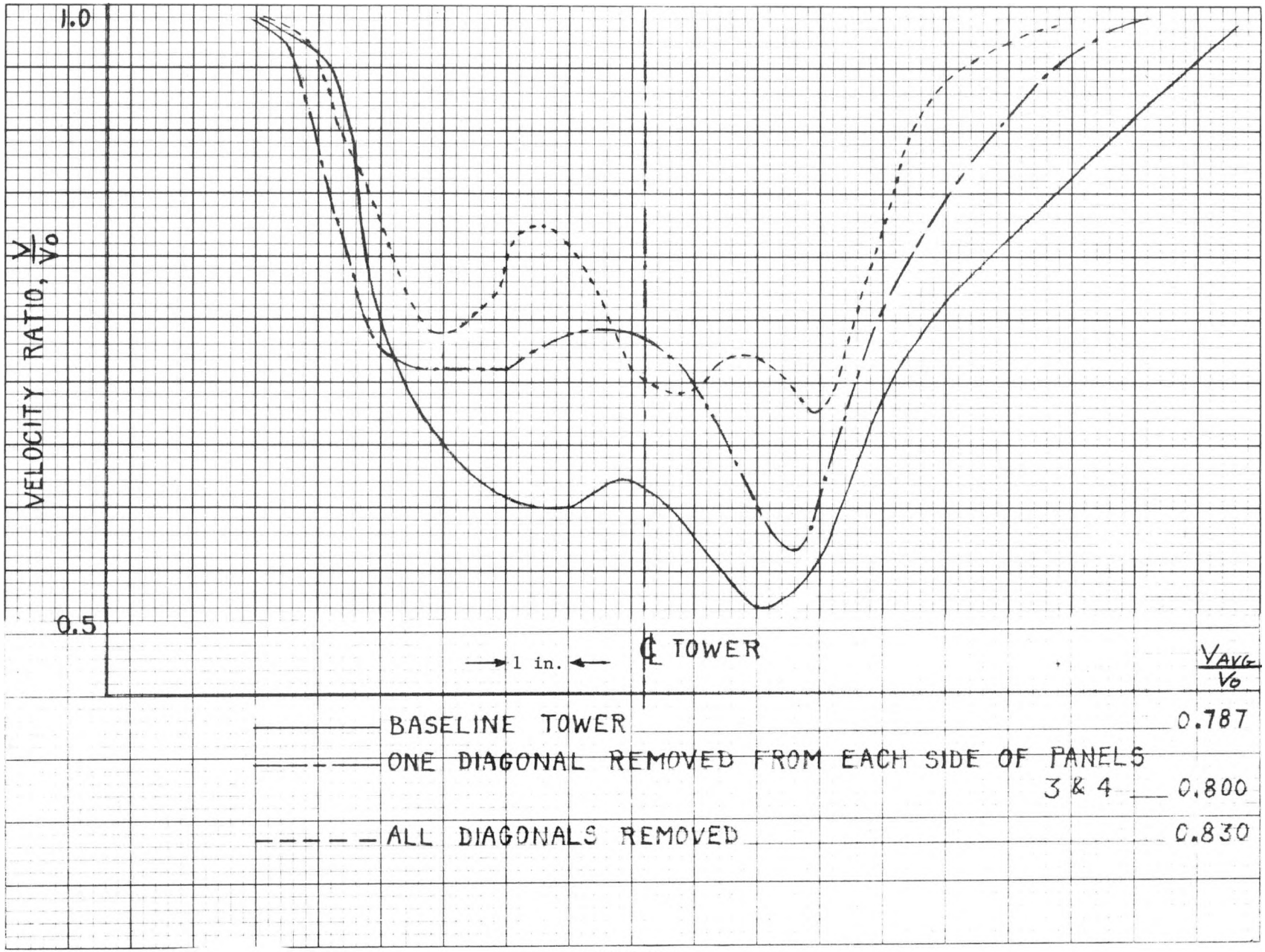

FIGURE 19a
Comparison of Velocity Ratio Profiles for Baseline Tower and Tower with Diagonals Removed at Elevation of 27.8 inches (Wind Direction of 10^{o})

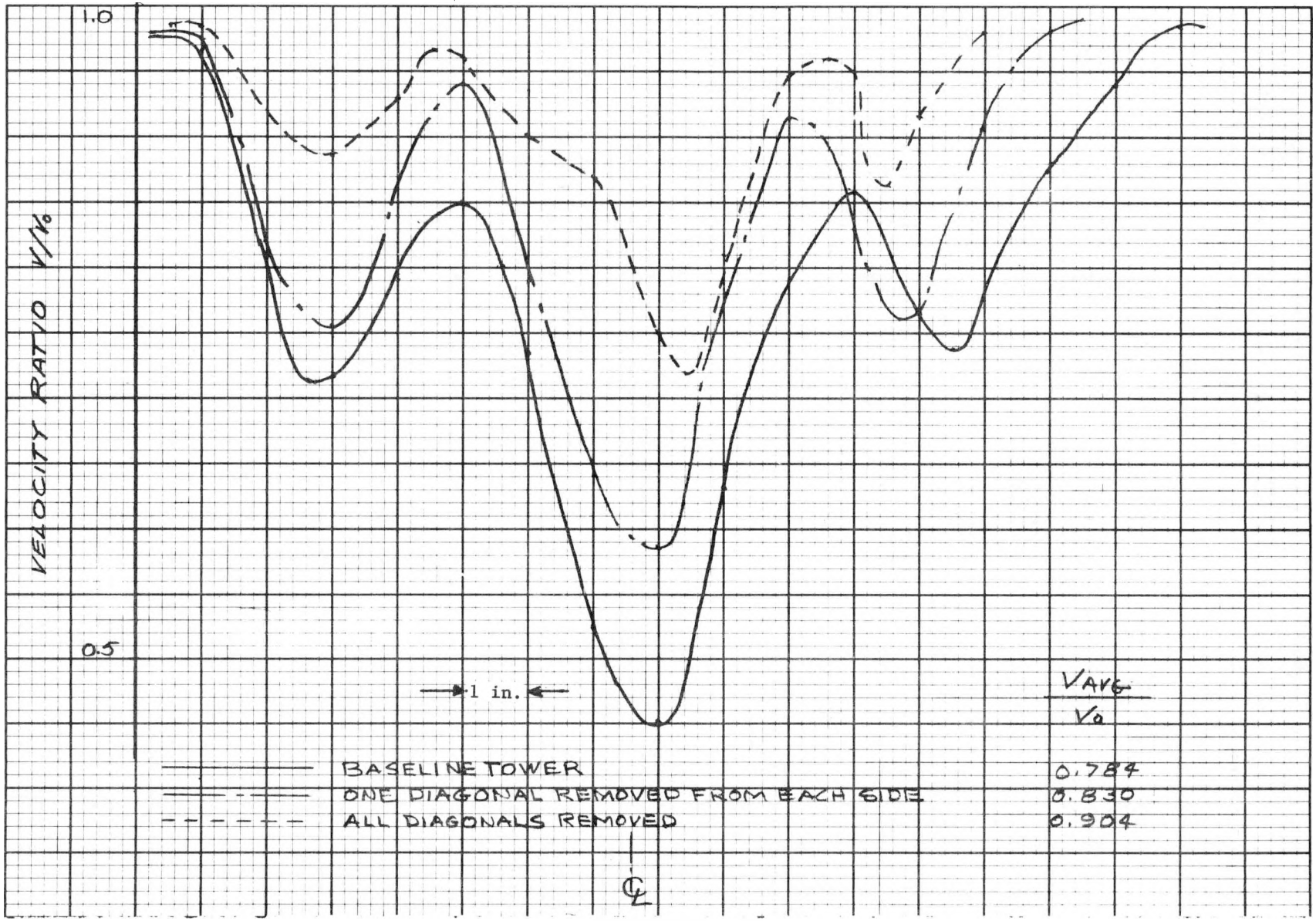

FIGURE 19b
Comparison of Velocity Ratio Profiles for Baseline Tower and Tower with Diagonals Removed at Elevation of 27.8 Inches (Wind Direction of 35°)

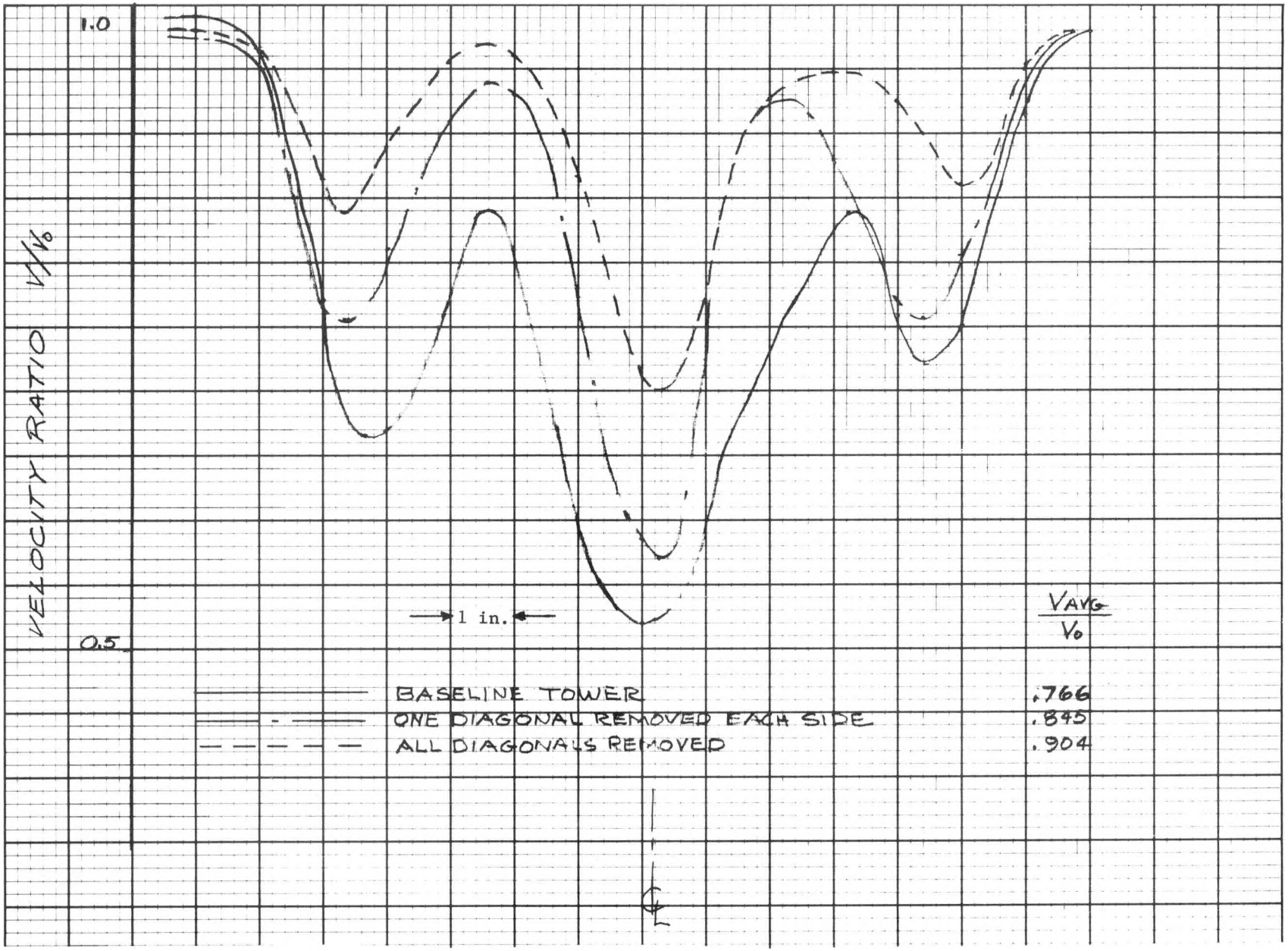

FIGURE 19c
Comparison of Velocity Ratio Profiles for Baseline Tower and Tower with Diagonals Removed at Elevation of 27.8 Inches (Wind Direction of 40°)

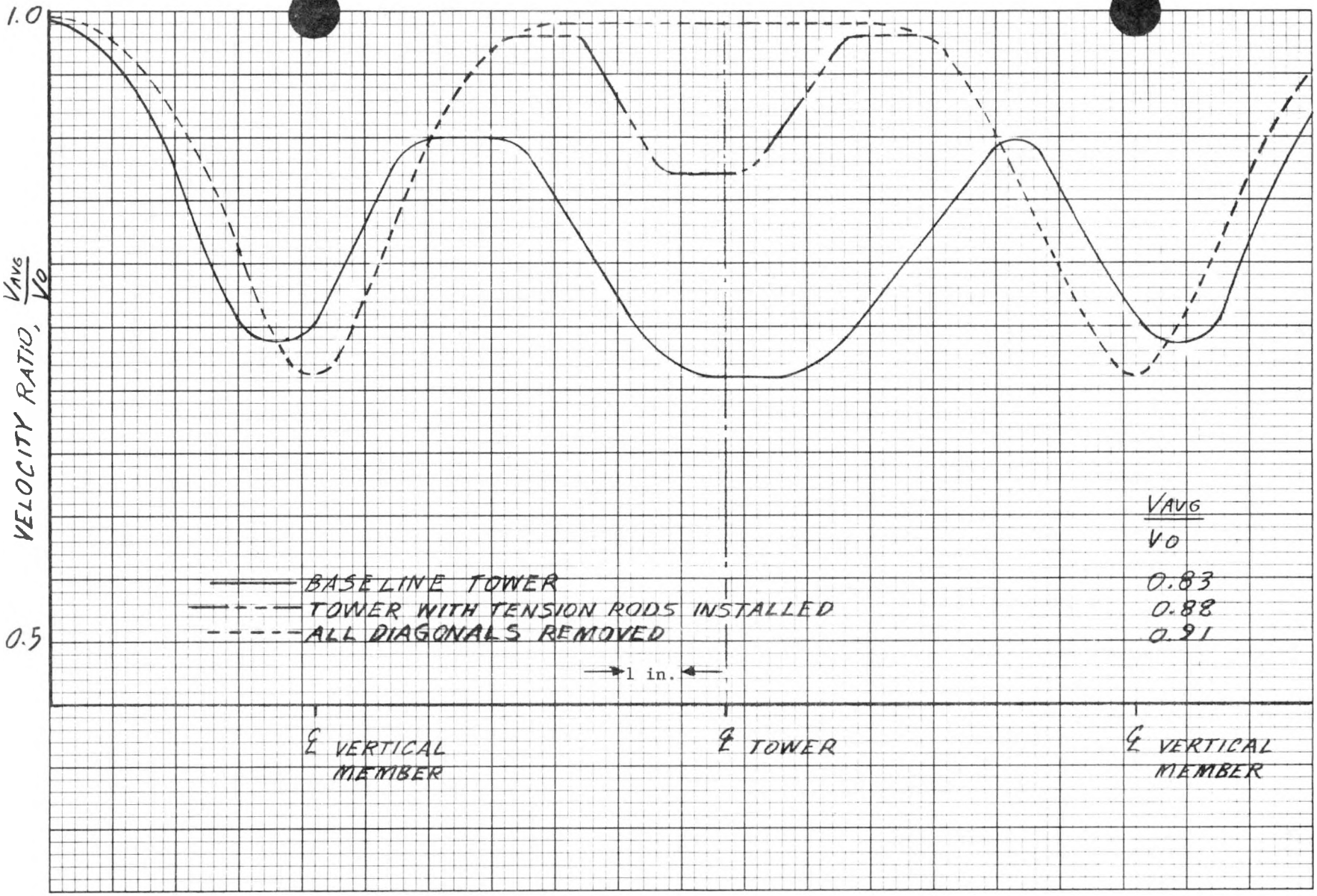

FIGURE 20a
Comparison of Velocity Ratio Profiles at Elevation of 22.7 Inches for Baseline Tower, Tower with All Diagonals Removed, and Tower With Tension Rods (Wind Direction 0^{o})

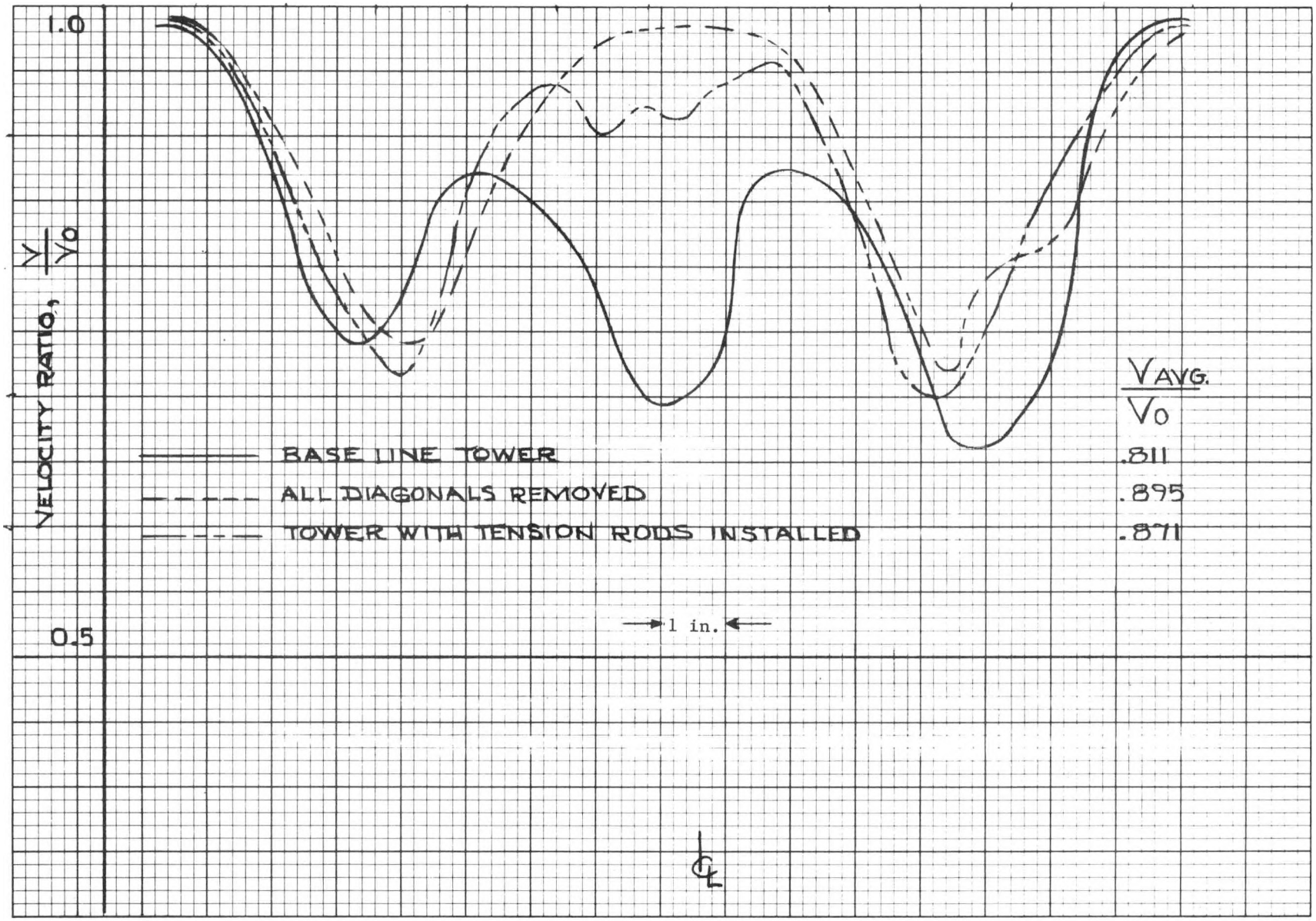

FIGURE 20b
Comparison of Velocity Ratio Profiles for Baseline Tower, Tower with all Diagonals Removed, and Tower with Tension Rods at Elevation of 22.7 inches Wind Direction of 10°

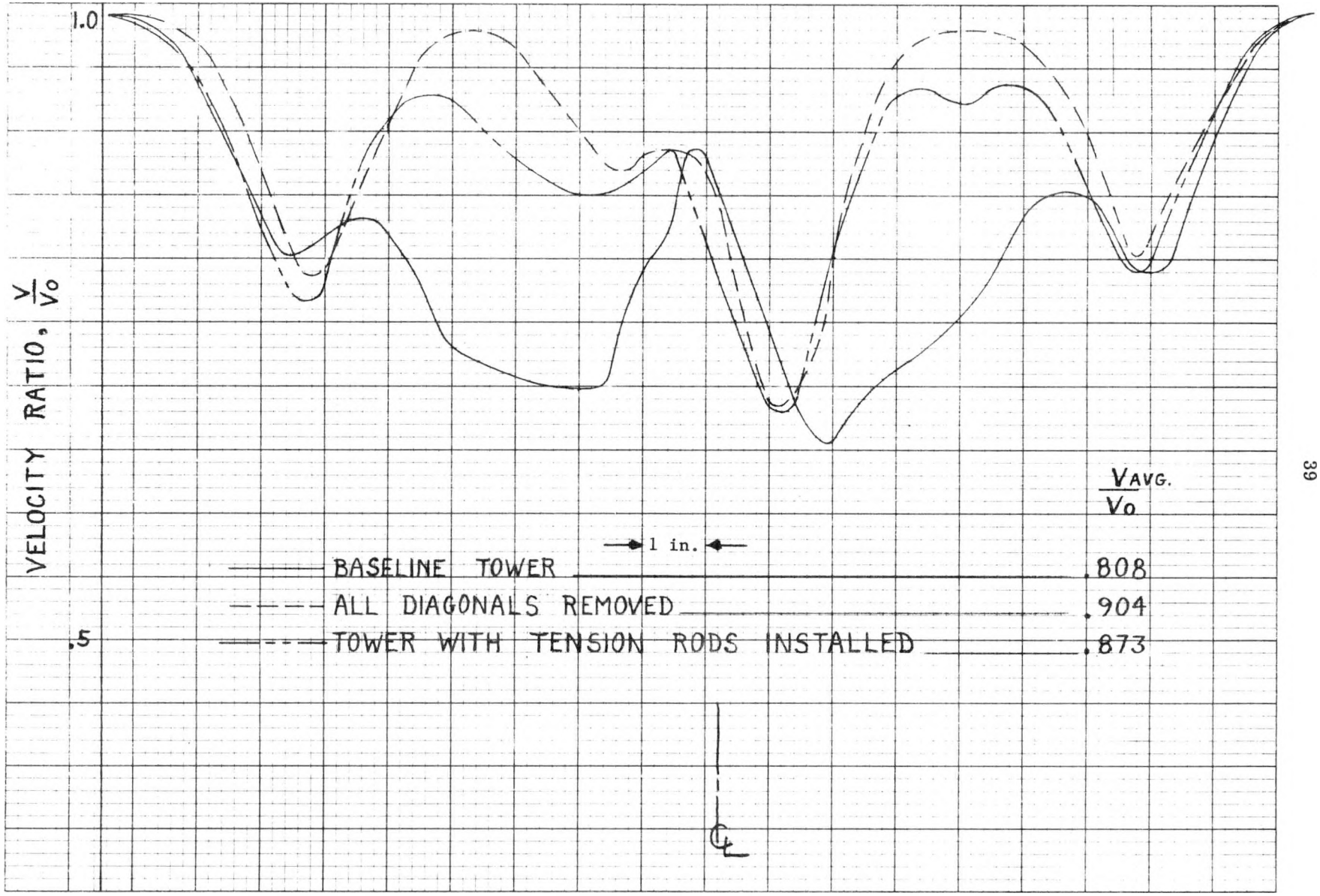

FIGURE 20c
Comparison of Velocity Ratio Profiles for Baseline Tower, Tower with all Diagonals Removed, and Tower with Tension Rods at Elevation of 22.7 Inches
Wind Direction of 35°

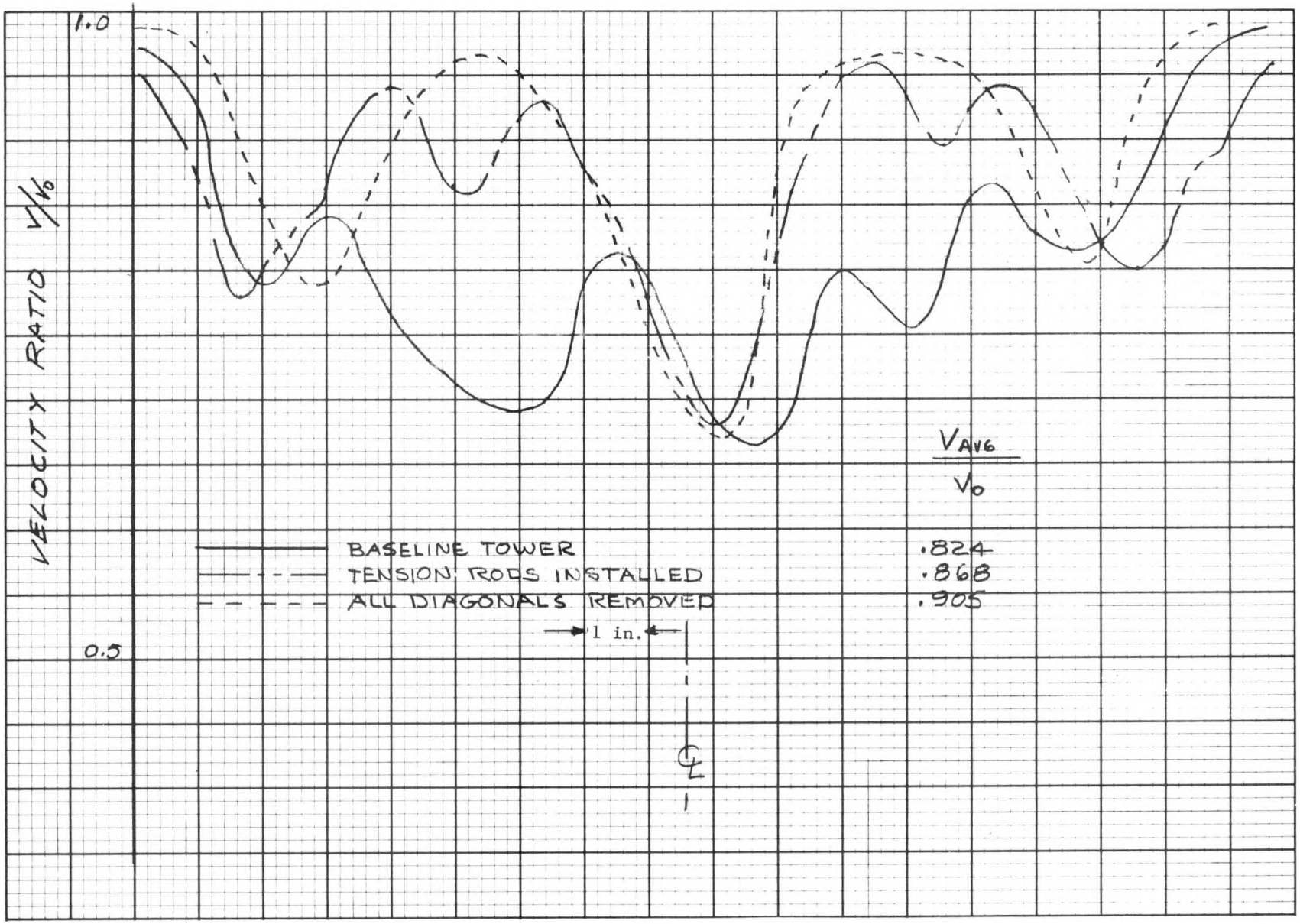

FIGURE 20d
Comparison of Velocity Ratio Profiles for Baseline Tower, Tower with all Diagonals Removed, and Tower with Tension Rods at Elevation of 22.7 Inches Wind Direction of 40°

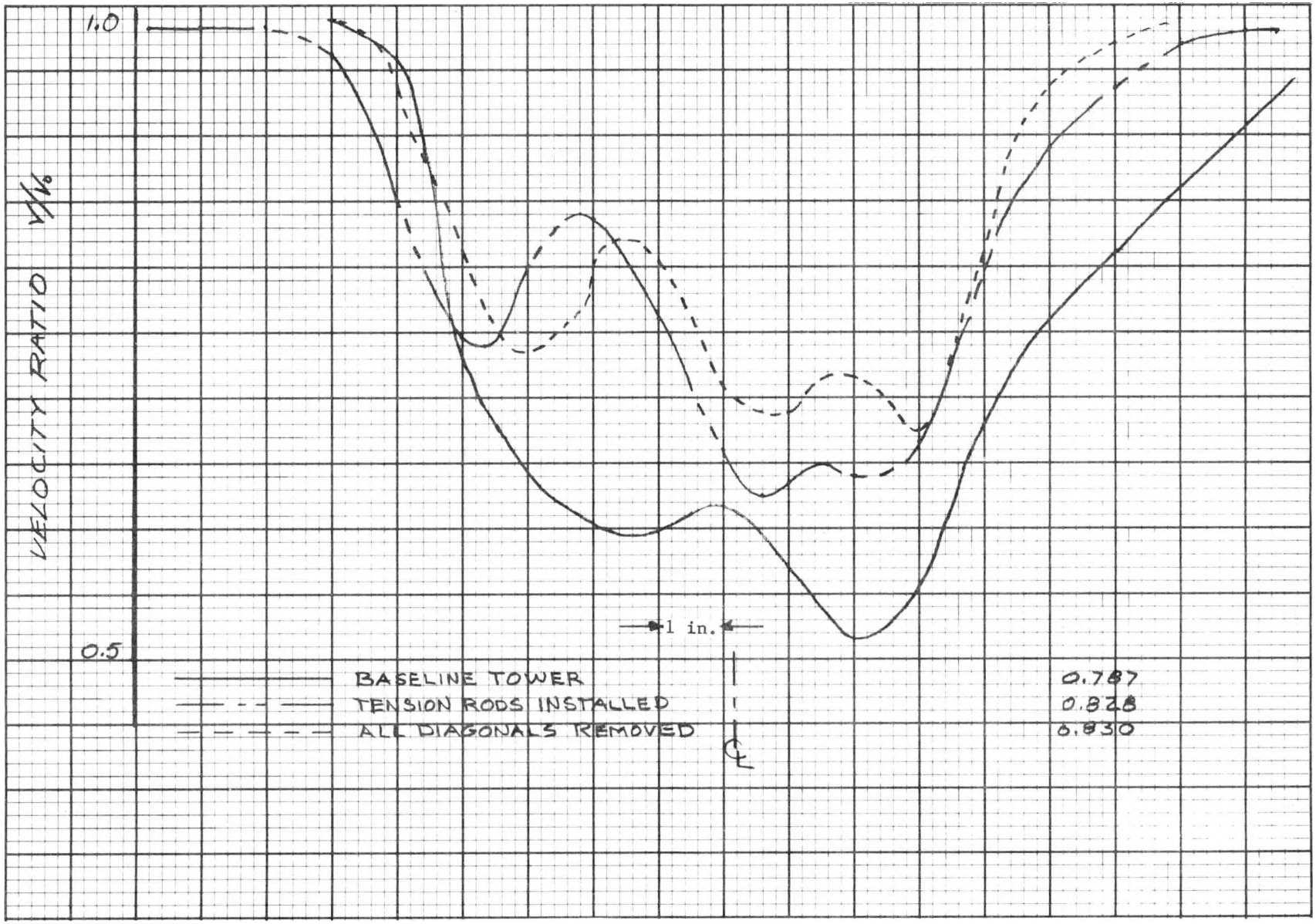

FIGURE 21a
Comparison of Velocity Ratio Profiles for Baseline Tower, Tower with all Diagonals Removed, and Tower with Tension Rods at Elevation of 27.8 Inches Wind Direction of 10°

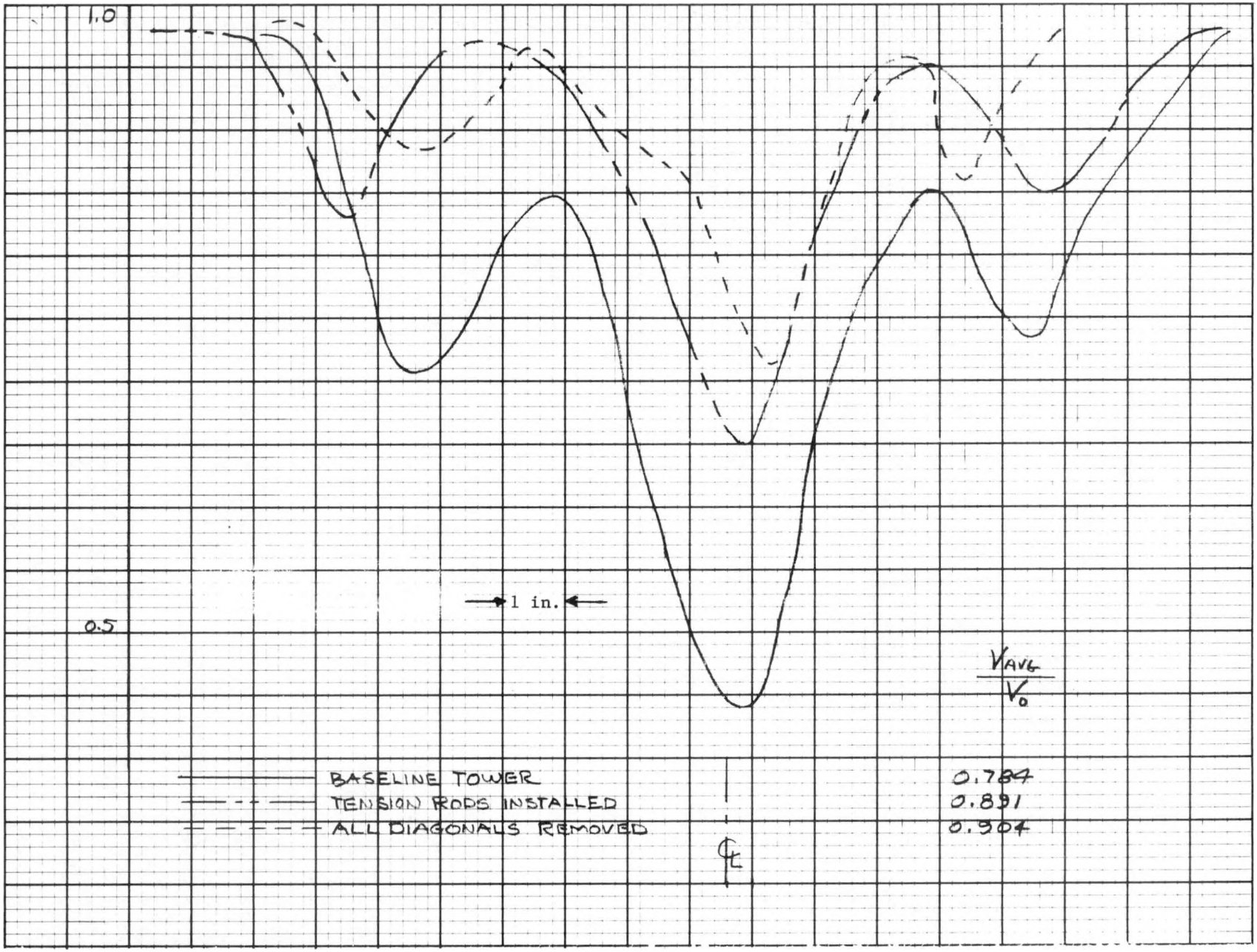

FIGURE 21b
Comparison of Velocity Ratio Profiles for Baseline Tower, Tower with all Diagonals Removed, and Tower with Tension Rods at Elevation of 27.8 Inches Wind Direction of 35°

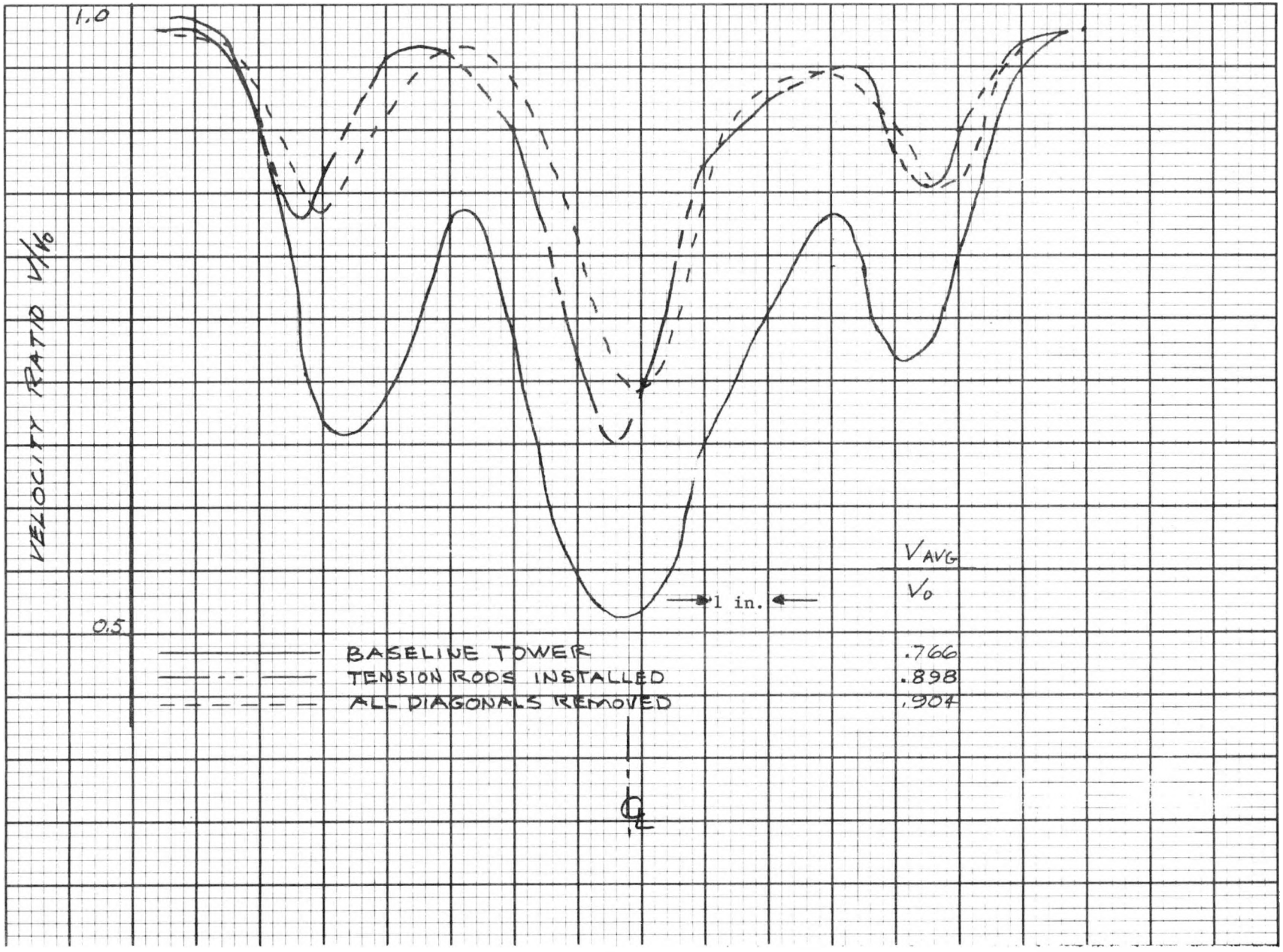

FIGURE 21c
Comparison of Velocity Ratio Profiles for Baseline Tower, Tower with all Diagonals Removed, and Tower with Tension Rods at Elevation of 27.8 Inches Wind Direction of 40°

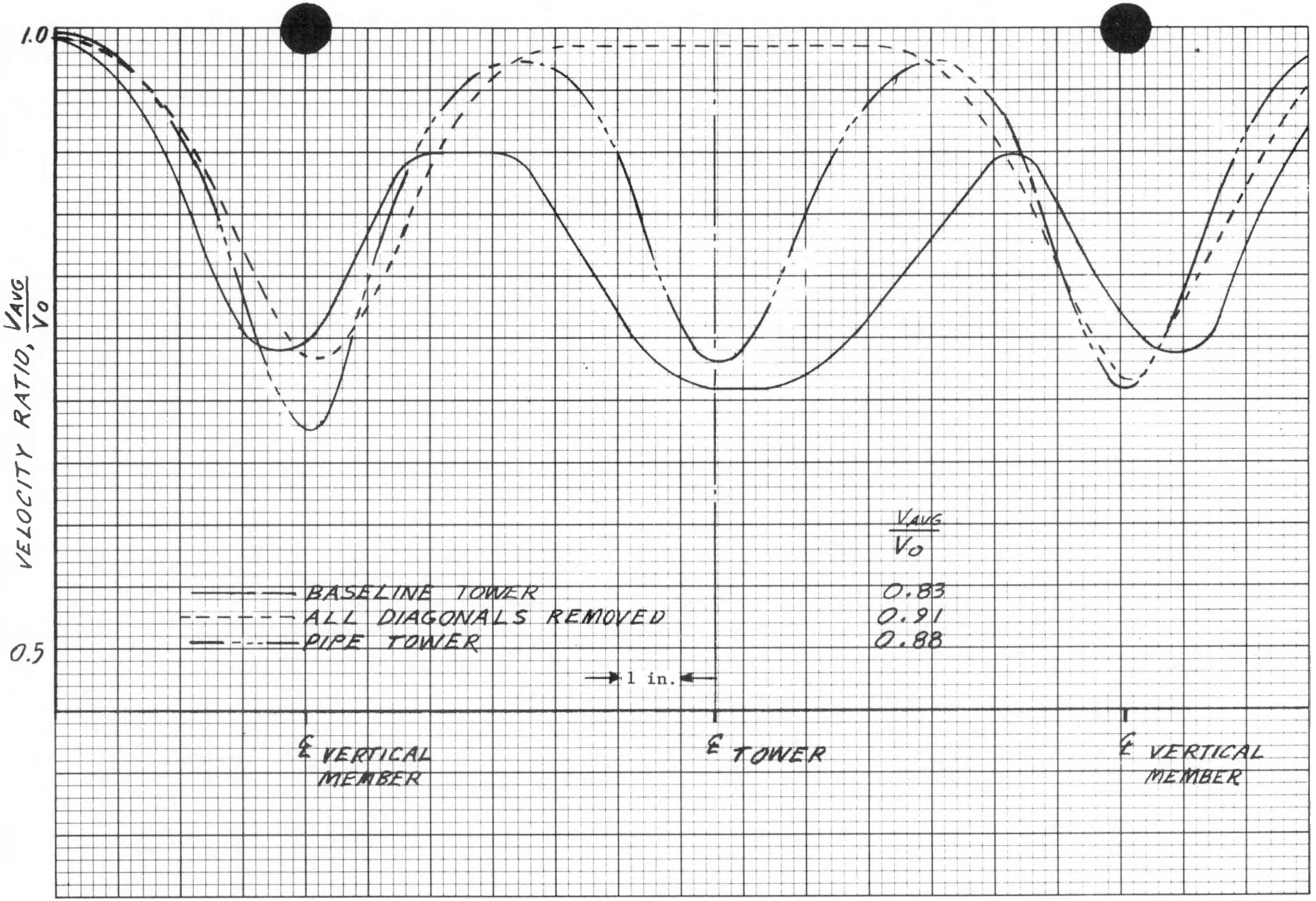

FIGURE 22a
Comparison of Velocity Ratio Profiles Behind Intersection of Diagonals for Baseline Tower, Tower with All Diagonals Removed, and All-Pipe Tower (Wind Direction 0^{o})

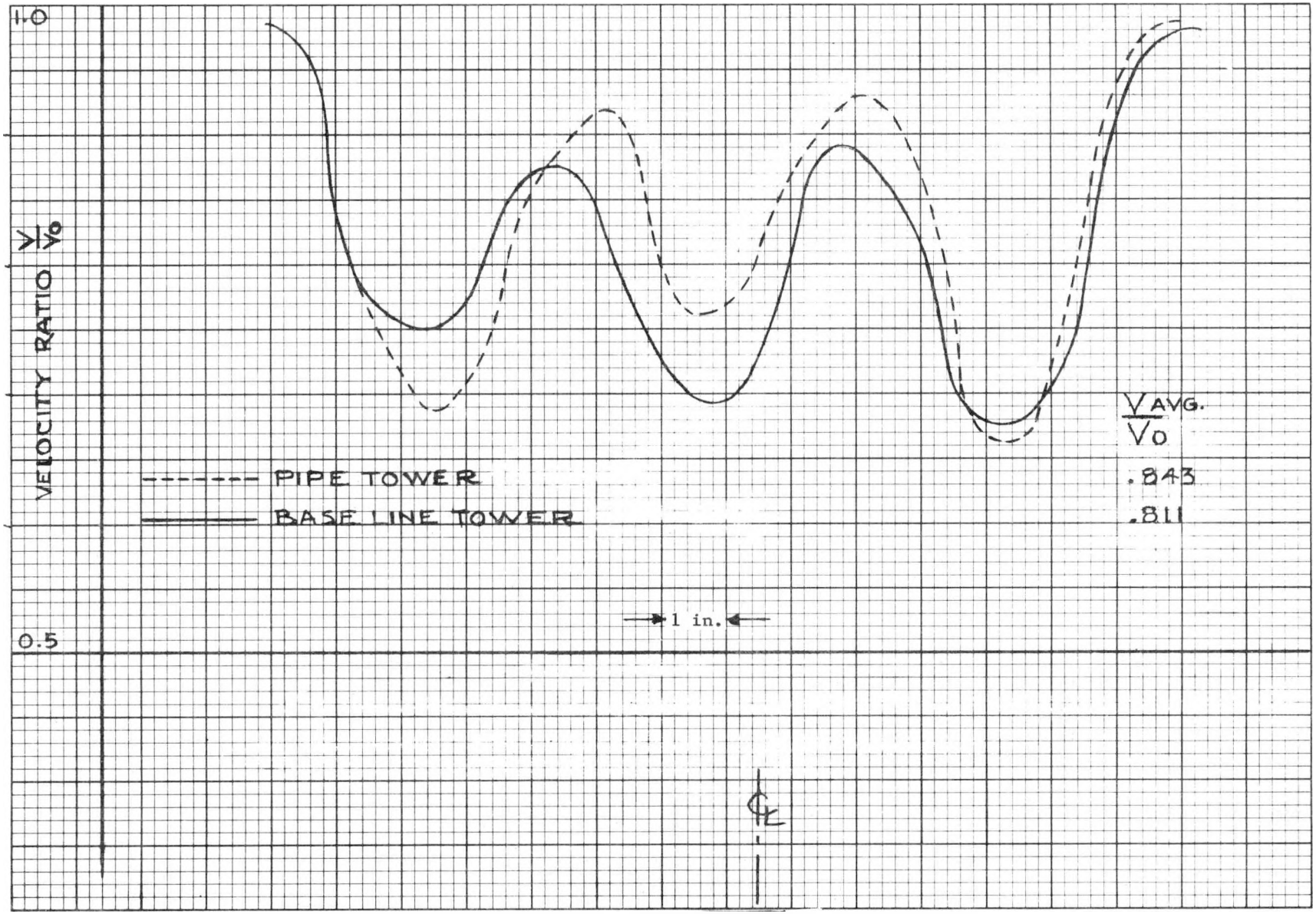

FIGURE 22b
Comparison of Velocity Ratio Profiles for Baseline Tower and All Pipe Tower Behind Intersection of Diagonals (Wind Direction of 10^{o})

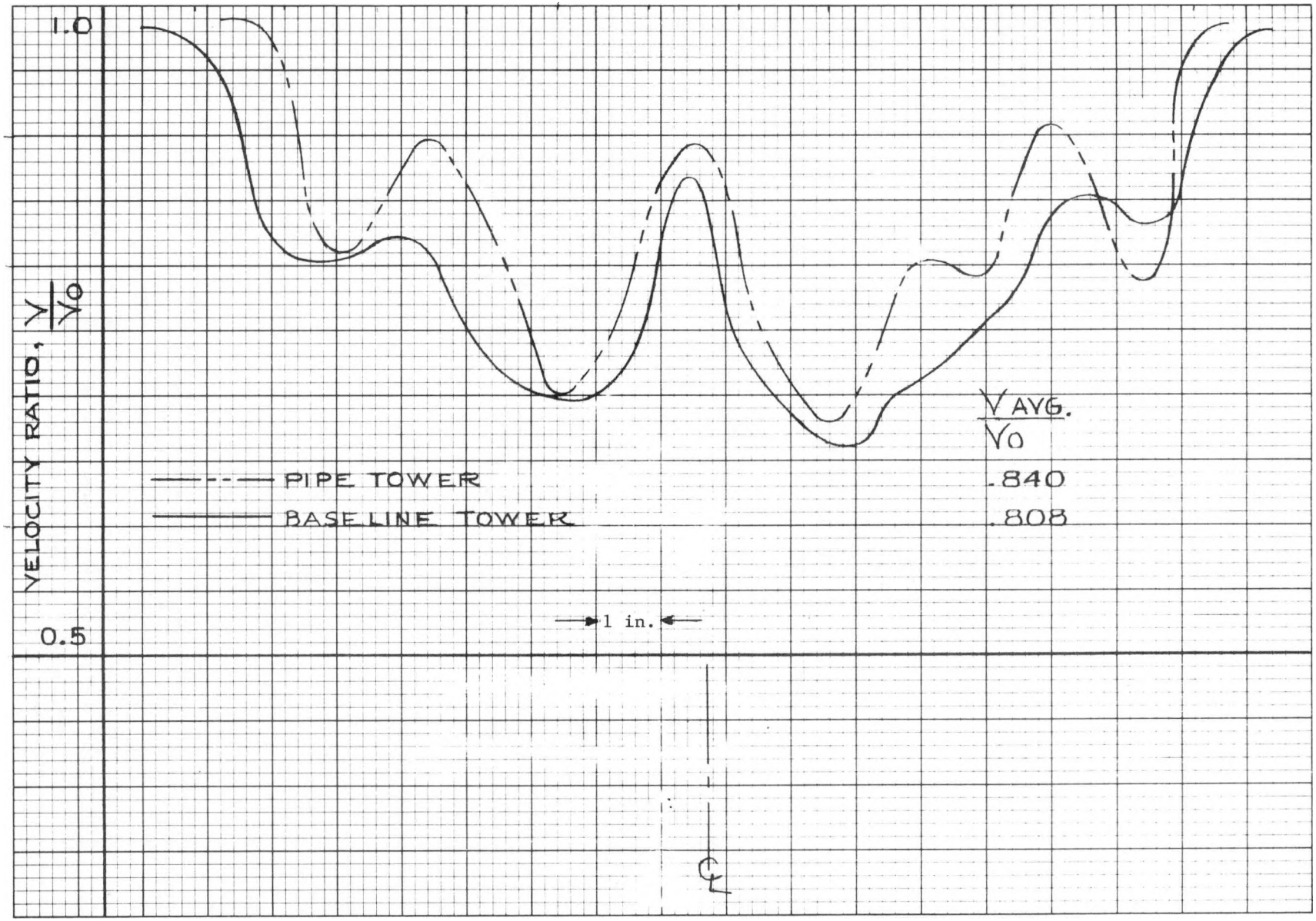

FIGURE 22c
Comparison of Velocity Ratio Profiles for Baseline Tower and All Pipe Tower Behind Intersection of Diagonals (Wind Direction of 35°)

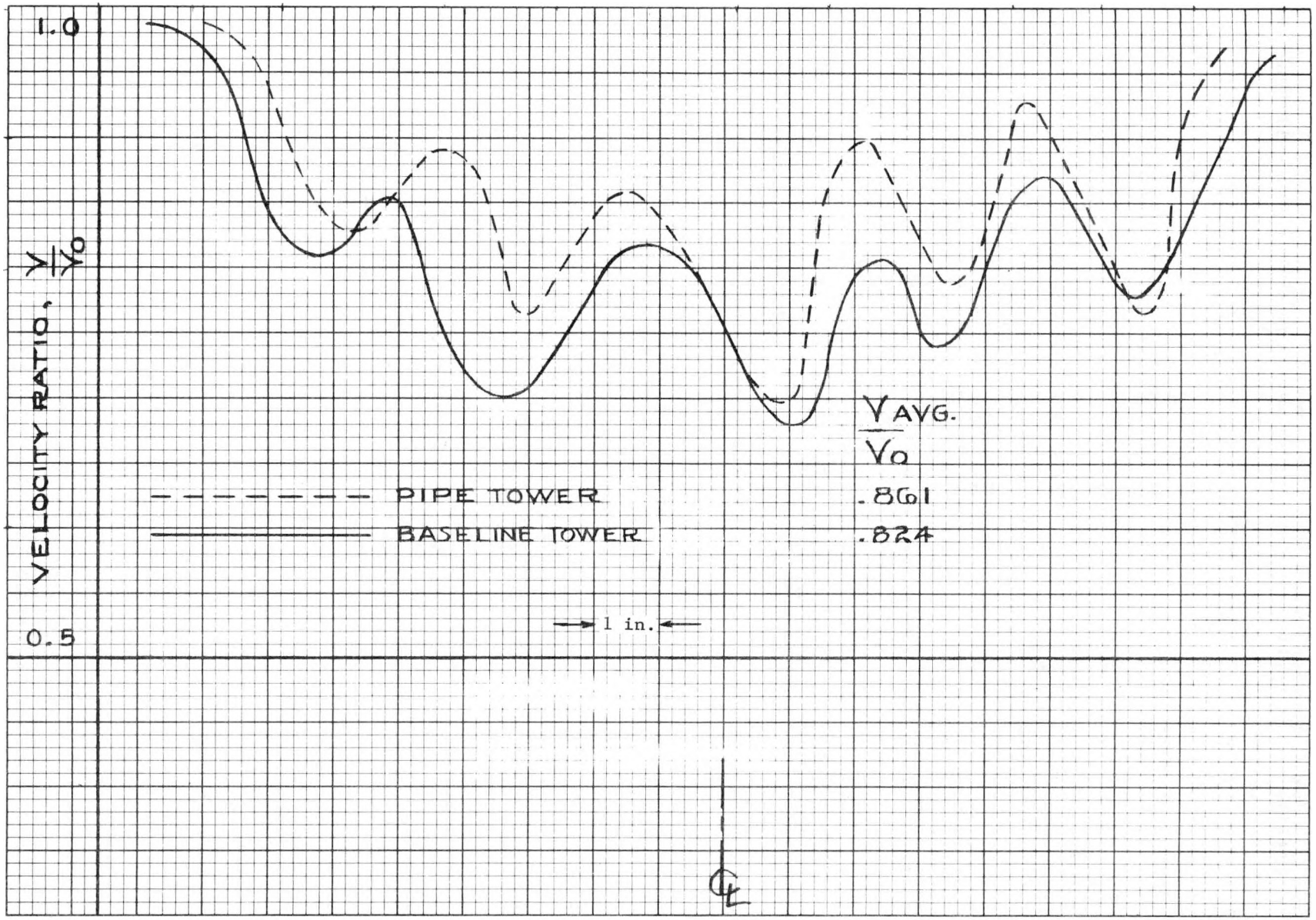

FIGURE 22d
Comparison of Velocity Ratio Profiles for Baseline Tower and All Pipe Tower Behind Intersection of Diagonals (Wind Direction of 40°)

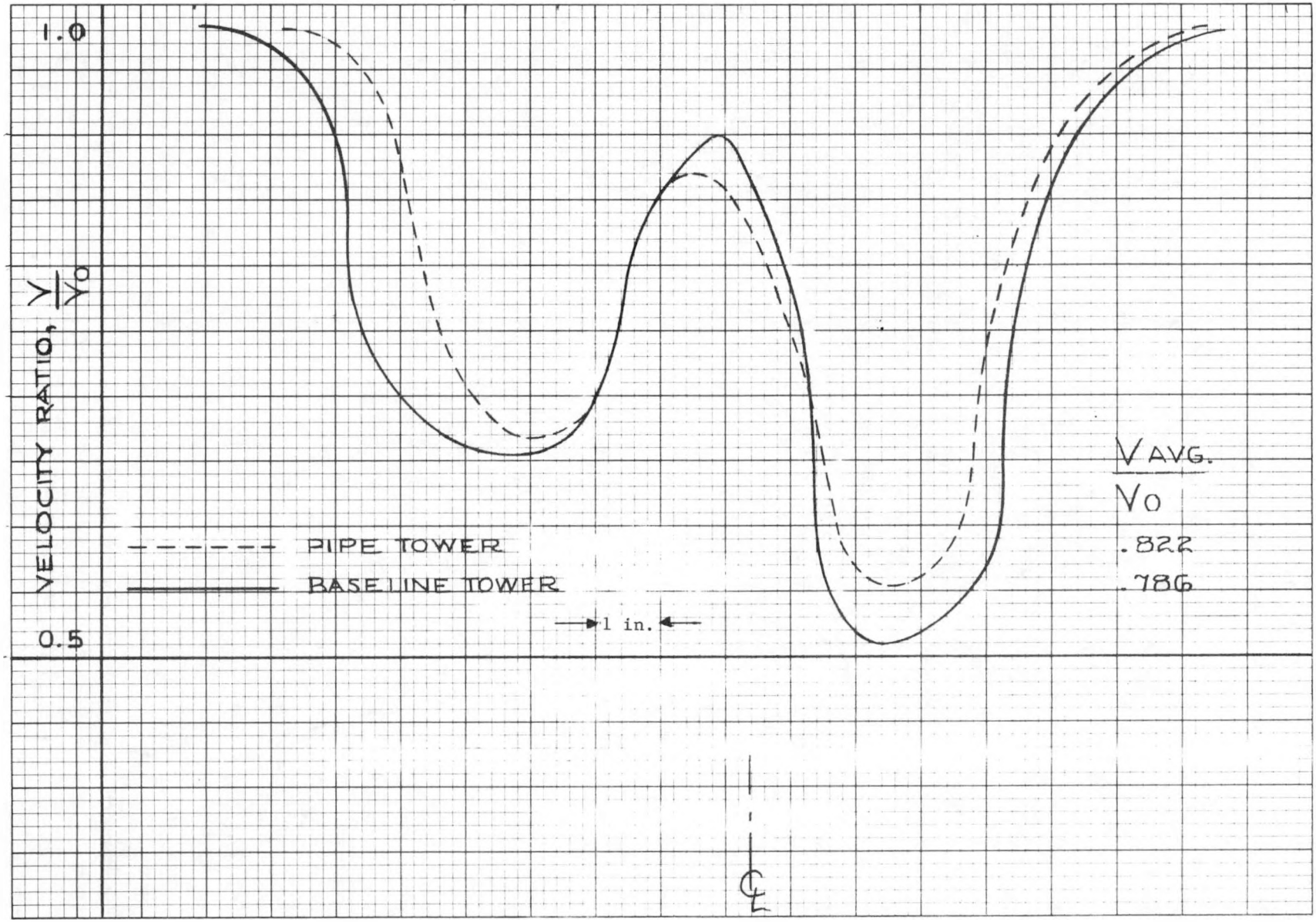

FIGURE 23a
Comparison of Velocity Ratio Profiles for Baseline Tower and All Pipe Tower Behind Horizontal Member (Wind Direction of 10°)

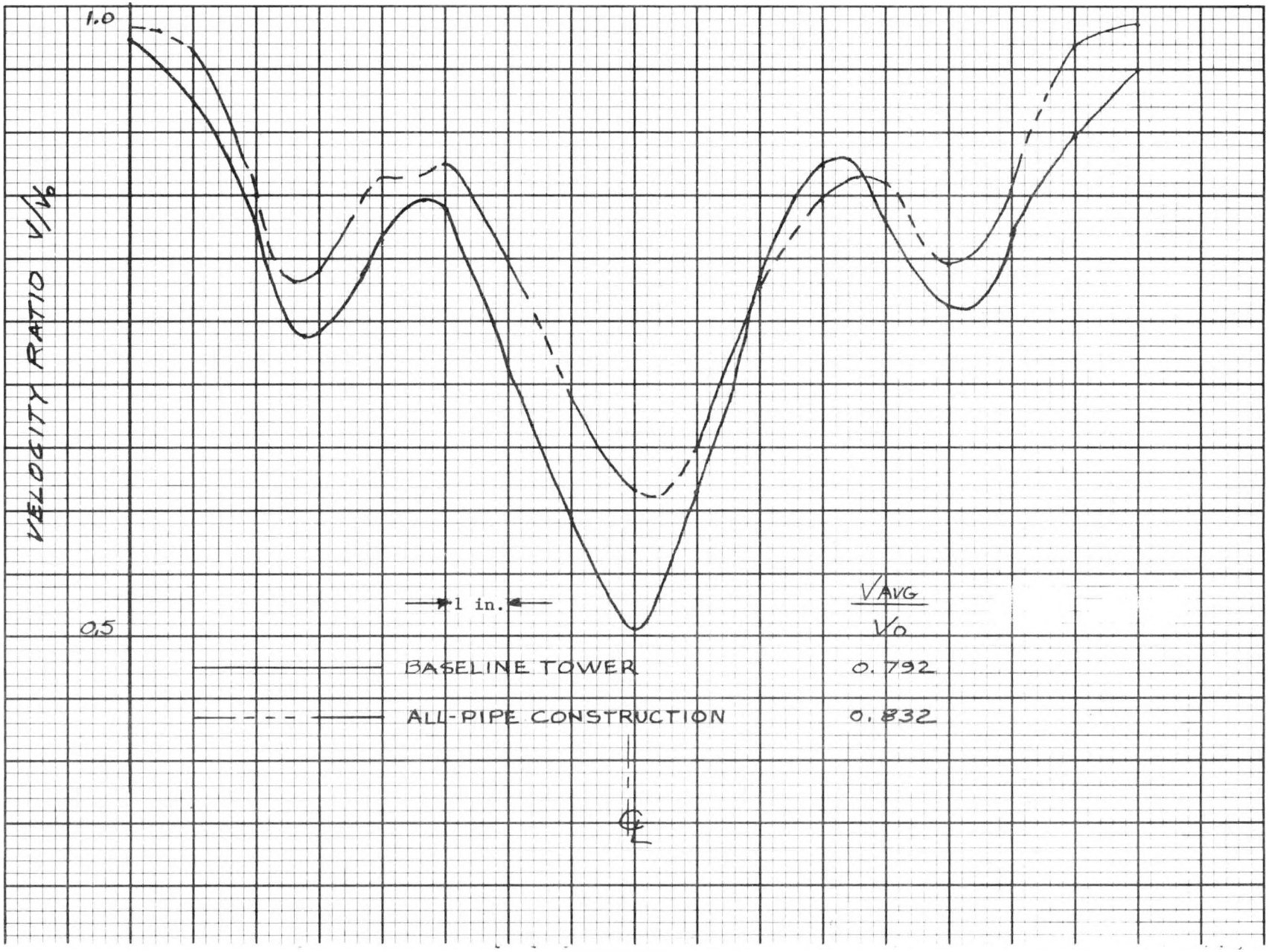

FIGURE 23b
Comparison of Velocity Ratio Profiles for Baseline Tower and All Pipe Tower Behind Horizontal Member (Wind Direction of 35°)

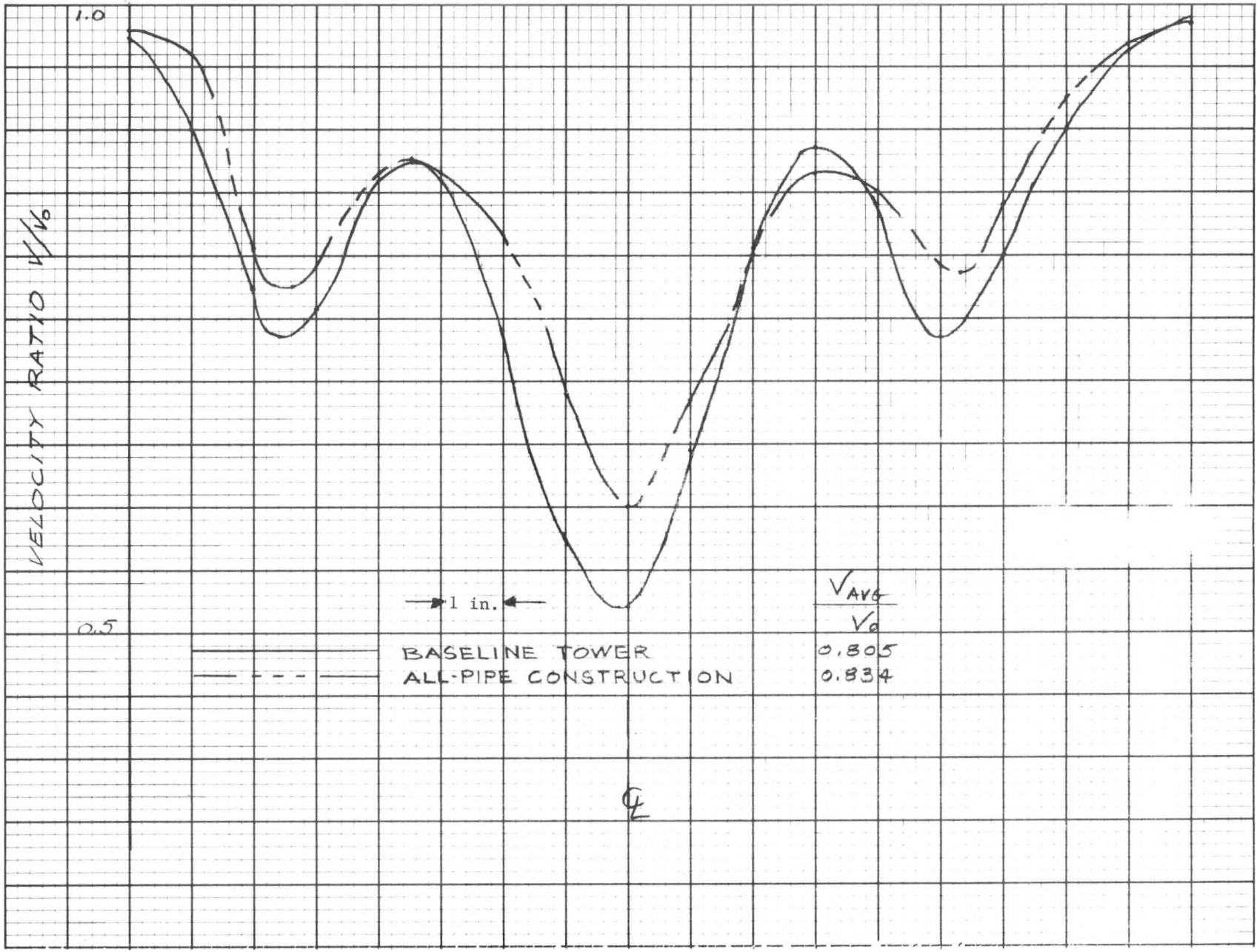

FIGURE 23c
Comparison of Velocity Ratio Profiles for Baseline Tower and All Pipe Tower Behind Horizontal Member (Wind Direction of 40°)

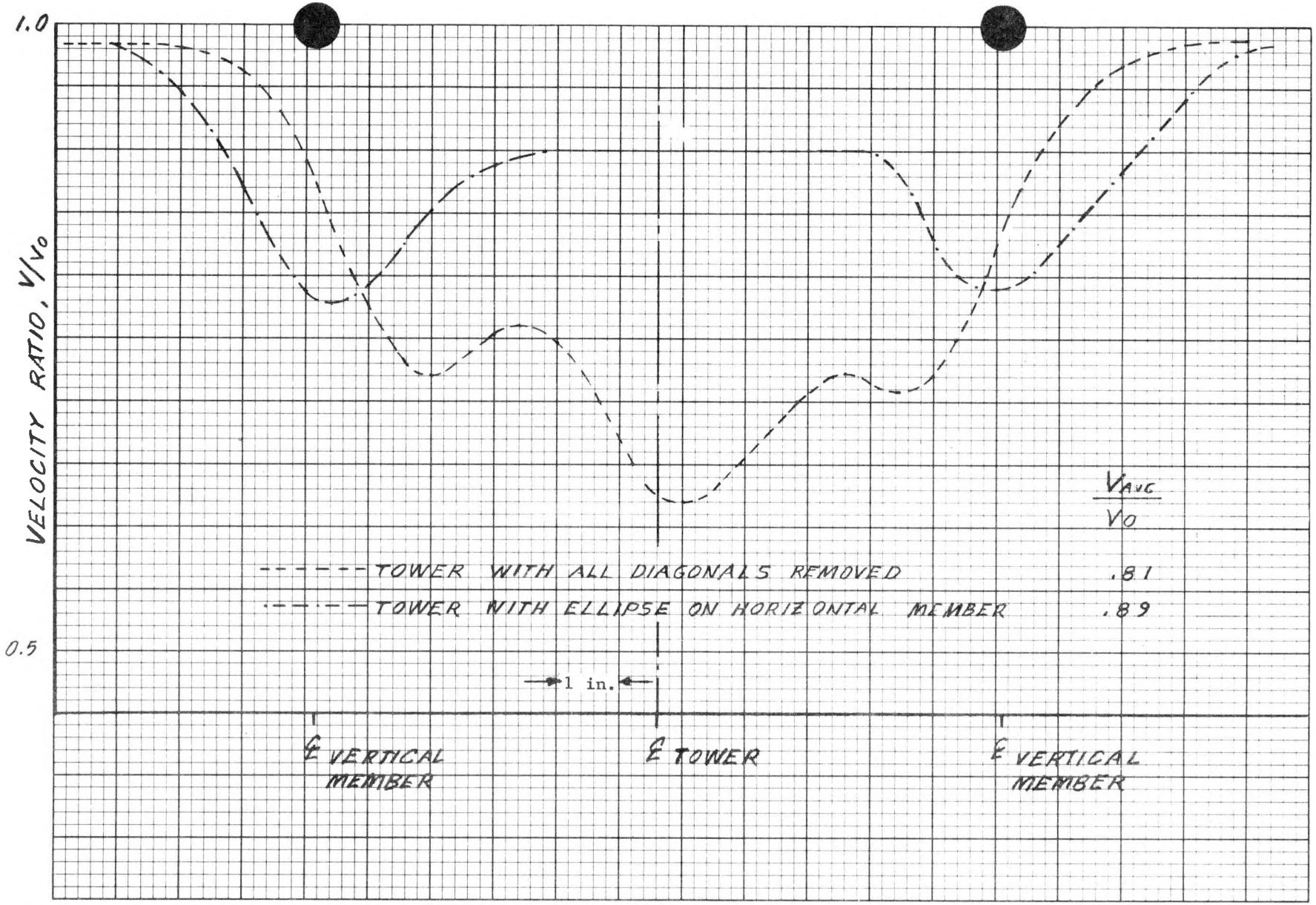

FIGURE 24a
Comparison of Velocity Ratio Profiles at Elevation of 26.5 Inches for Tower With and Without Ellipses Installed on Horizontal Member with All Diagonals Removed (Wind Direction 0°)

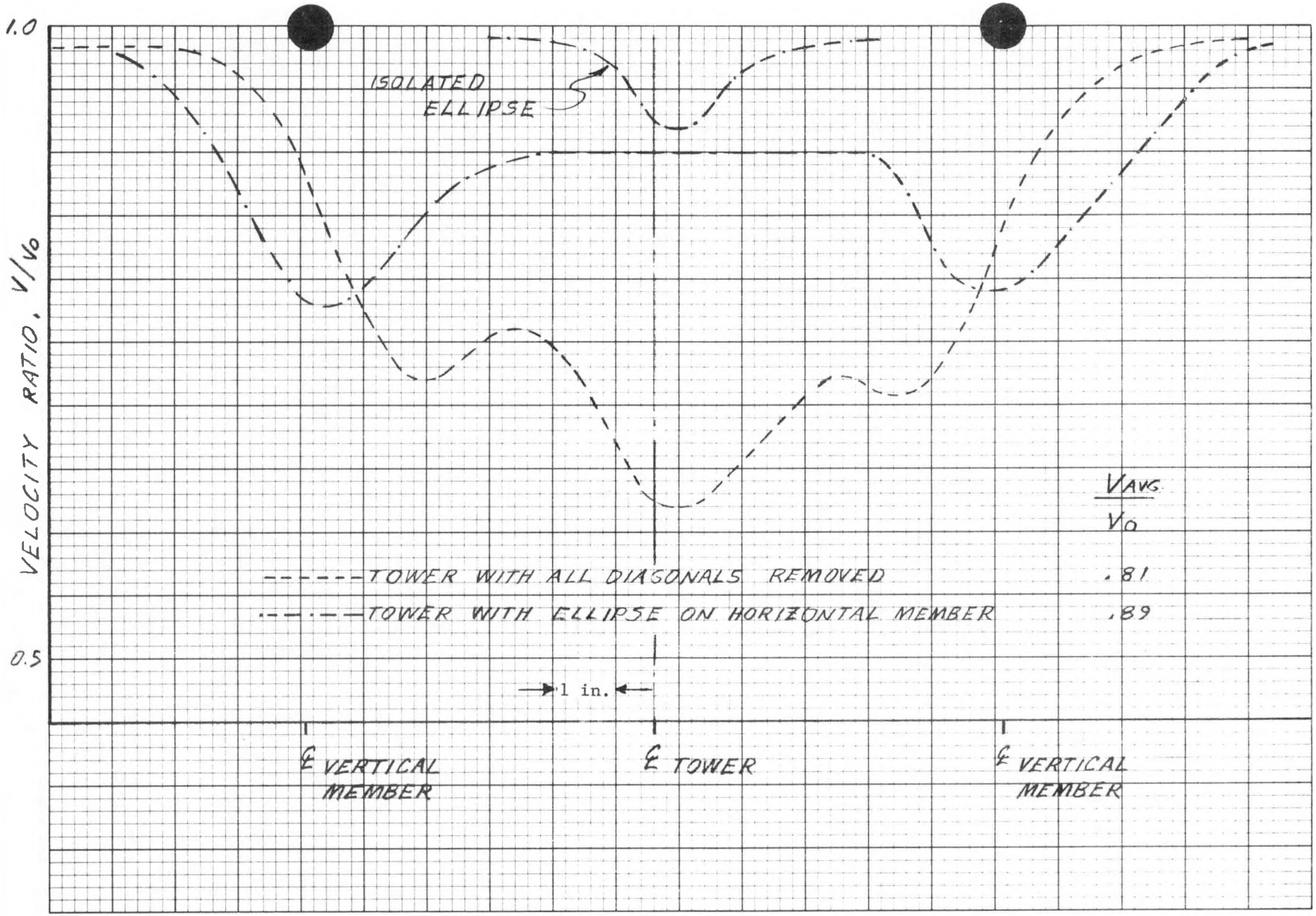

FIGURE 24b
Comparison of Velocity Ratio Profiles at Elevation of 26.5 Inches for Tower With and Without Ellipses Installed on Horizontal Member with All Diagonals Removed and for Isolated Ellipse (Wind Direction 0°)

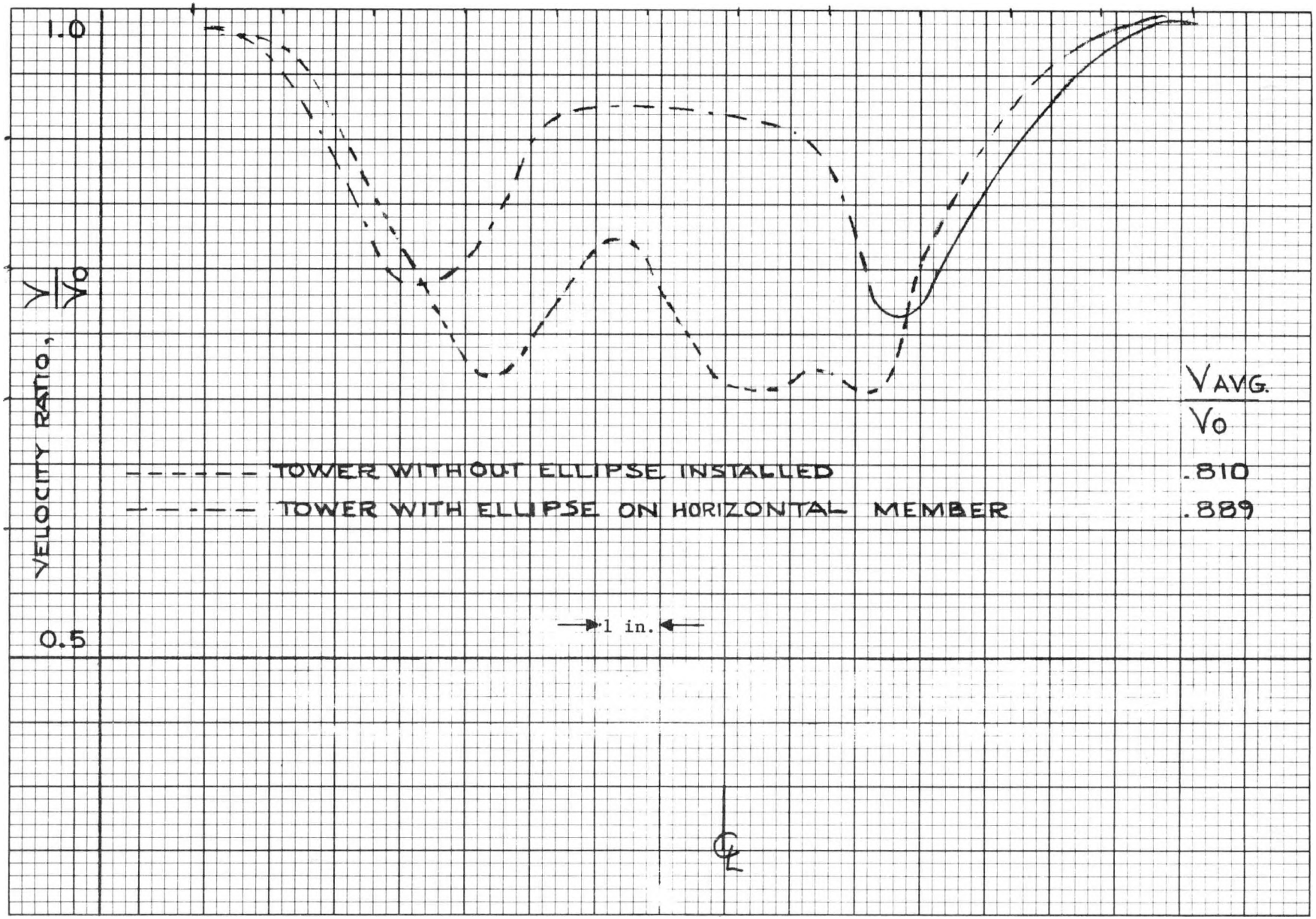

FIGURE 24c
Comparison of Velocity Ratio Profiles With and Without Ellipses Installed on Horizontal Member with All Diagonals Removed (Elevation of 26.5 inches)
Wind Direction of 10^{o}

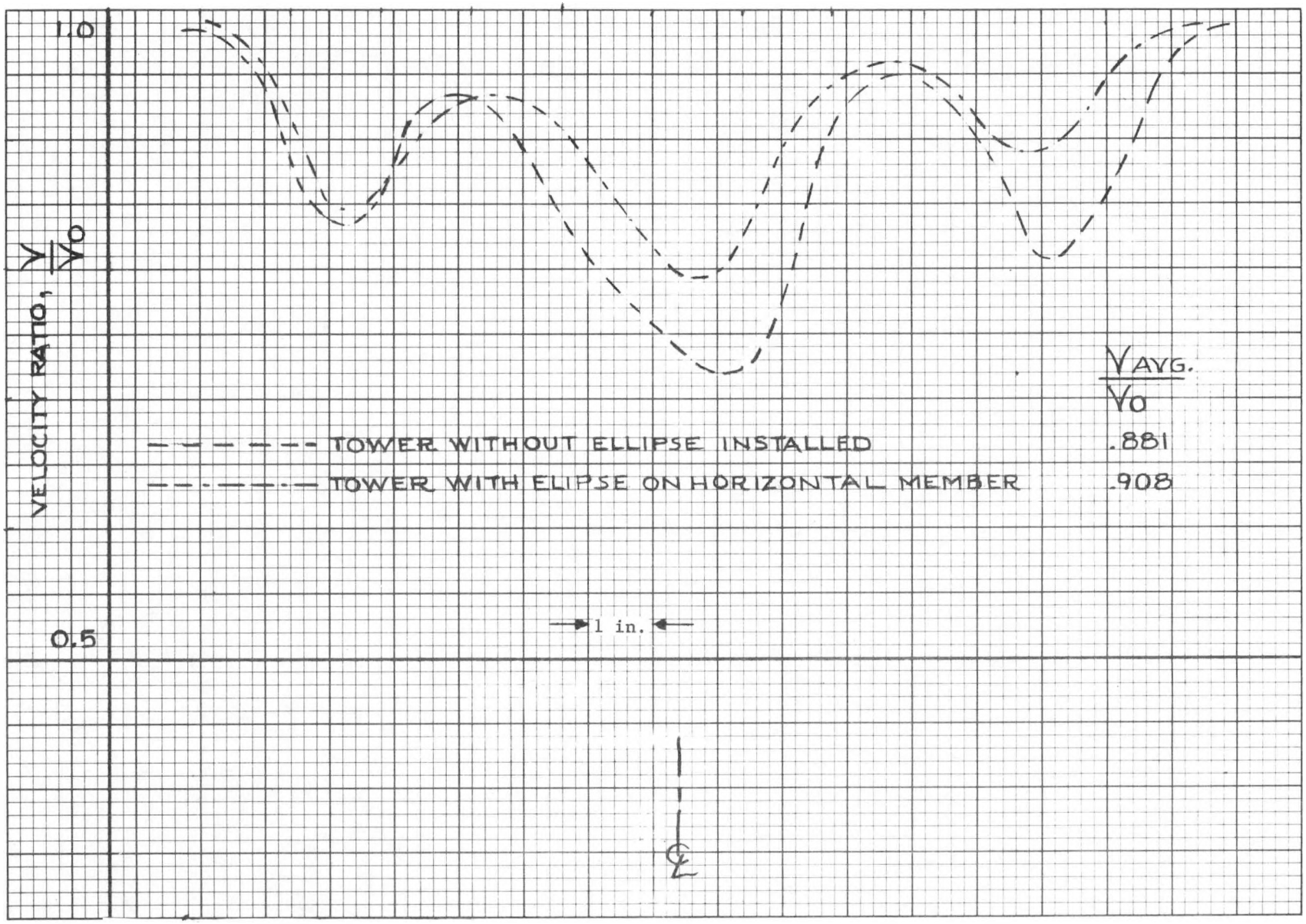

FIGURE 24d
Comparison of Velocity Ratio Profiles With and Without Ellipses Installed on Horizontal Member with All Diagonals Removed (Elevation of 26.5 inches) Wind Direction of 35°

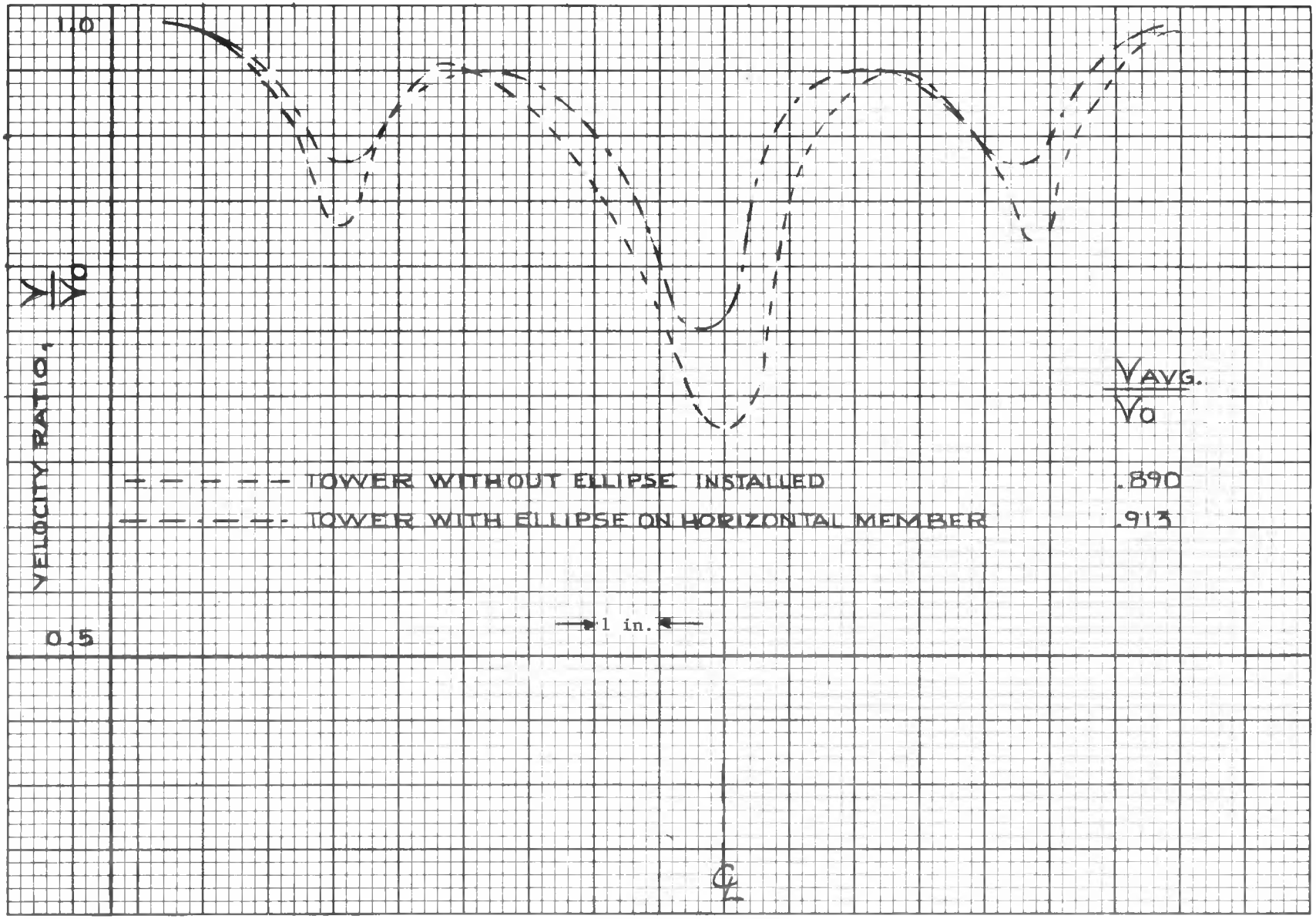

FIGURE 24e
Comparison of Velocity Ratio Profiles With and Without Ellipses Installed on Horizontal Member with All Diagonals Removed (Elevation of 26.5 inches)
Wind Direction of 40°

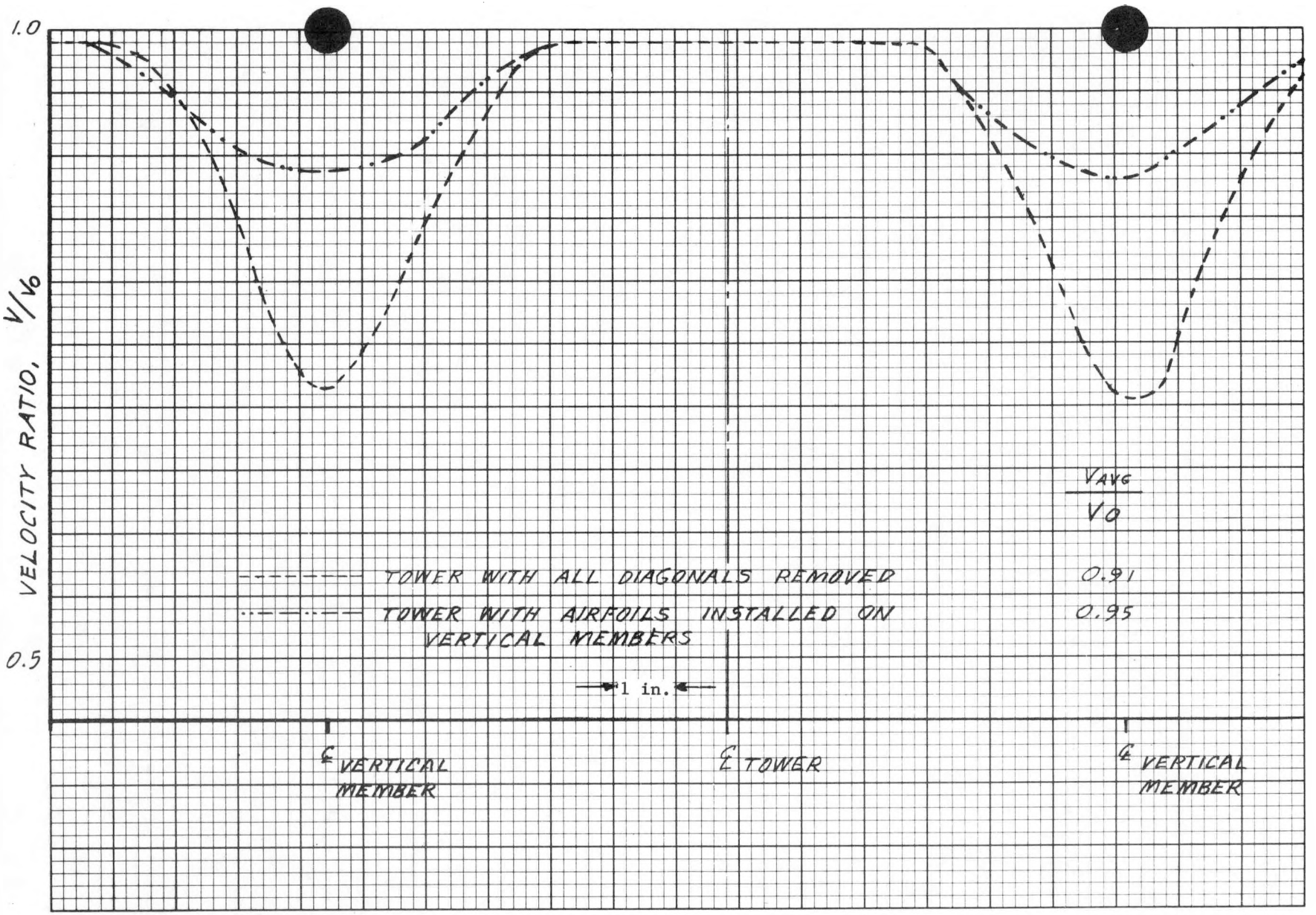

FIGURE 25a
Comparison of Velocity Ratio Profile at Elevation of 24.2 Inches for Tower With and Without Airfoils Installed on Vertical Member (Wind Direction 0°)

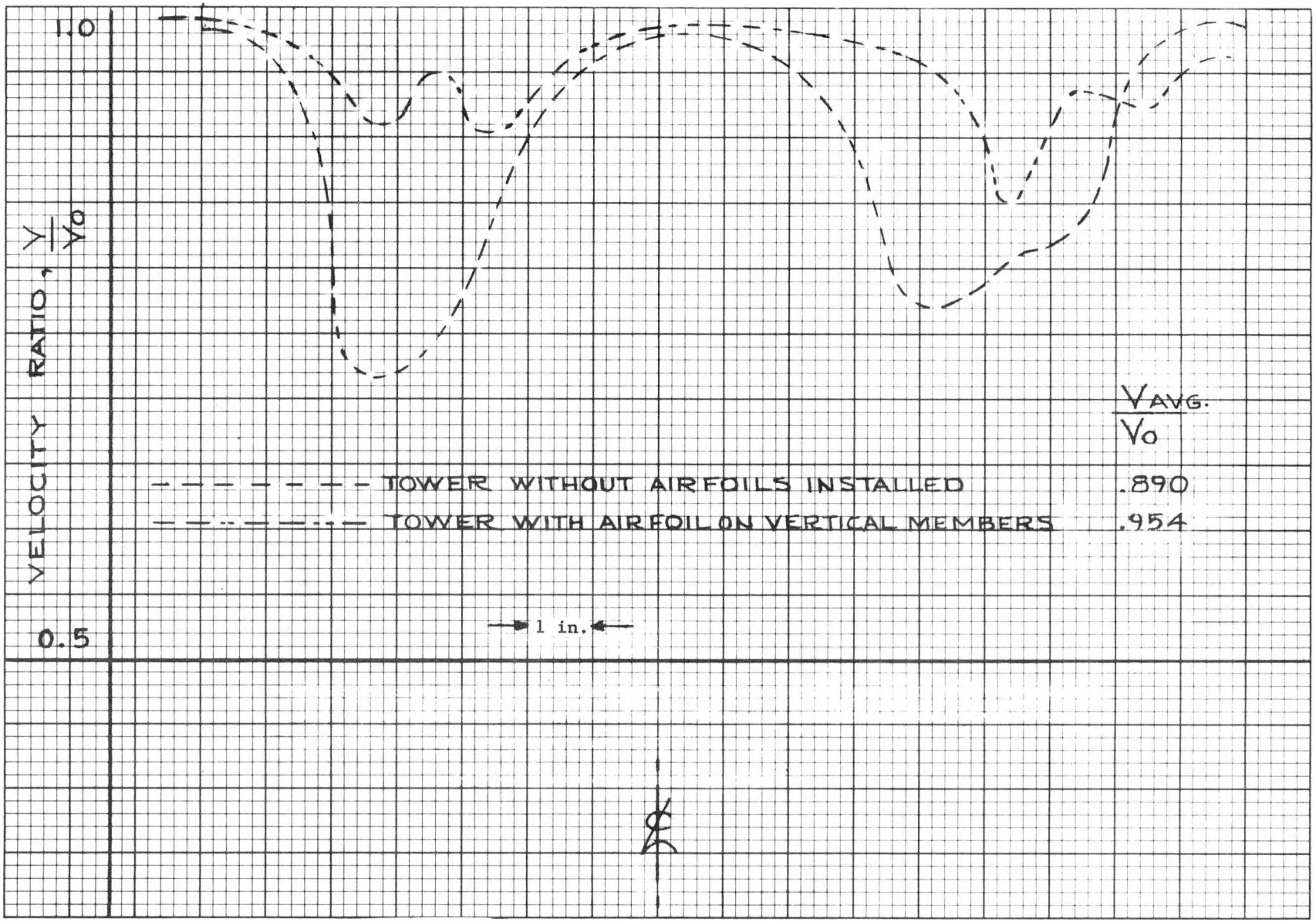

FIGURE 25b
Comparison of Velocity Ratio Profile With and Without Airfoils Installed on Vertical Members with All Diagonals Removed (Elevation of 24.2 inches)
Wind Direction of 10°

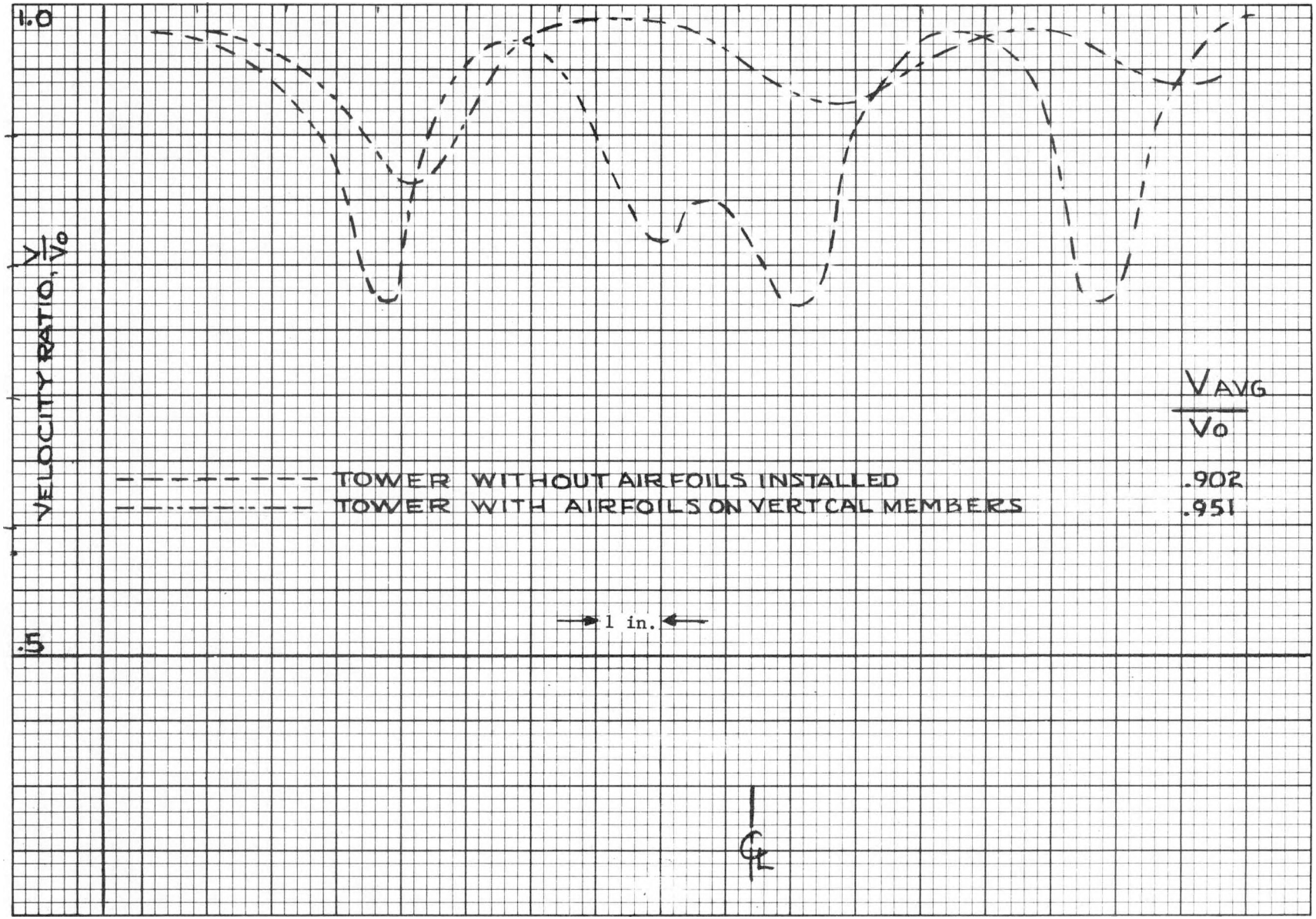

FIGURE 25c
Comparison of Velocity Ratio Profile With and Without Airfoils Installed on Vertical Members with All Diagonals Removed (Elevation of 24.2 inches) Wind Direction of 35°

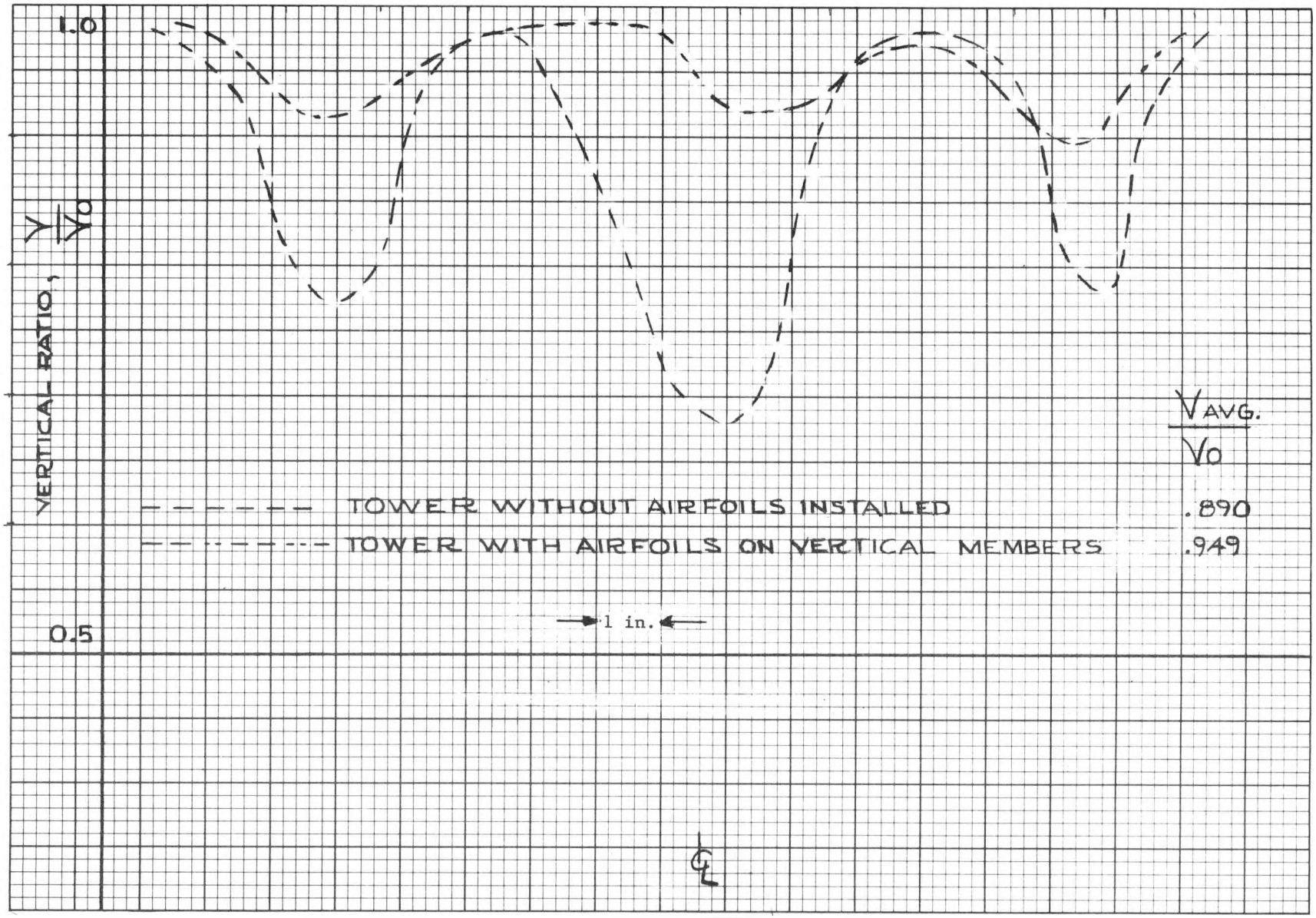

FIGURE 25d
Comparison of Velocity Ratio Profile With and Without Airfoils Installed on Vertical Members with All Diagonals Removed (Elevation of 24.2 inches)
Wind Direction of 40°

APPENDIX B

Variation of V_{min}/V_o, V_{ℓ}/V_o, and Average Velocity, Ratio with Elevation at Wind Directions of 0^o, 10^o, 35^o, 40^o; All Tower Configurations.

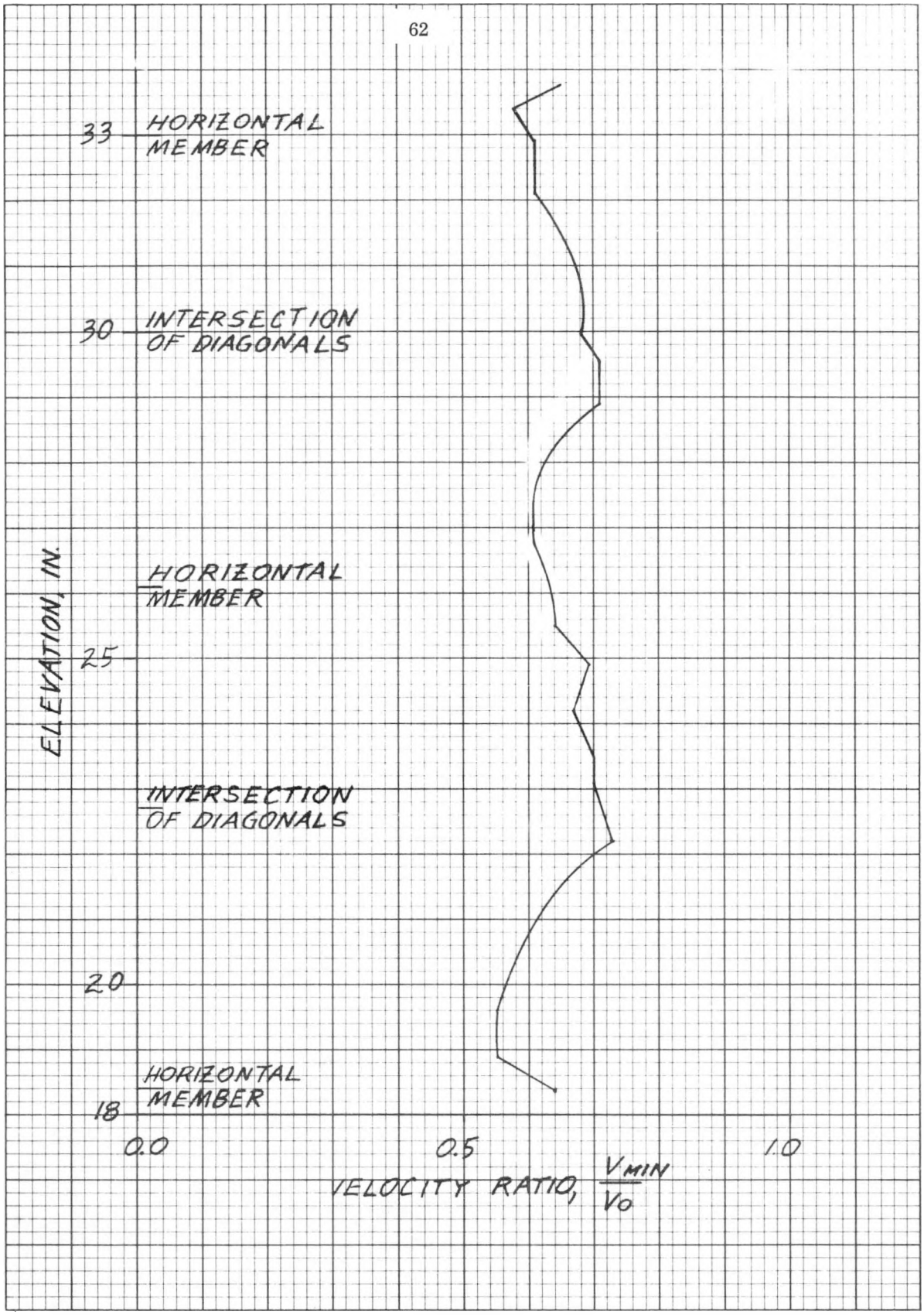

FIGURE 26
Variation of Minimum Velocity Ratio with Elevation for Baseline Tower (Wind Direction 0^{o})

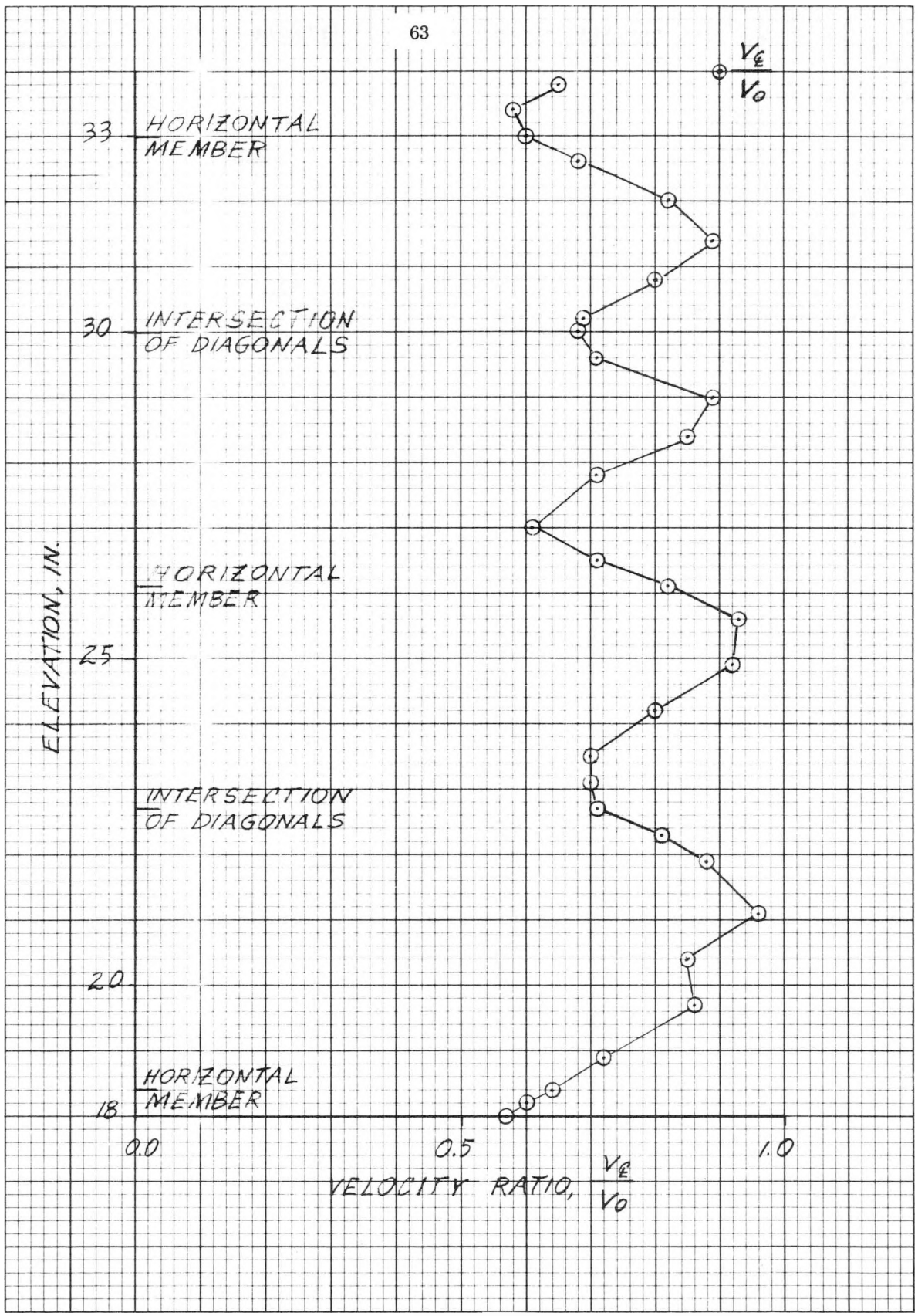

FIGURE 27a
Variation of Velocity Ratio with Elevation Downstream of the Baselinc Tower Centerline (Wind Direction 0^{o})

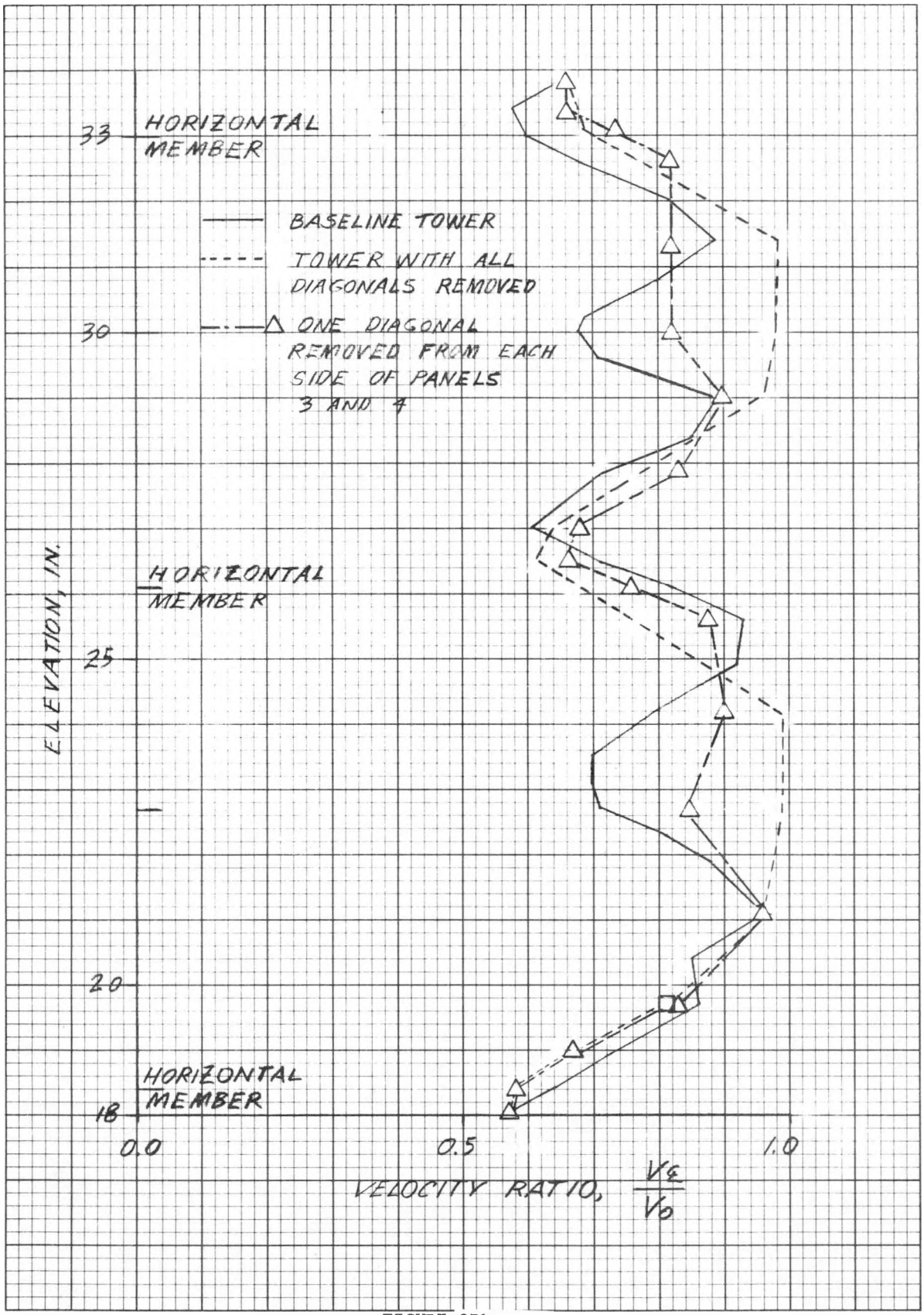

FIGURE 27b

Comparison of Variation of Centerline Velocity Ratio with Elevation for Baseline Tower and Tower with Diagonals Removed (Wind Direction 0^{o})

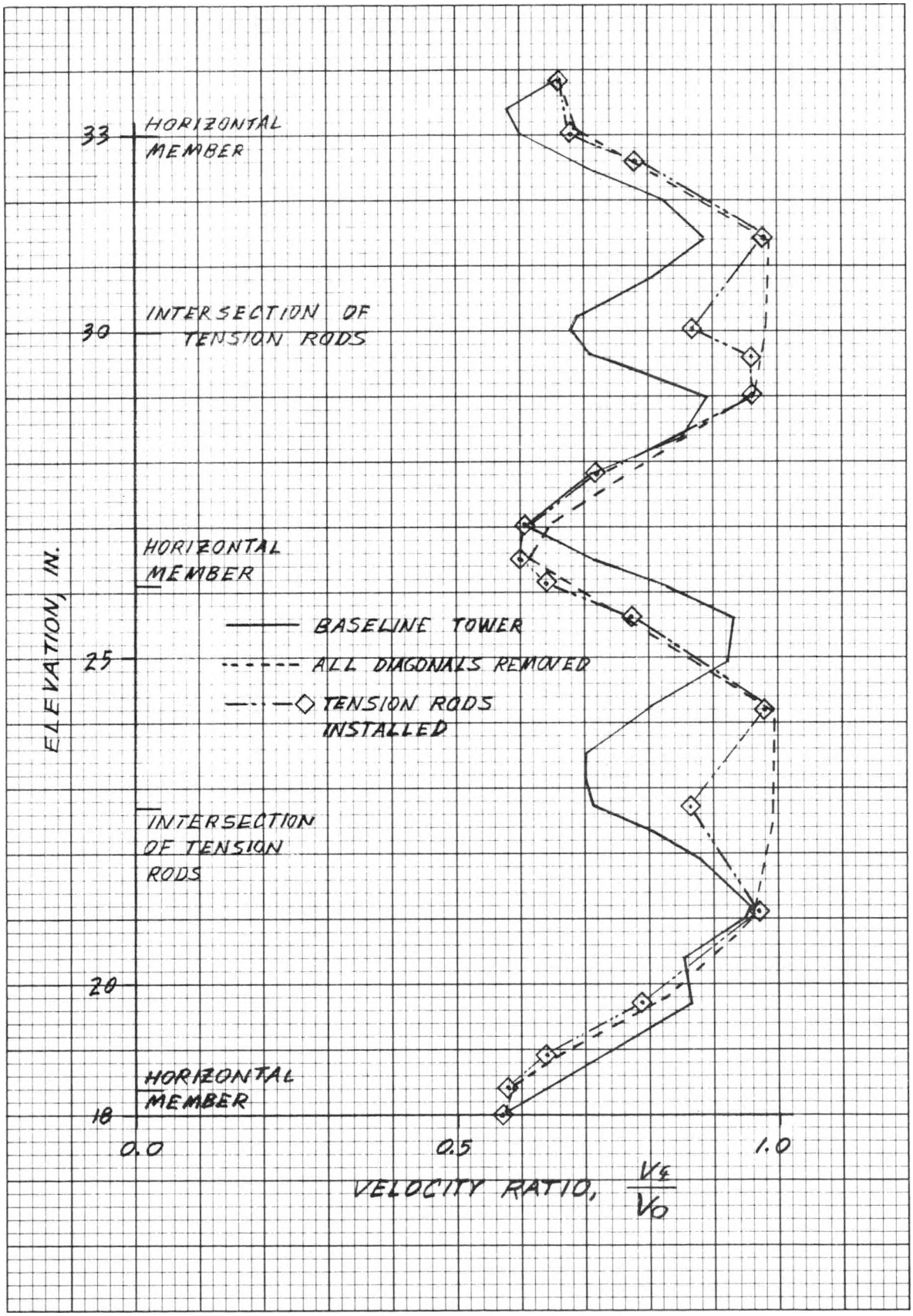

FIGURE 27c

Comparison of Variation of Centerline Velocity Ratio with Elevation for Baseline Tower, Tower with All Diagonals Removed, and Tower with Tension Rods (Wind Direction 0°)

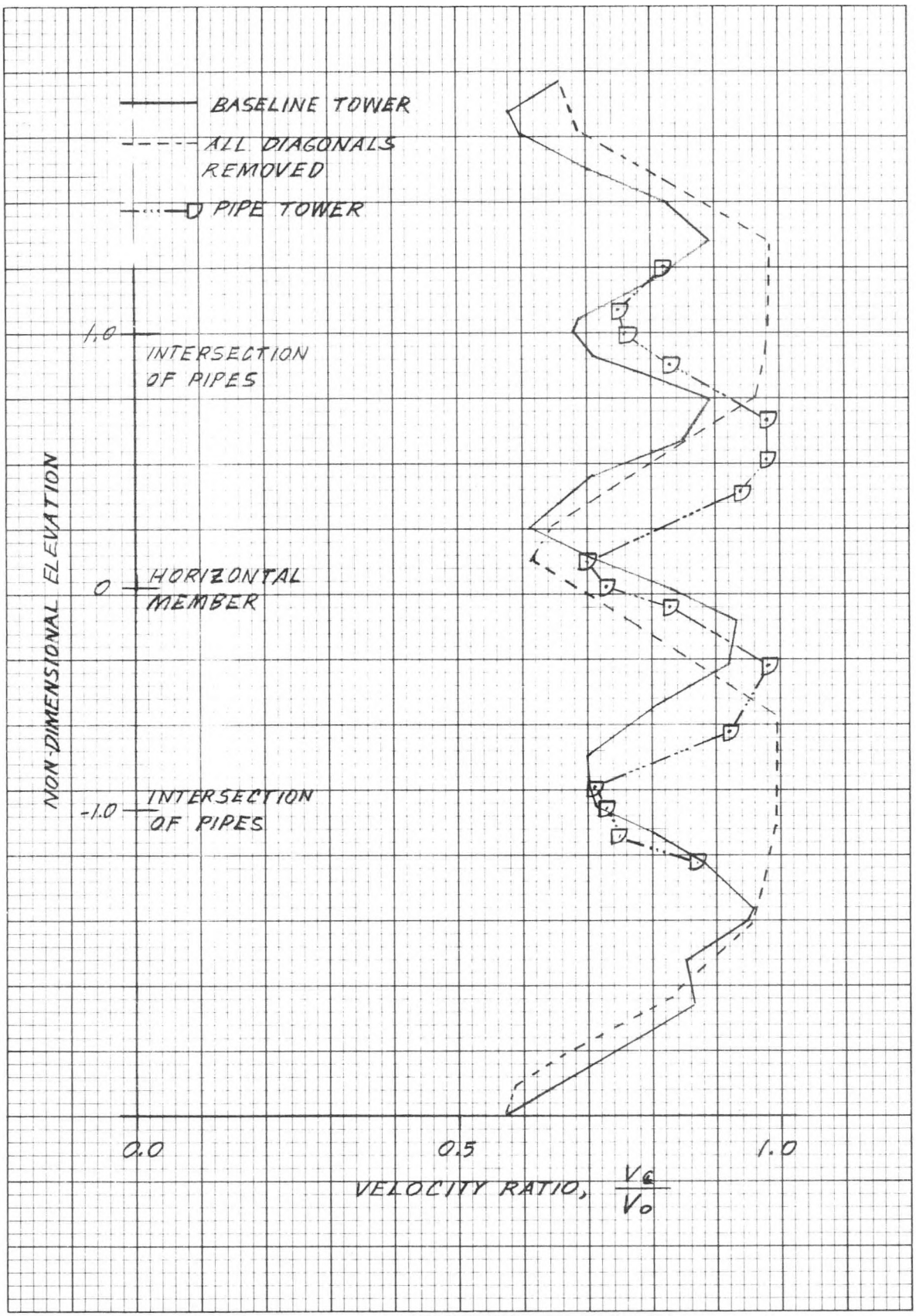

FIGURE 27d

Comparison of Variation of Centerline Velocity Ratio with Elevation for Baseline Tower, Tower with All Diagonals Removed, and All-Pipe Tower (Wind Direction 0°)

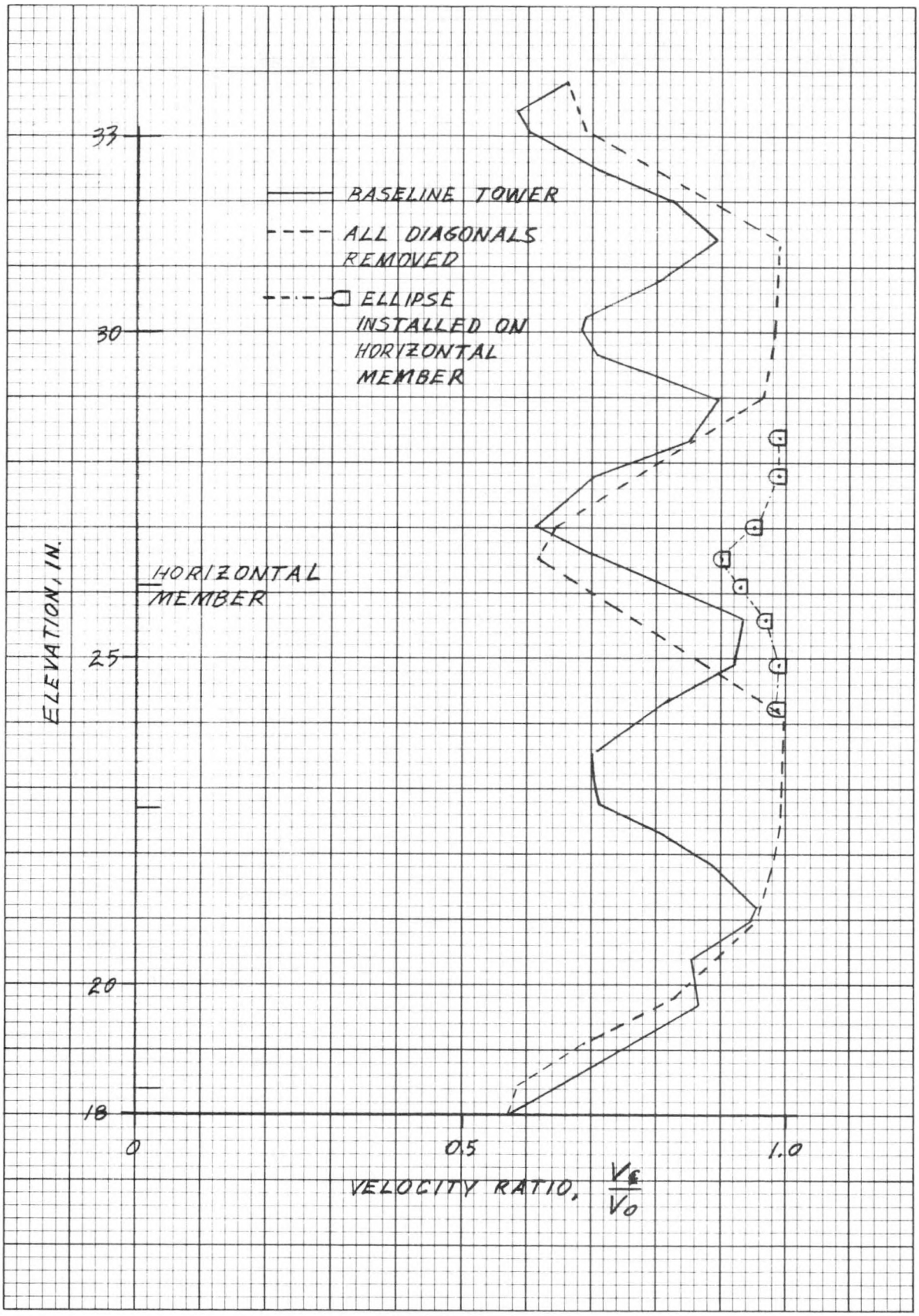

FIGURE 27e
Comparison of Variation of Centerline Velocity Ratio with Elevation for Baseline Tower and and for Tower with and without Ellipses Installed on Horizontal Member with All Diagonals Removed (Wind Direction 0°)

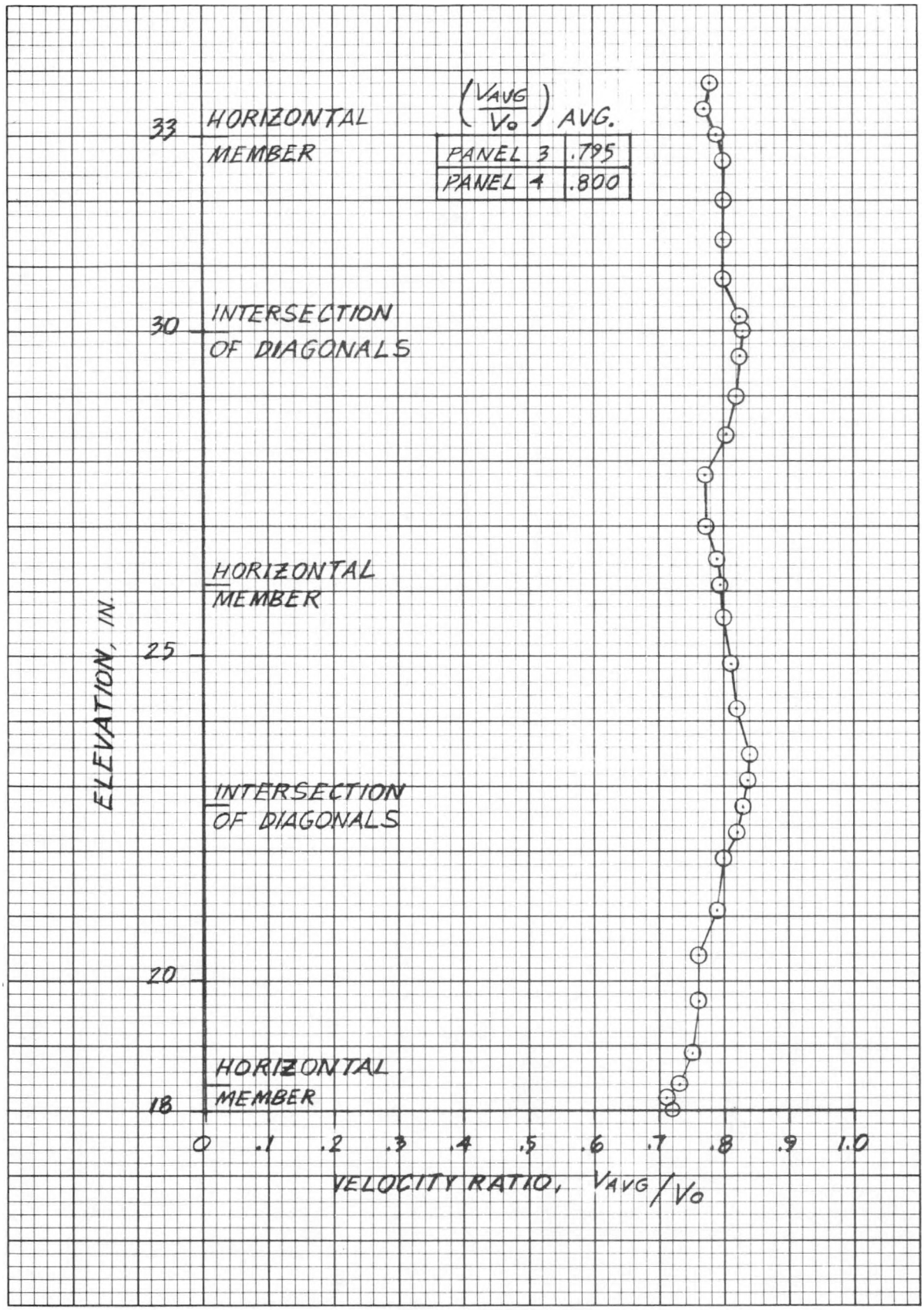

FIGURE 28a
Variation of Average Velocity Ratio with Elevation for Baseline Tower
(Wind Direction 0^{o})

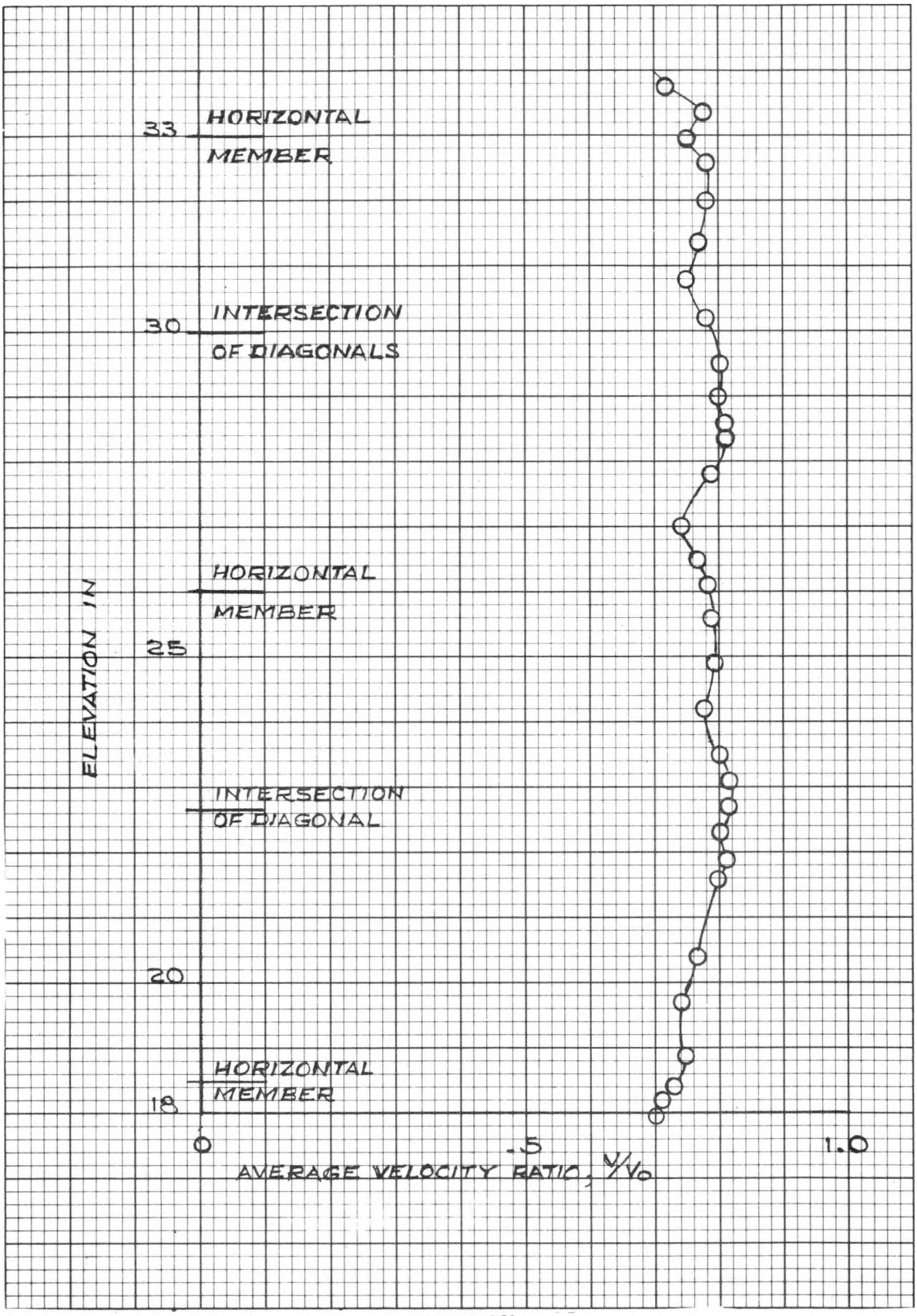

FIGURE 28b
Variation of Average Velocity Ratio with Elevation for Baseline Tower
Wind Direction 10^{o}

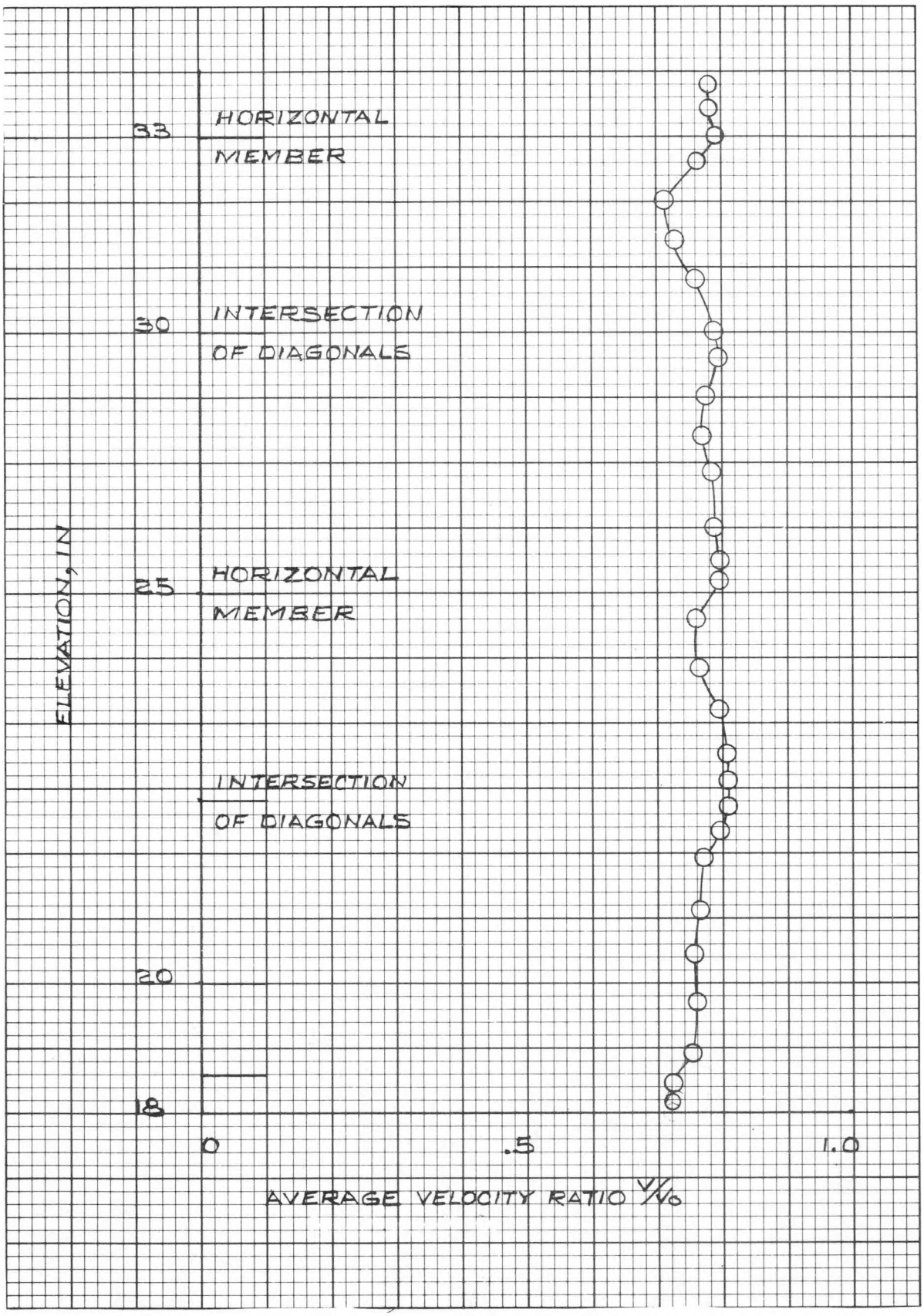

FIGURE 28c
Variation of Average Velocity Ratio with Elevation for Baseline Tower
Wind Direction of 35°

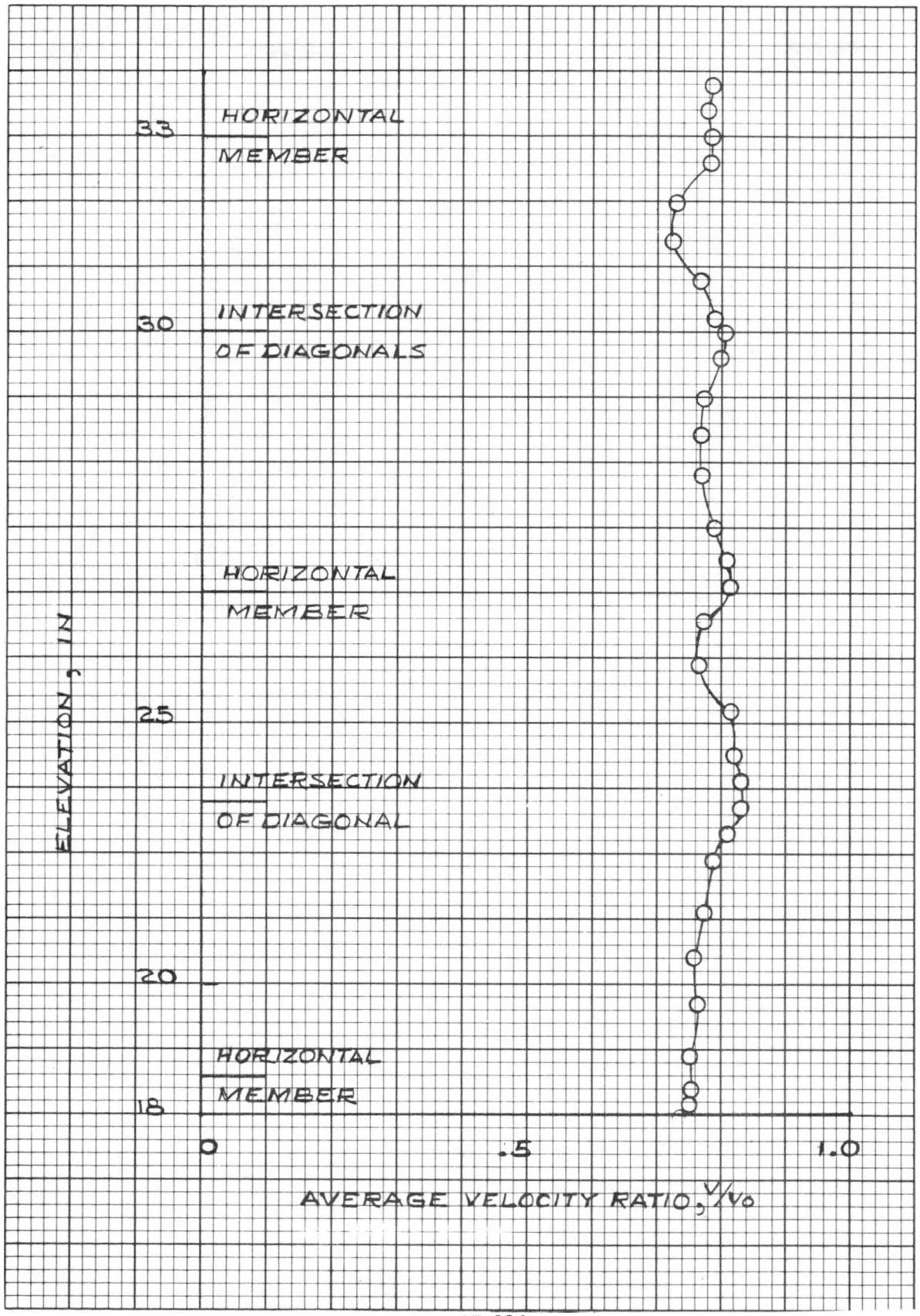

FIGURE 28d
Variation of Average Velocity Ratio with Elevation for Baseline Tower
Wind Direction of 40°

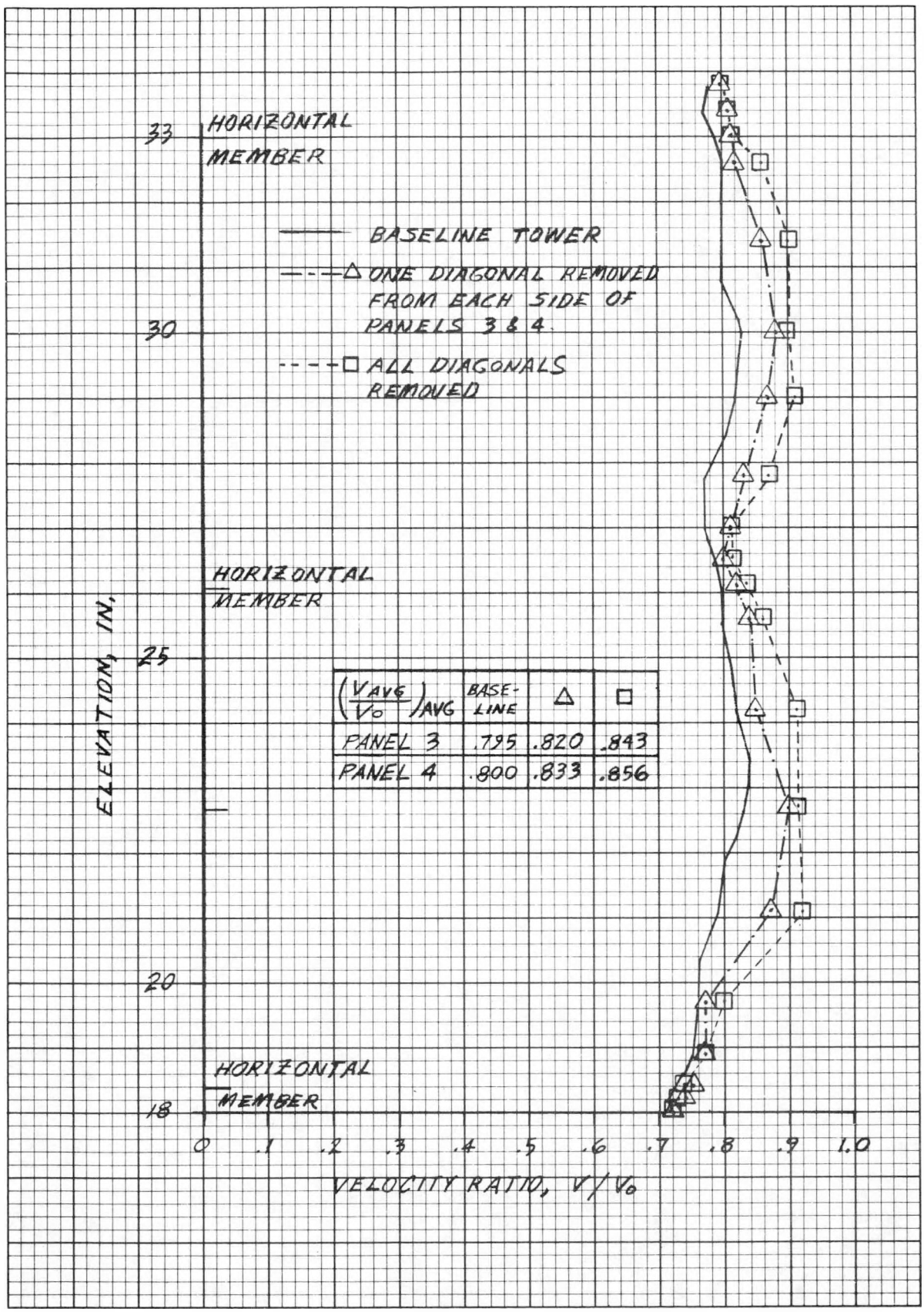

$(V_{AVG}/V_0)_{AVG}$	BASE-LINE	△	□
PANEL 3	.795	.820	.843
PANEL 4	.800	.833	.856

FIGURE 29a
Comparison of Variation of Average Velocity Ratio with Elevation for Baseline Tower and Tower with Diagonals Removed (Wind Direction 0^o)

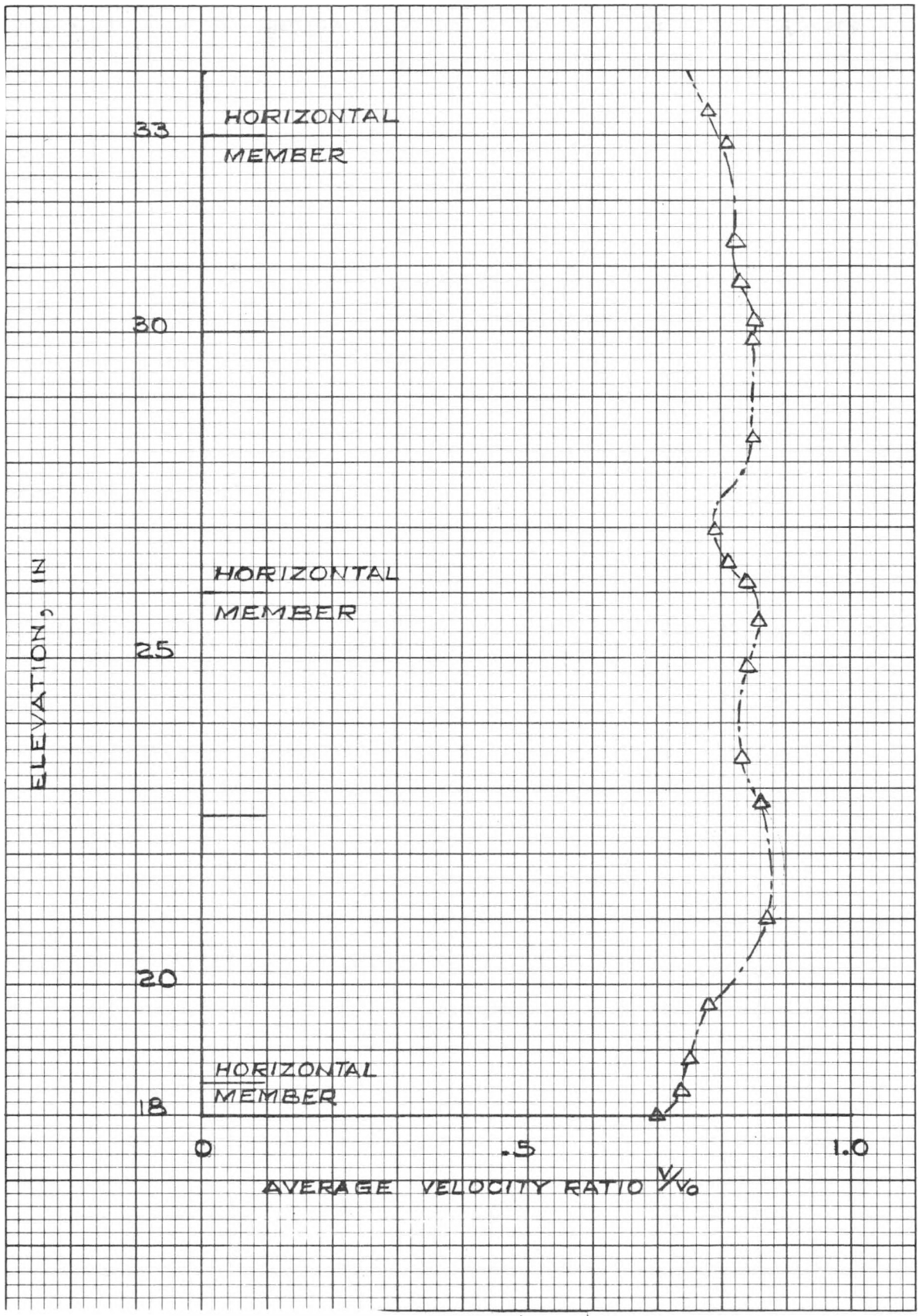

FIGURE 29b

Variation of Average Velocity Ratio with Elevation for Tower with One Diagonal Removed from Each Side of Panels 3 and 4 (Wind Direction of 10^{o})

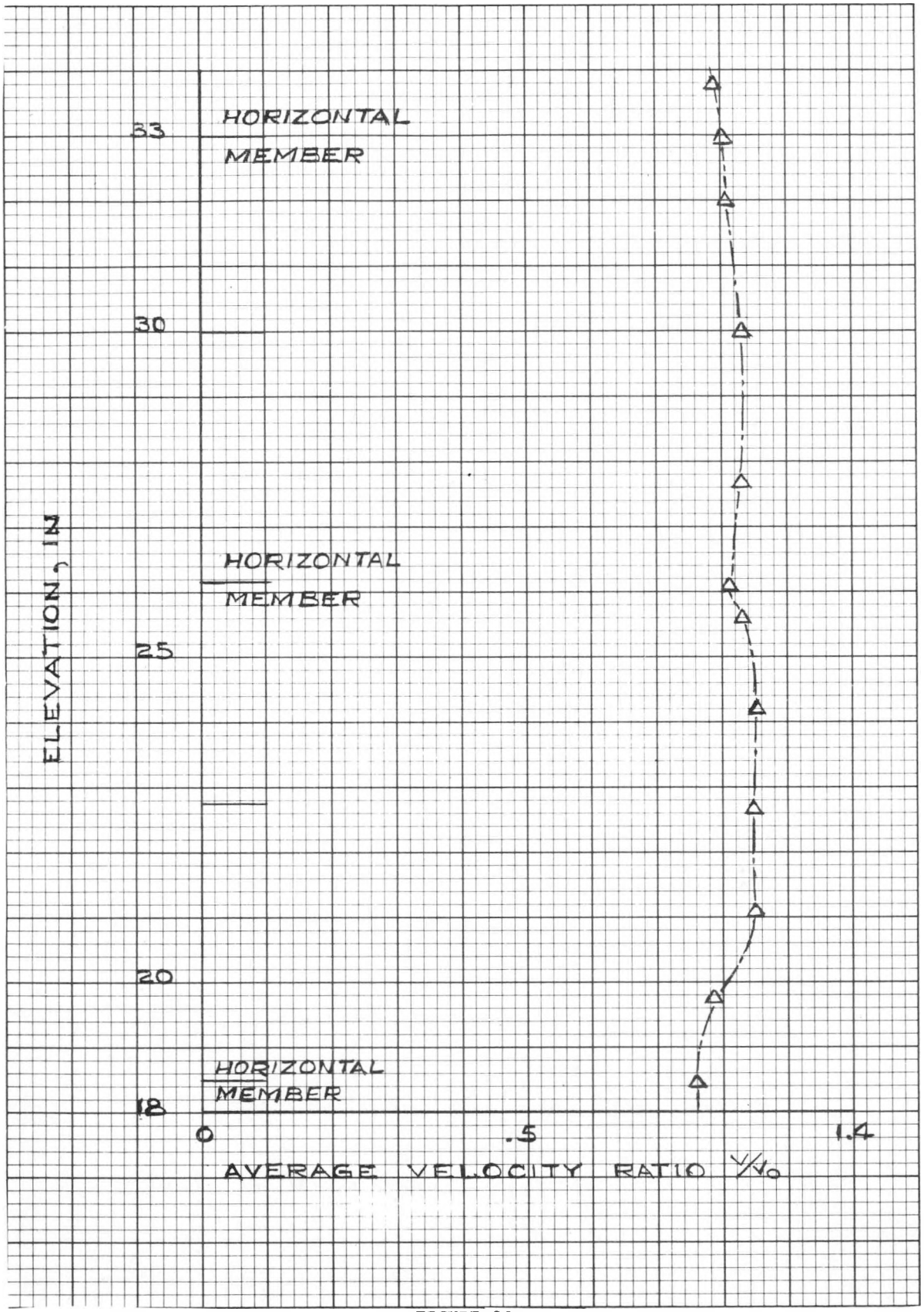

FIGURE 29c
Variation of Average Velocity Ratio with Elevation for Tower with One Diagonal Removed from Each Side of Panels 3 and 4 (Wind Direction of 35^{o})

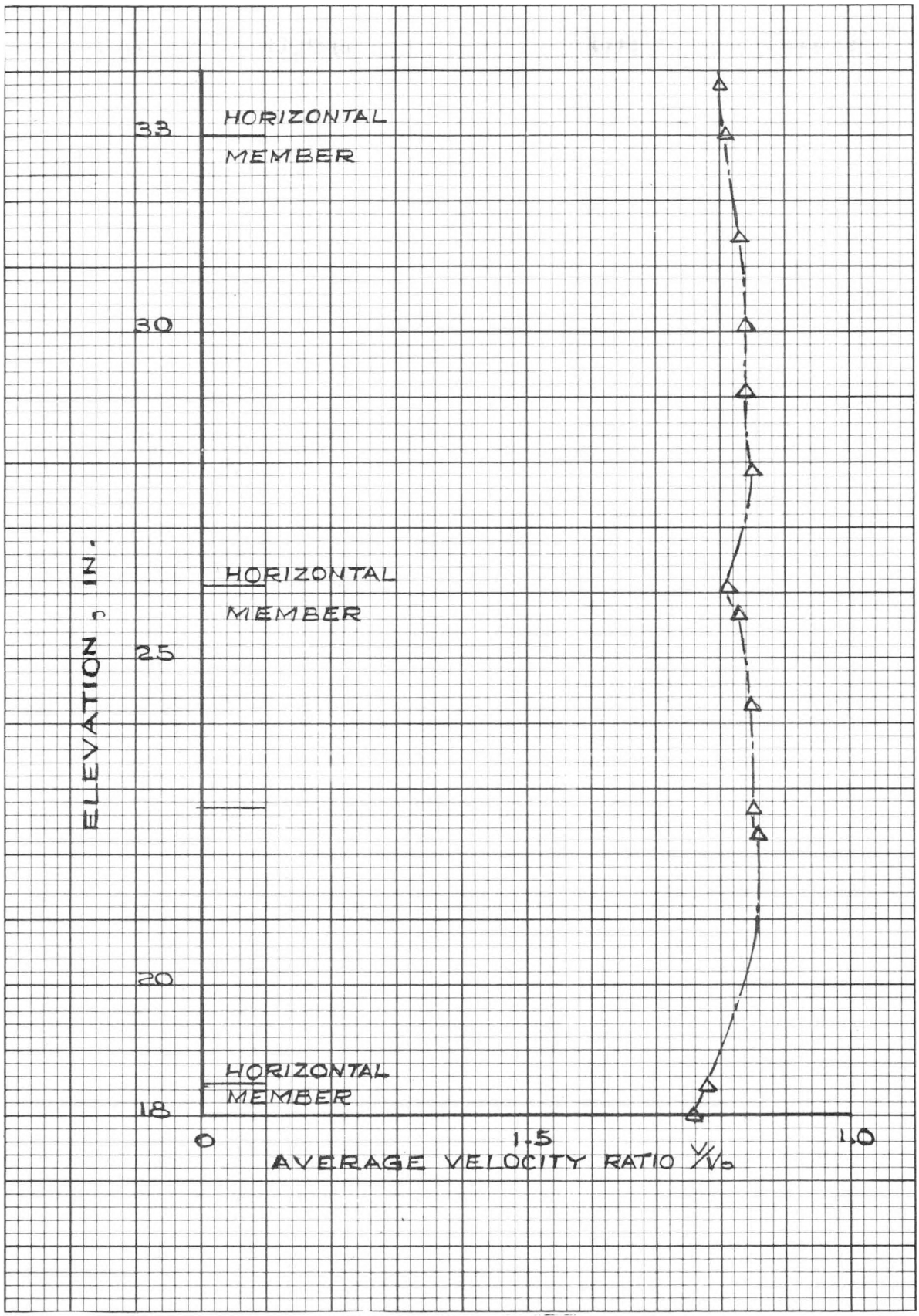

FIGURE 29d
Variation of Average Velocity Ratio with Elevation for Tower with One Diagonal Removed from Each Side of Panels 3 and 4 (Wind Direction of 40^{o})

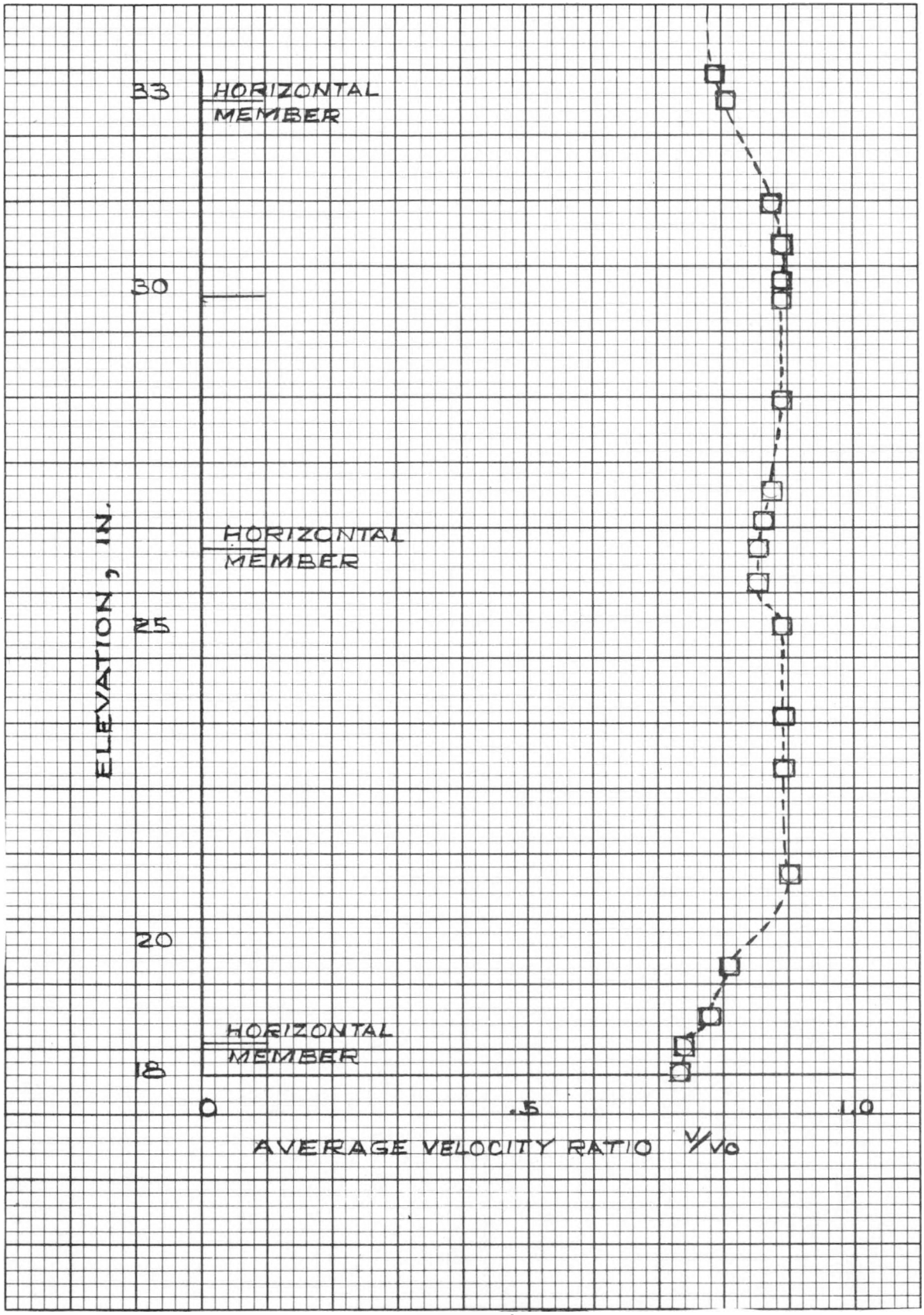

FIGURE 30a
Variation of Average Velocity Ratio with All Diagonals Removed from Panels 3 and 4 (Wind Direction of 10^{o})

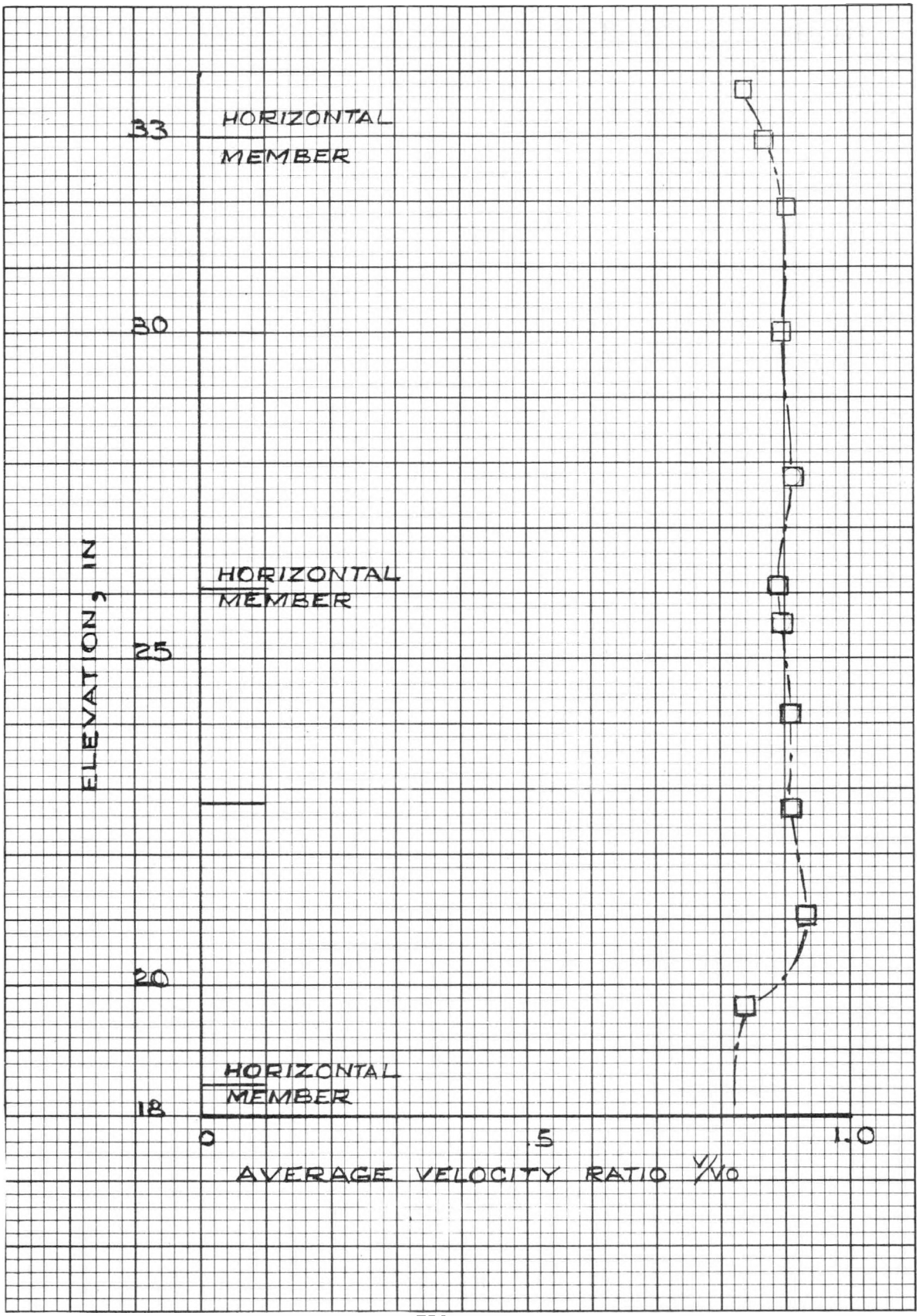

FIGURE 30b
Variation of Average Velocity Ratio with All Diagonals Removed from Panels 3 and 4 (Wind Direction of 35°)

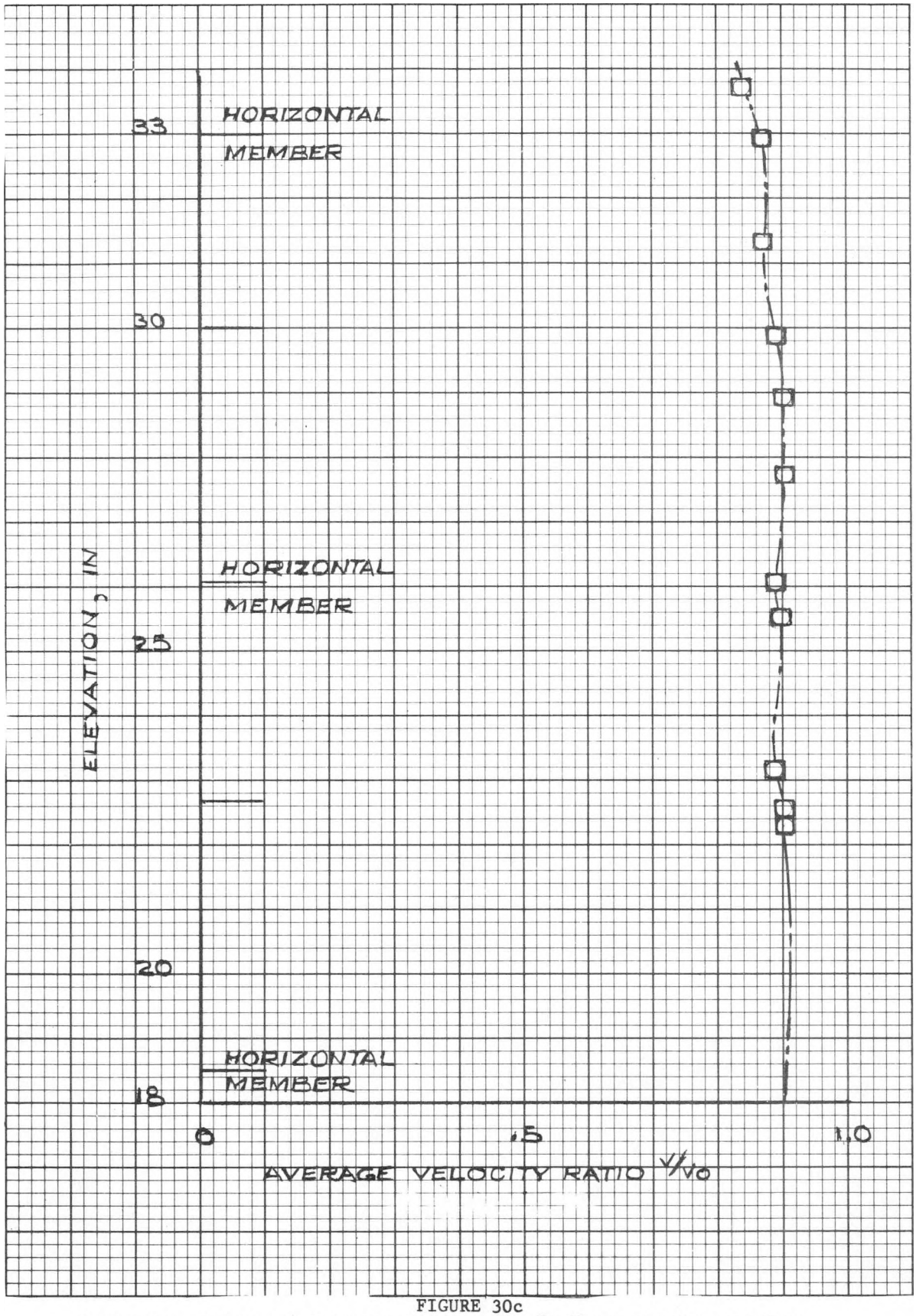

FIGURE 30c
Variation of Average Velocity Ratio with All Diagonals Removed from Panels 3 and 4 (Wind Direction of 40^{o})

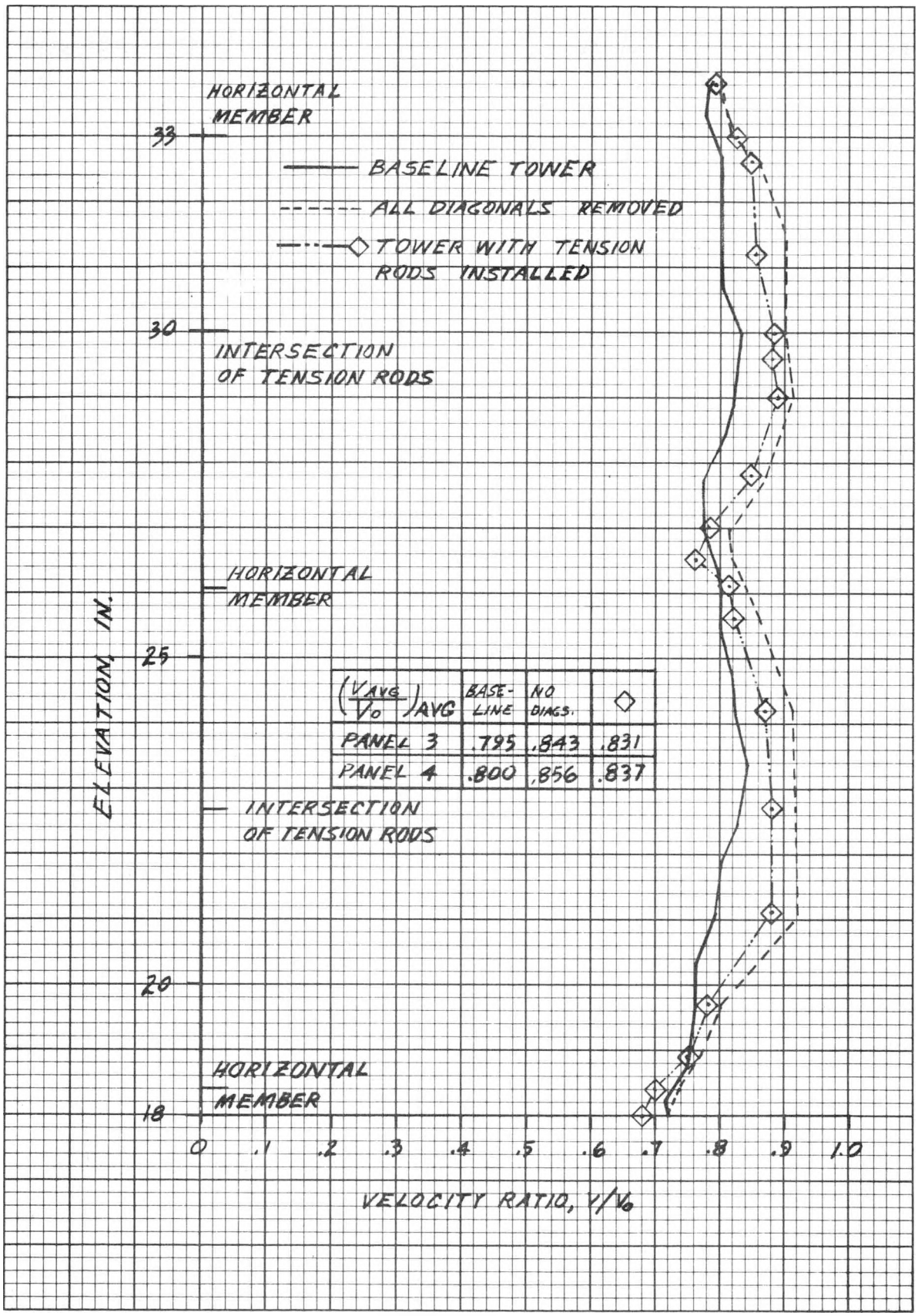

FIGURE 31a

Comparison of Variation of Average Velocity Ratio with Elevation for Baseline Tower, Tower with All Diagonals Removed, and Tower With Tension Rods (Wind Direction 0°)

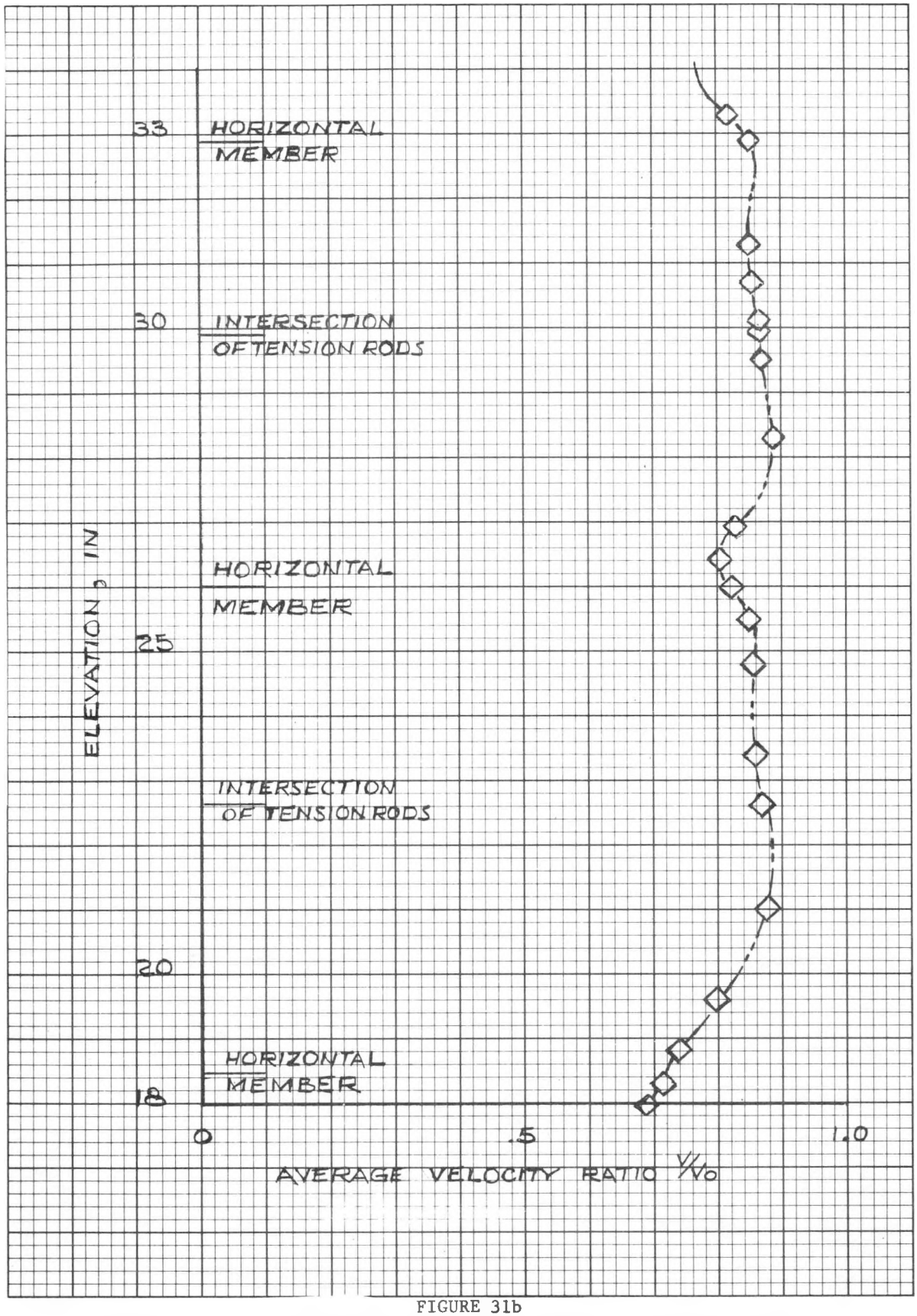

FIGURE 31b
Variation of Average Velocity Ratio with Tension Rods Installed as Diagonals in Panels 3 and 4 (Wind Direction of 10^{o})

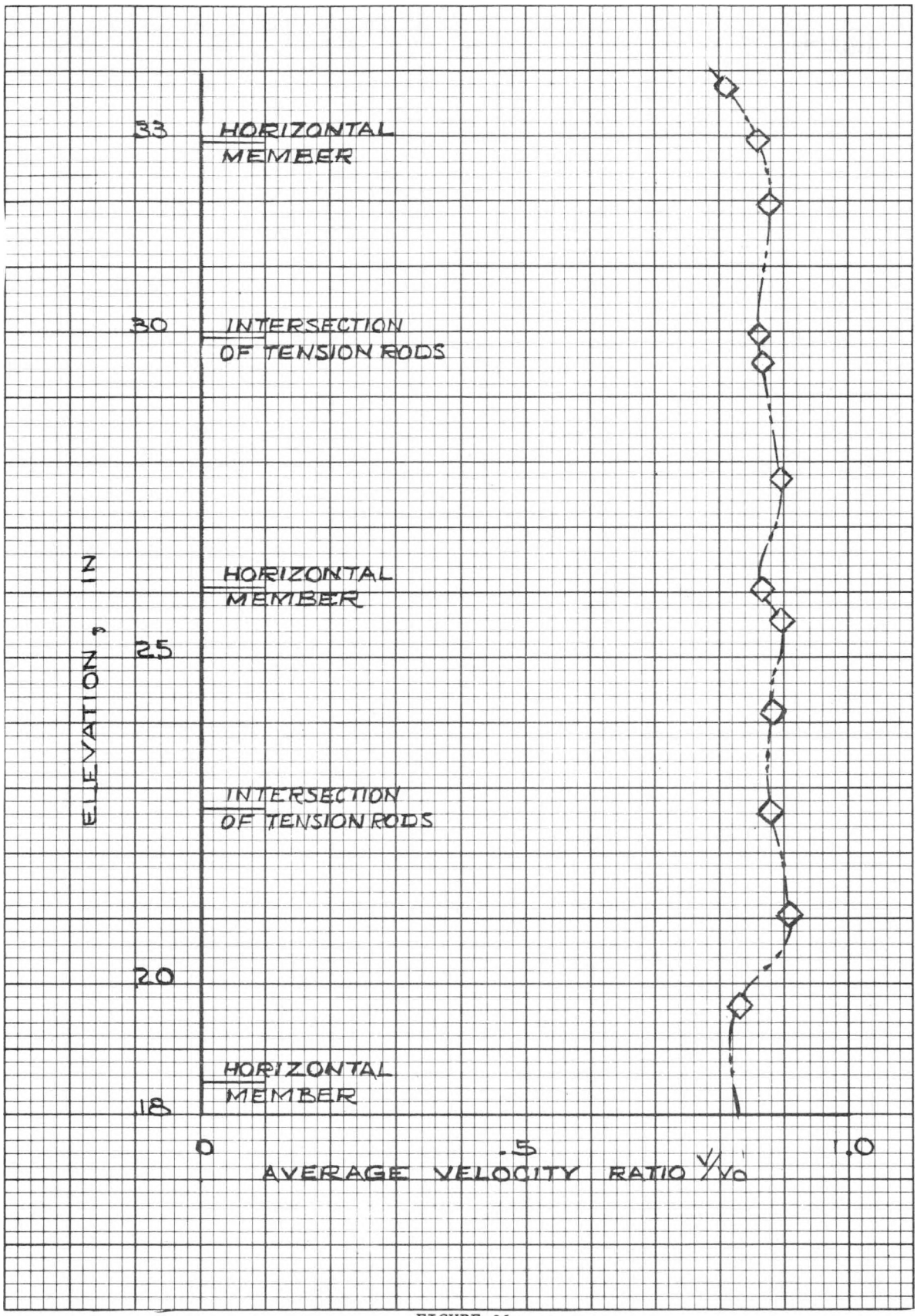

FIGURE 31c
Variation of Average Velocity Ratio with Tension Rods Installed as Diagonals in Panels 3 and 4 (Wind Direction of 35°)

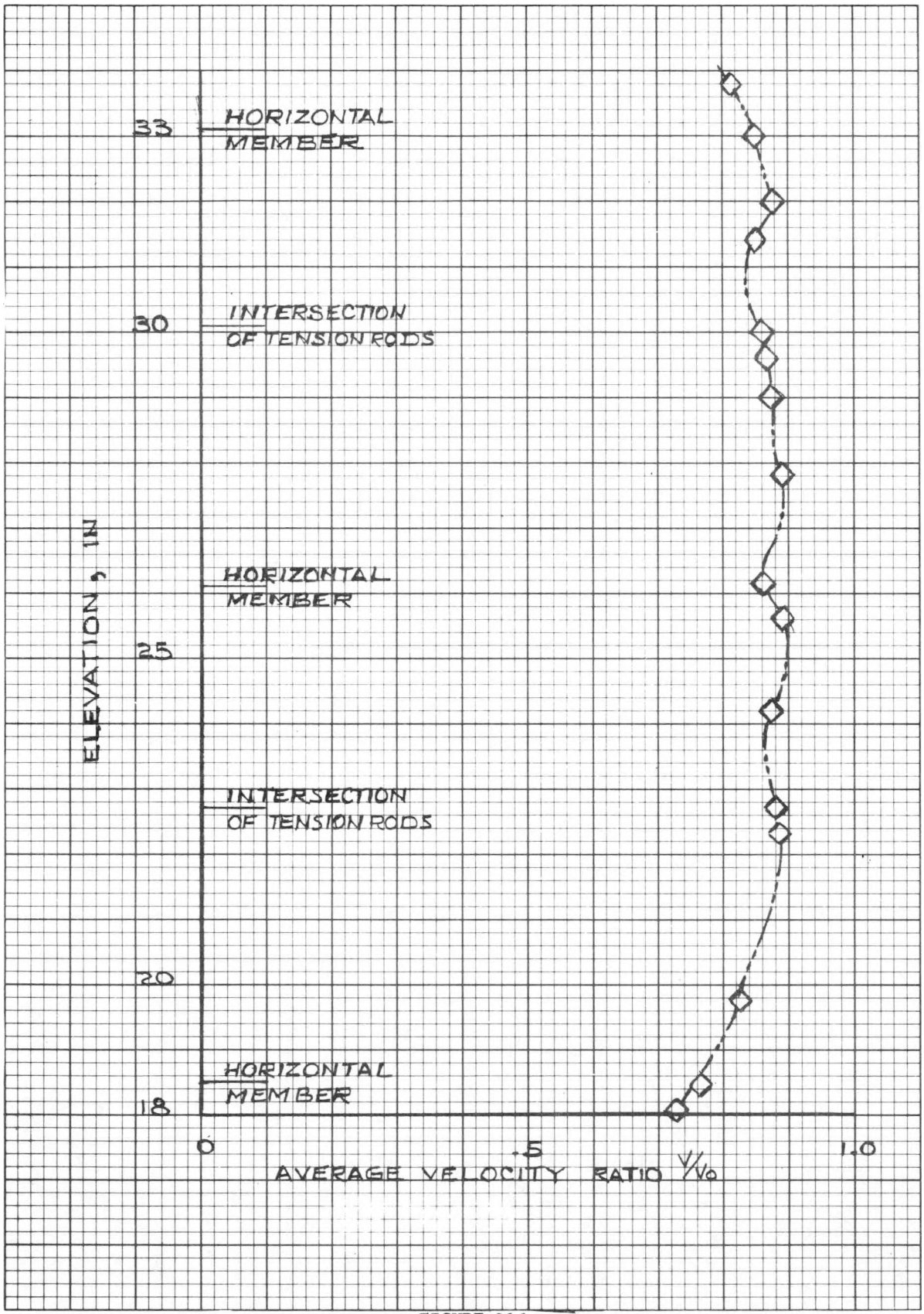

FIGURE 31d
Variation of Average Velocity Ratio with Tension Rods Installed as Diagonals in Panels 3 and 4 (Wind Direction of 40^{o})

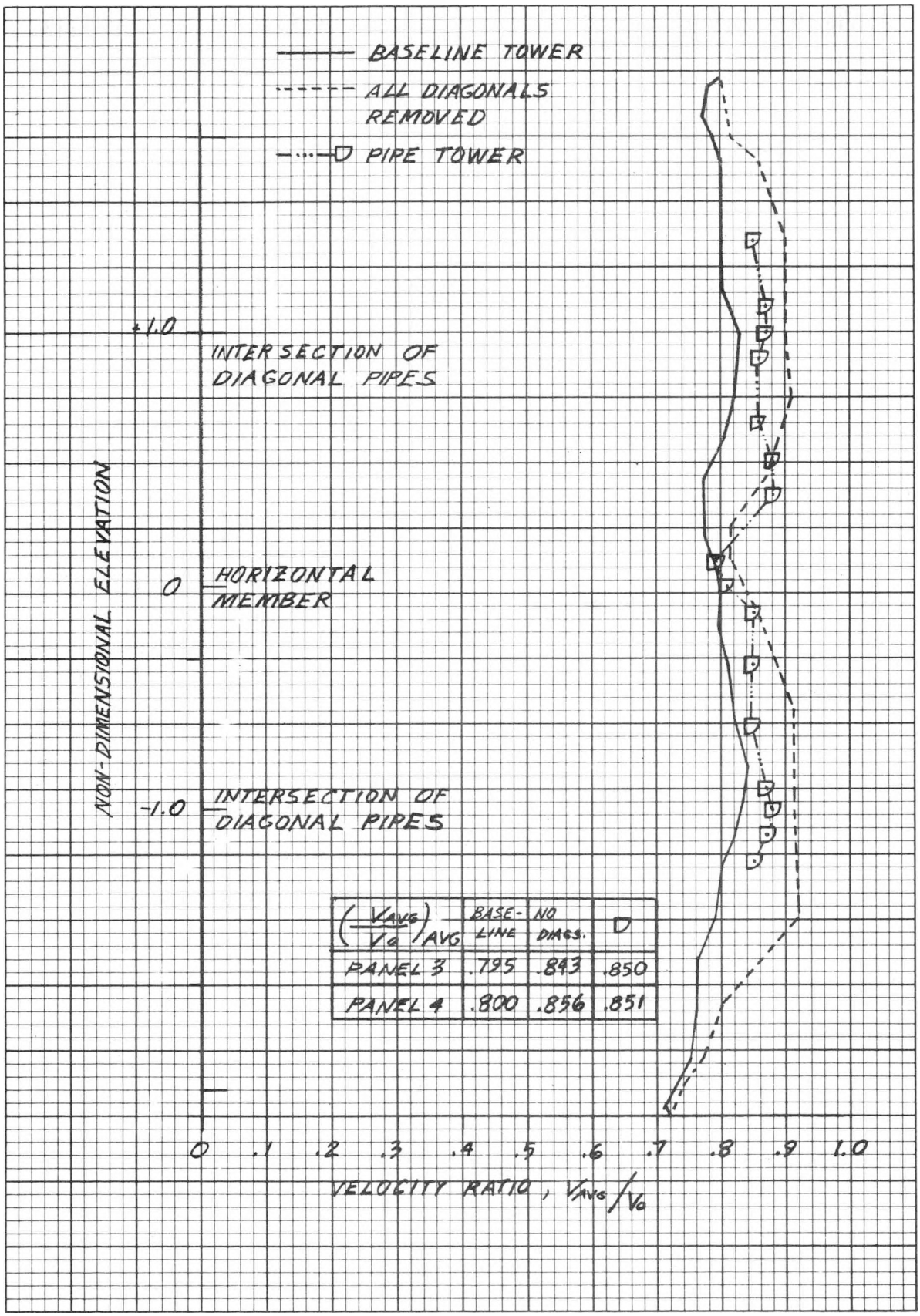

$(V_{AVG}/V_G)_{AVG}$	BASE-LINE	NO DIAGS.	D
PANEL 3	.795	.843	.850
PANEL 4	.800	.856	.851

FIGURE 32a
Comparison of Variation of Average Velocity Ratio with Elevation for Baseline Tower, Tower with All Diagonals Removed, and All-Pipe Tower (Wind Direction 0°)

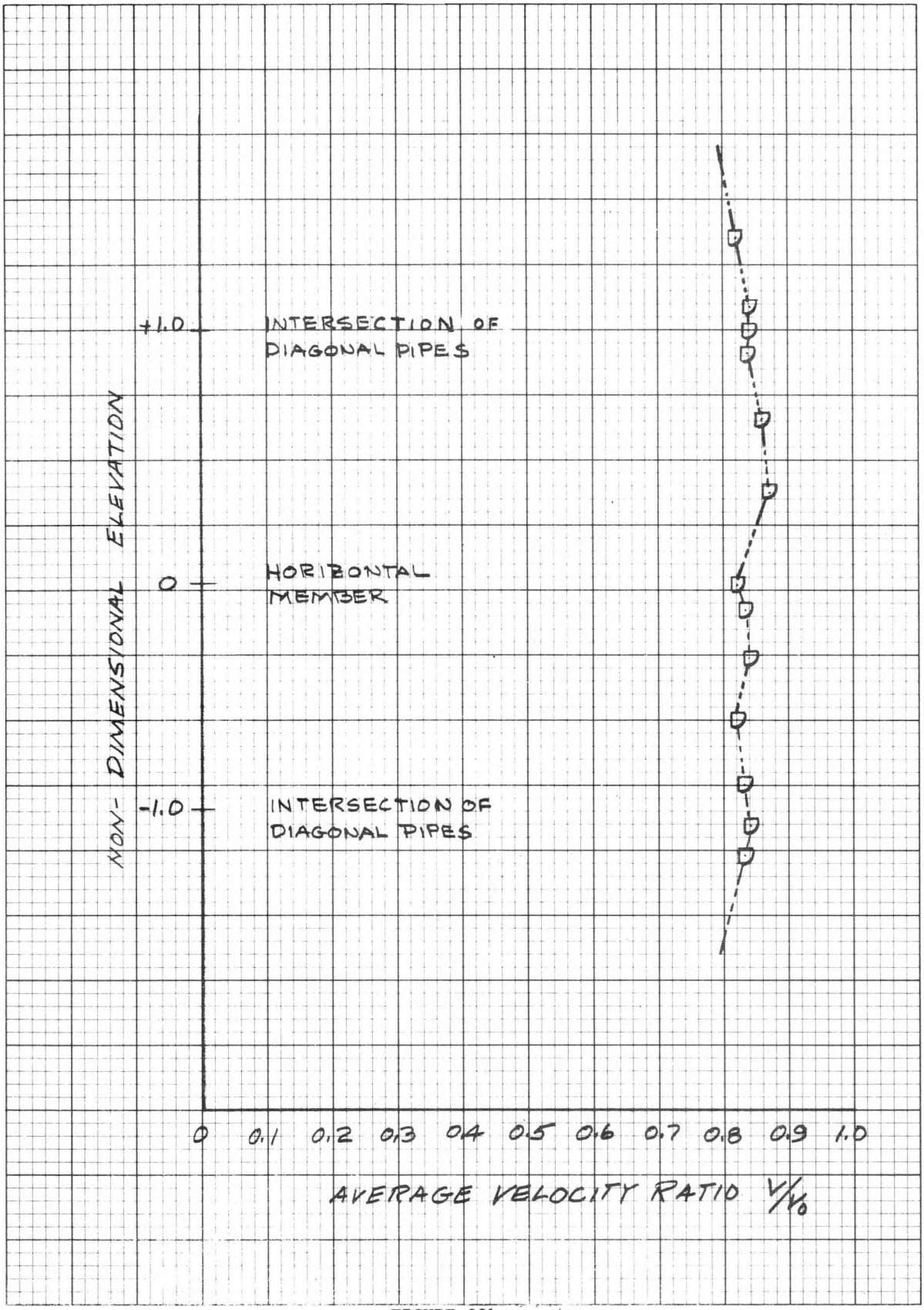

FIGURE 32b
Variation of Average Velocity Ratio for All-Pipe Tower
Wind Direction of 10^{o}

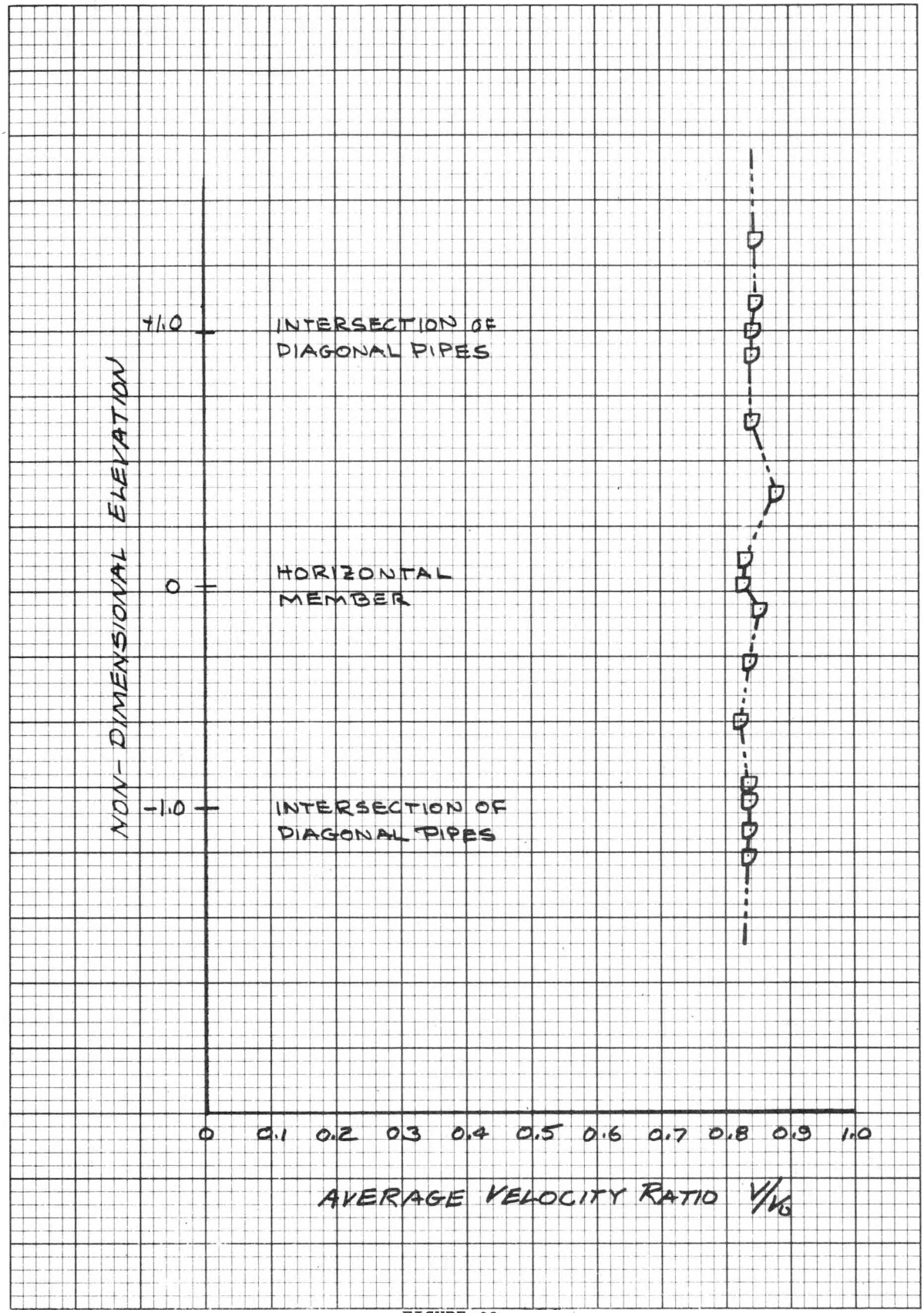

FIGURE 32c
Variation of Average Velocity Ratio for All-Pipe Tower
Wind Direction of 35^{o}

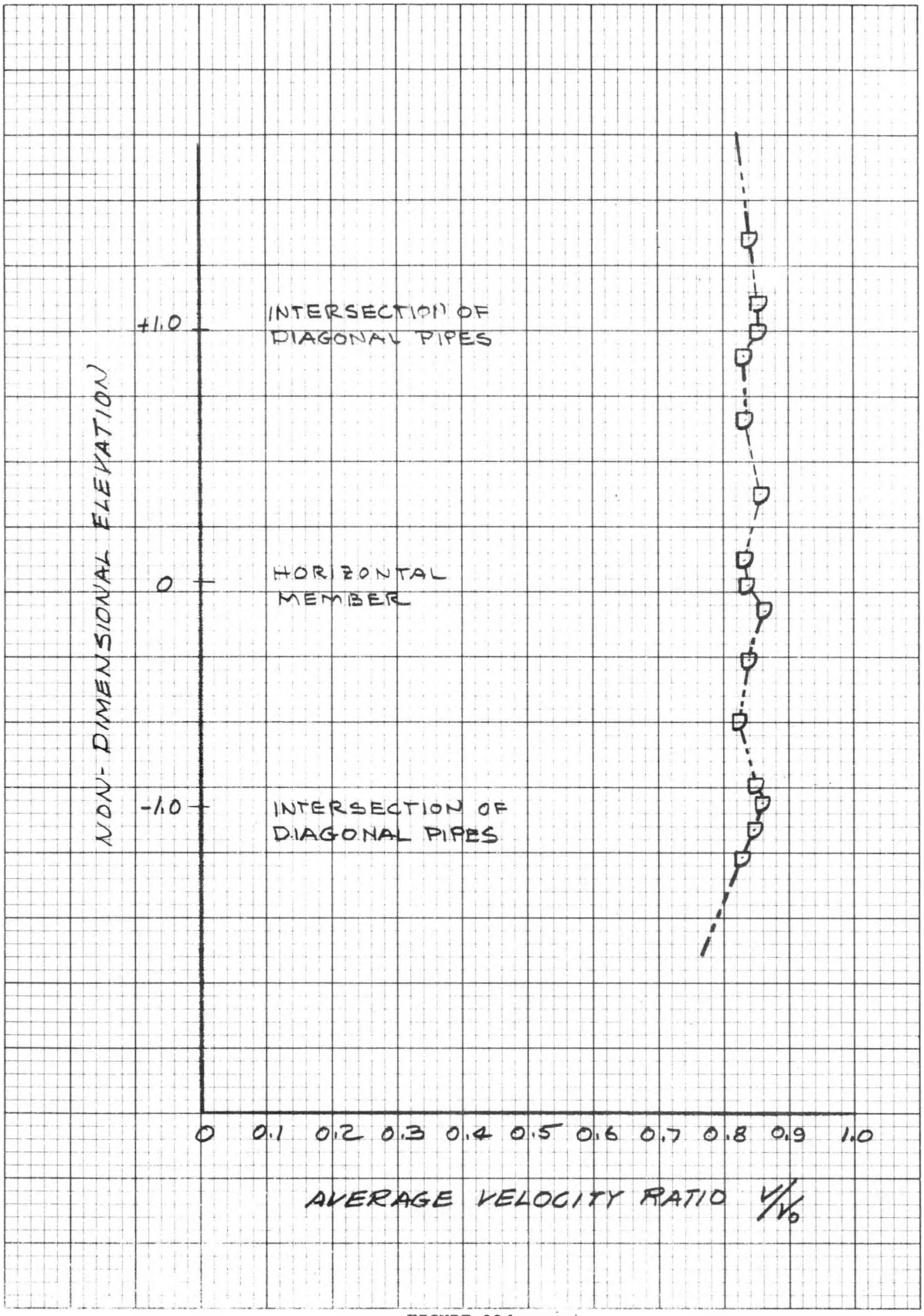

FIGURE 32d
Variation of Average Velocity Ratio for All-Pipe Tower
Wind Direction of 40°

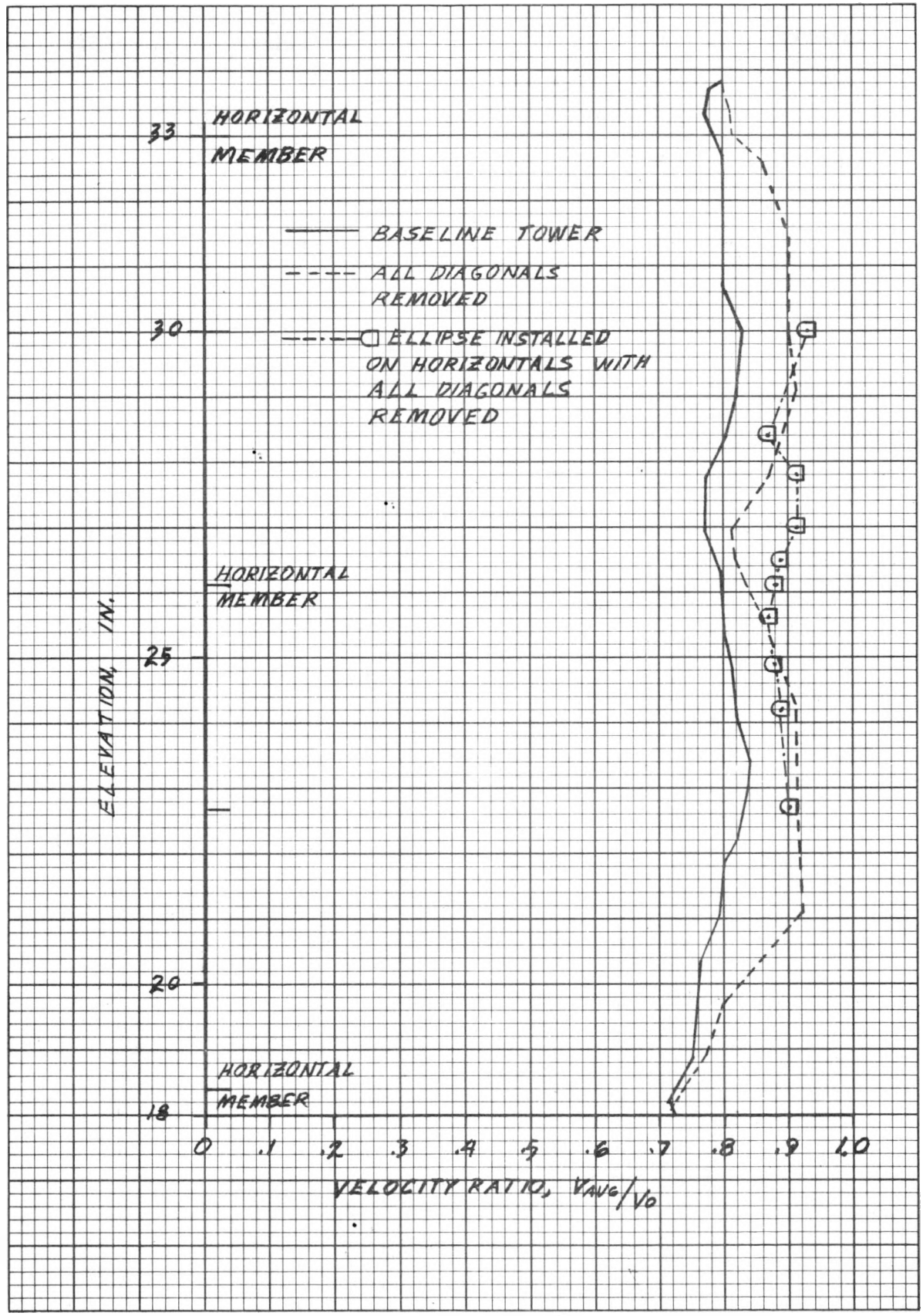

FIGURE 33a

Comparison of Variation of Average Velocity Ratio with Elevation of Baseline Tower and for Tower With and Without Ellipses Installed on Horizontal Member with All Diagonals Removed (Wind Direction 0°)

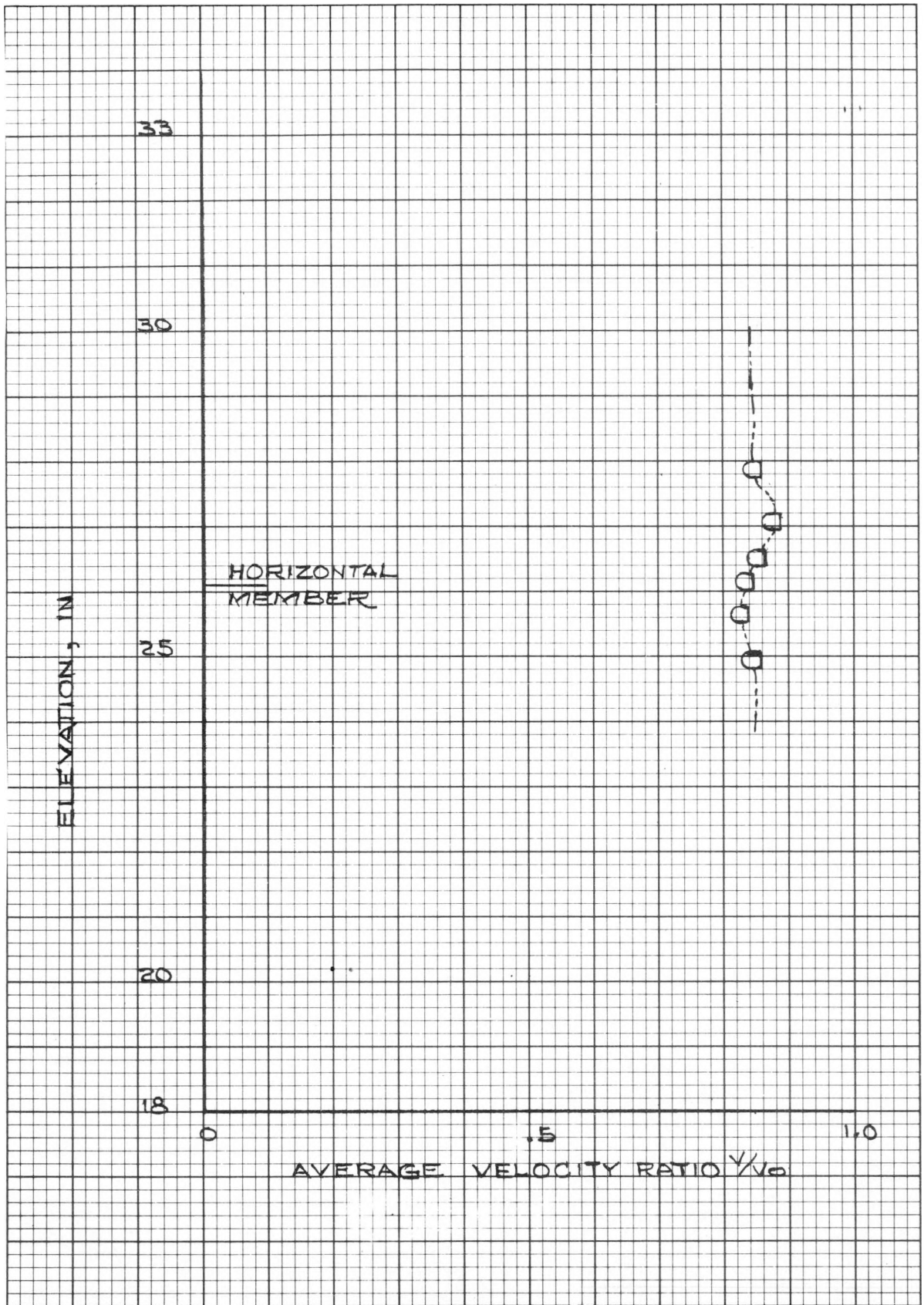

FIGURE 33b
Variation of Average Velocity Ratio for Tower with Ellipses Installed on Horizontal Member with All Diagonals Removed (Wind Direction of 10^{o})

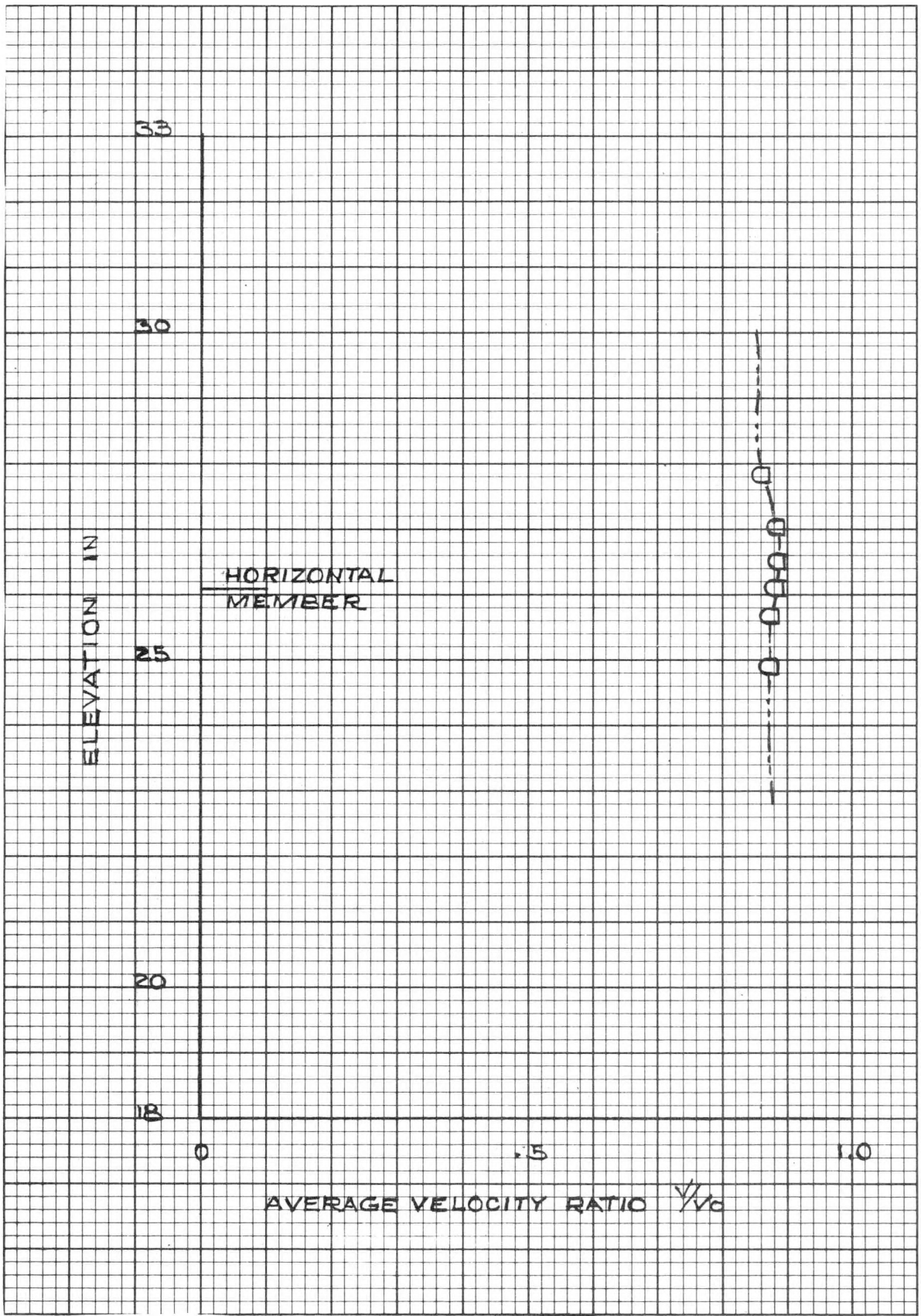

FIGURE 33c
Variation of Average Velocity Ratio for Tower with Ellipses Installed on Horizontal Member with All Diagonals Removed (Wind Direction of 35°)

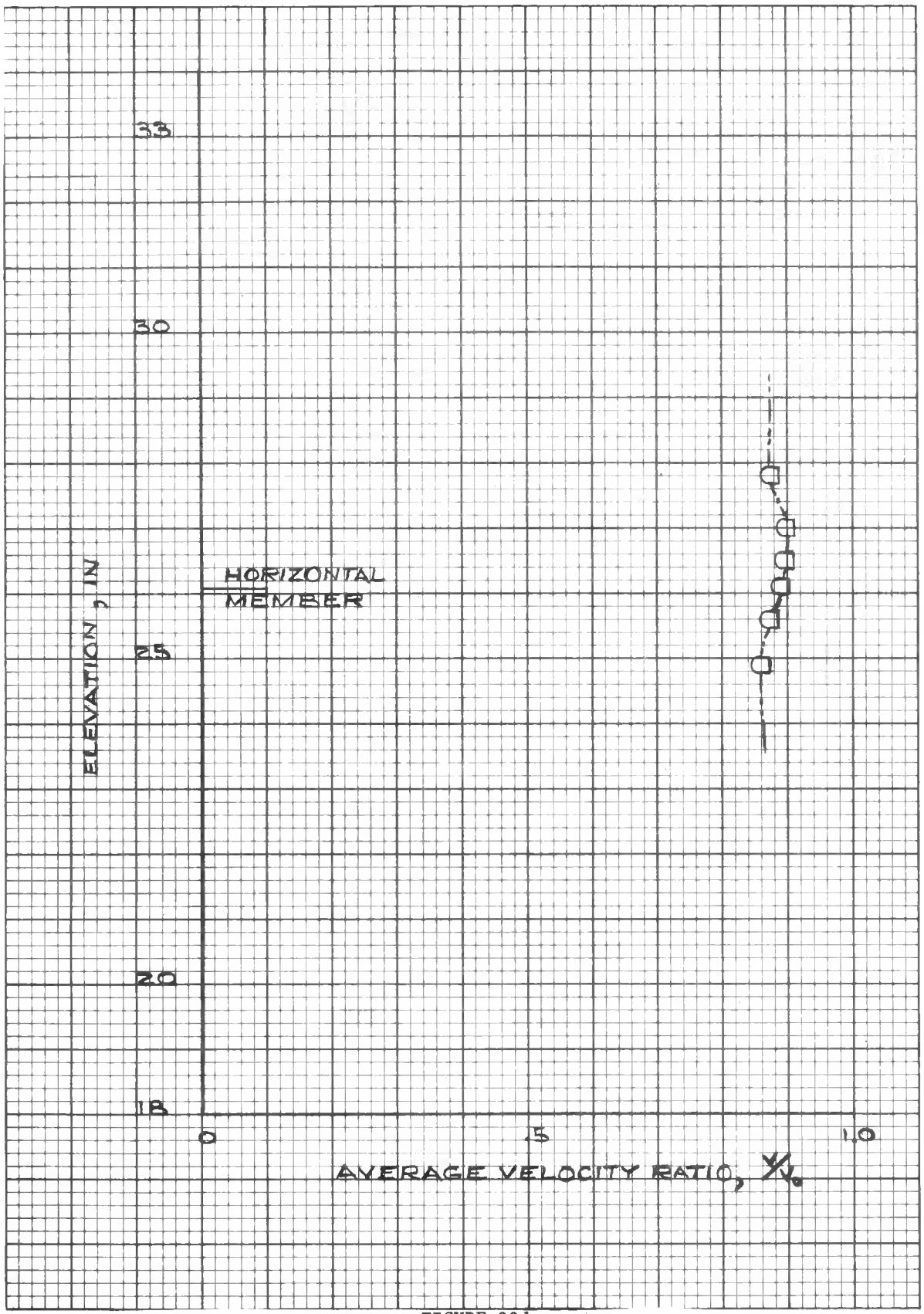

FIGURE 33d
Variation of Average Velocity Ratio for Tower with Ellipses Installed on Horizontal Member with All Diagonals Removed (Wind Direction of 40°)

APPENDIX C

Variation of Wake to Tower Width Ratio with Elevation at Wind Directions of 0°, 10°, 35°, 40°; All Tower Configurations.

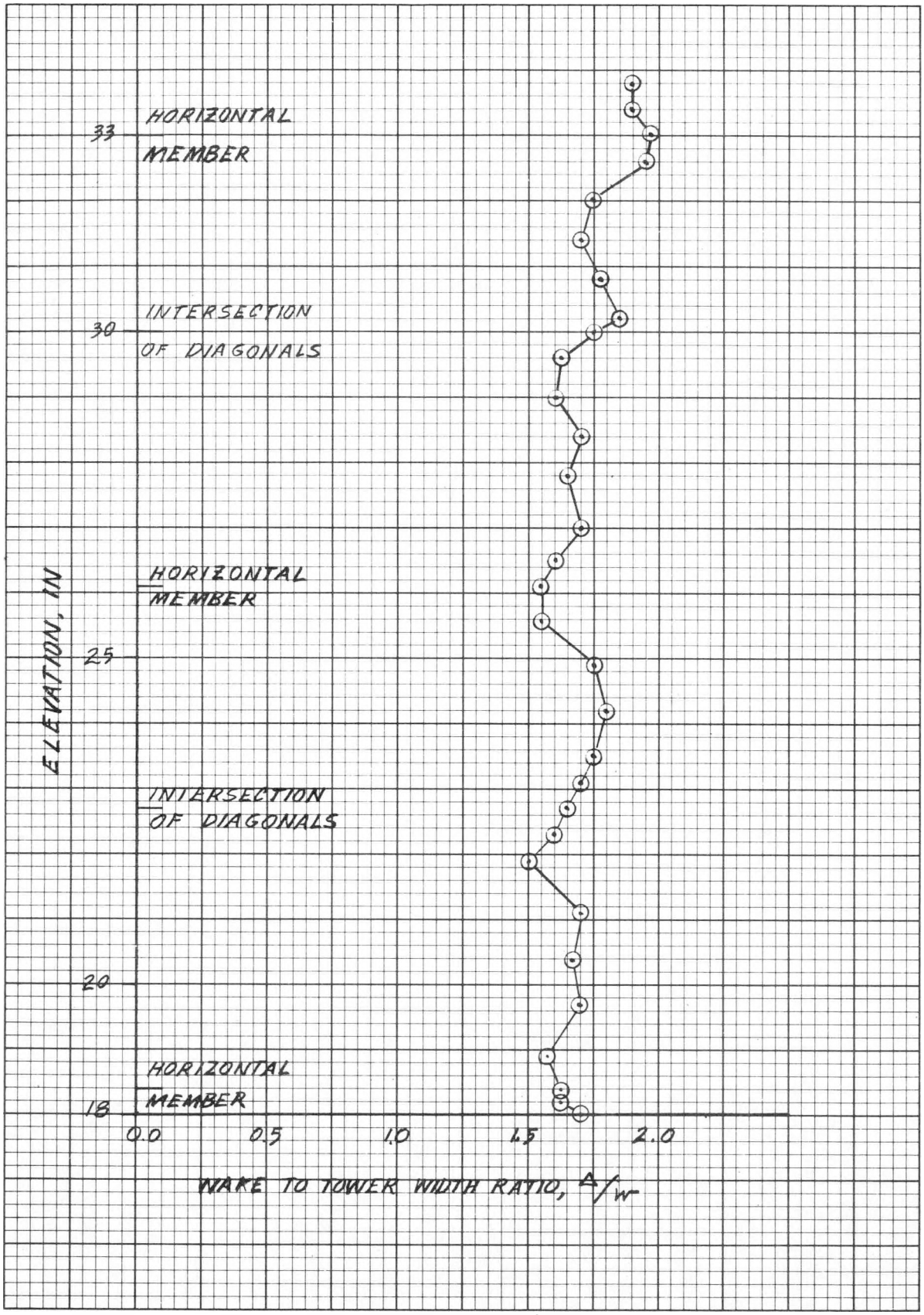

FIGURE 34a
Variation of Wake-to-Tower Width Ratio with Elevation for Baseline Tower (Wind Direction 0^{o})

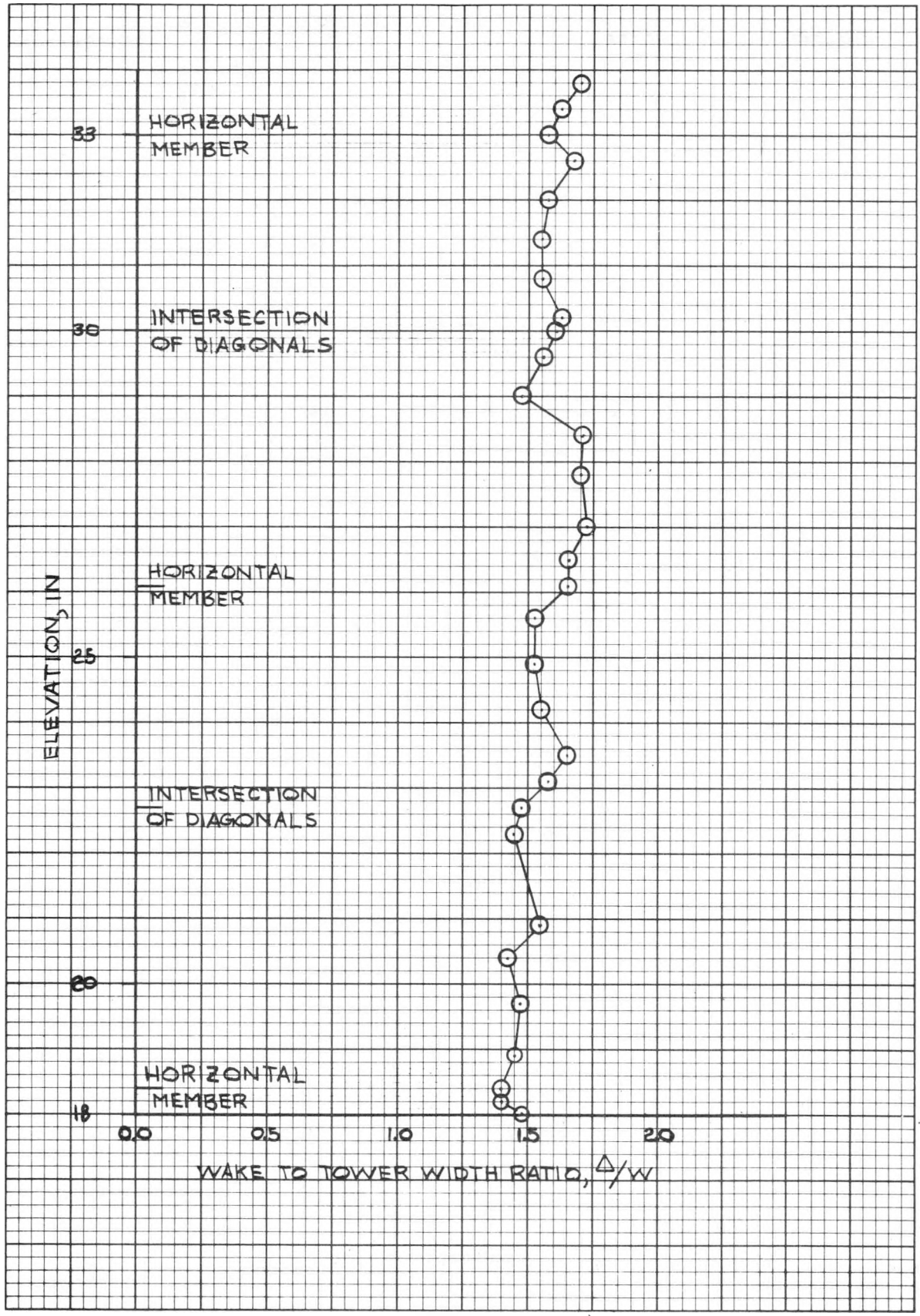

FIGURE 34b
Variation of Wake-to-Tower Width Ratio with Elevation for Baseline Tower Wind Direction of 10^{o}

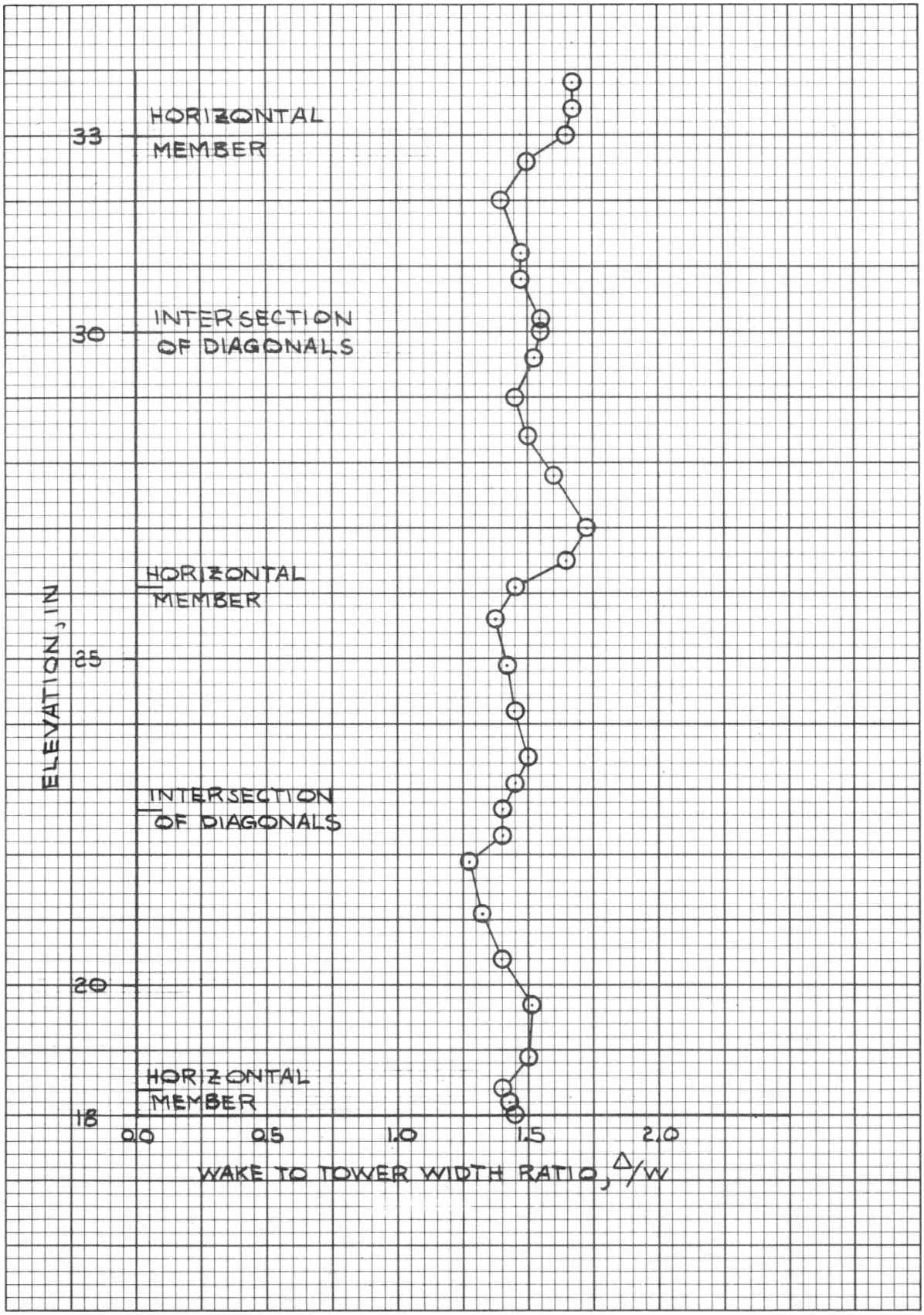

FIGURE 34c
Variation of Wake-to-Tower Width Ratio with Elevation for Baseline Tower Wind Direction of 35°

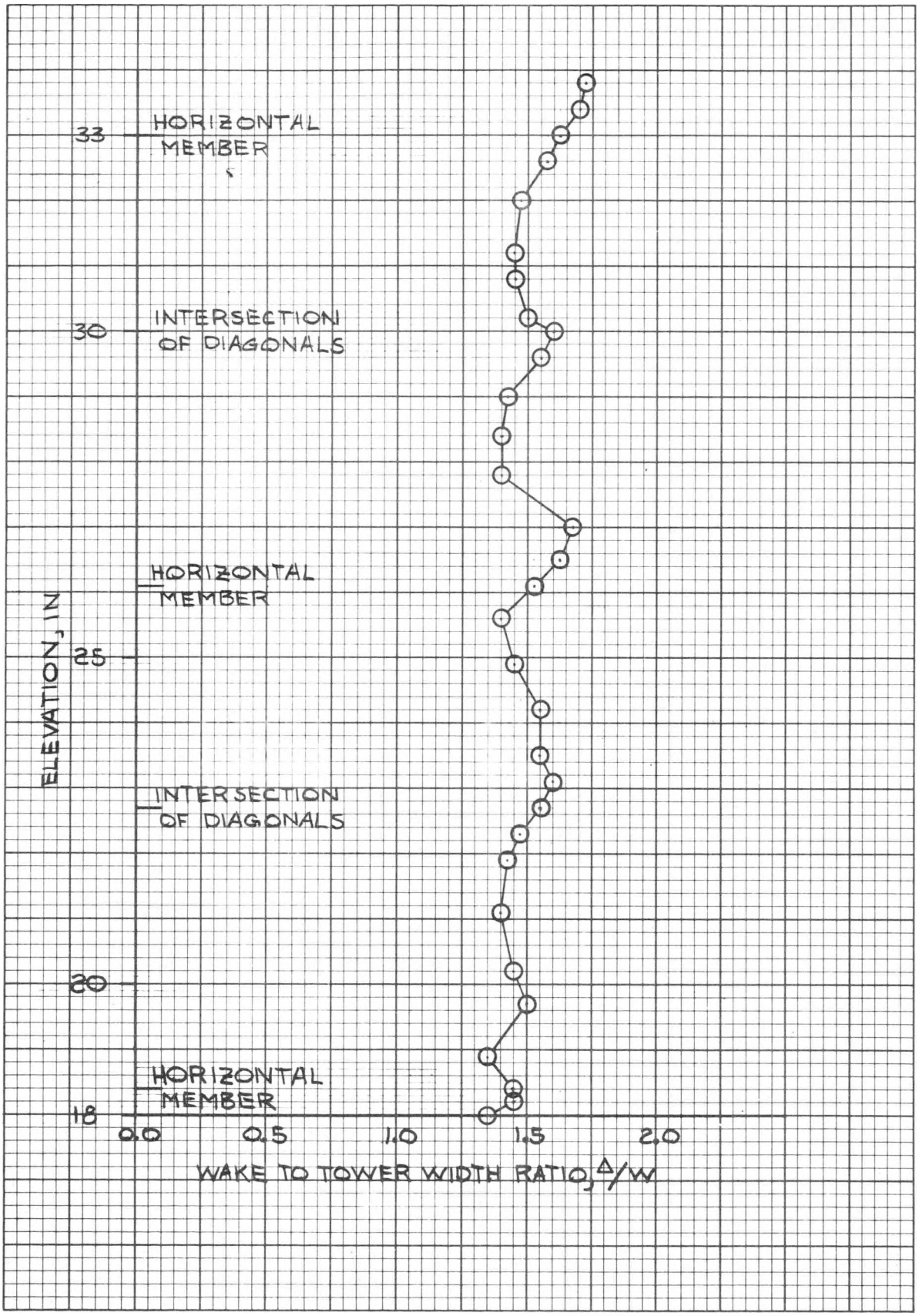

FIGURE 34d
Variation of Wake-to-Tower Width Ratio with Elevation for Baseline Tower Wind Direction of 40°

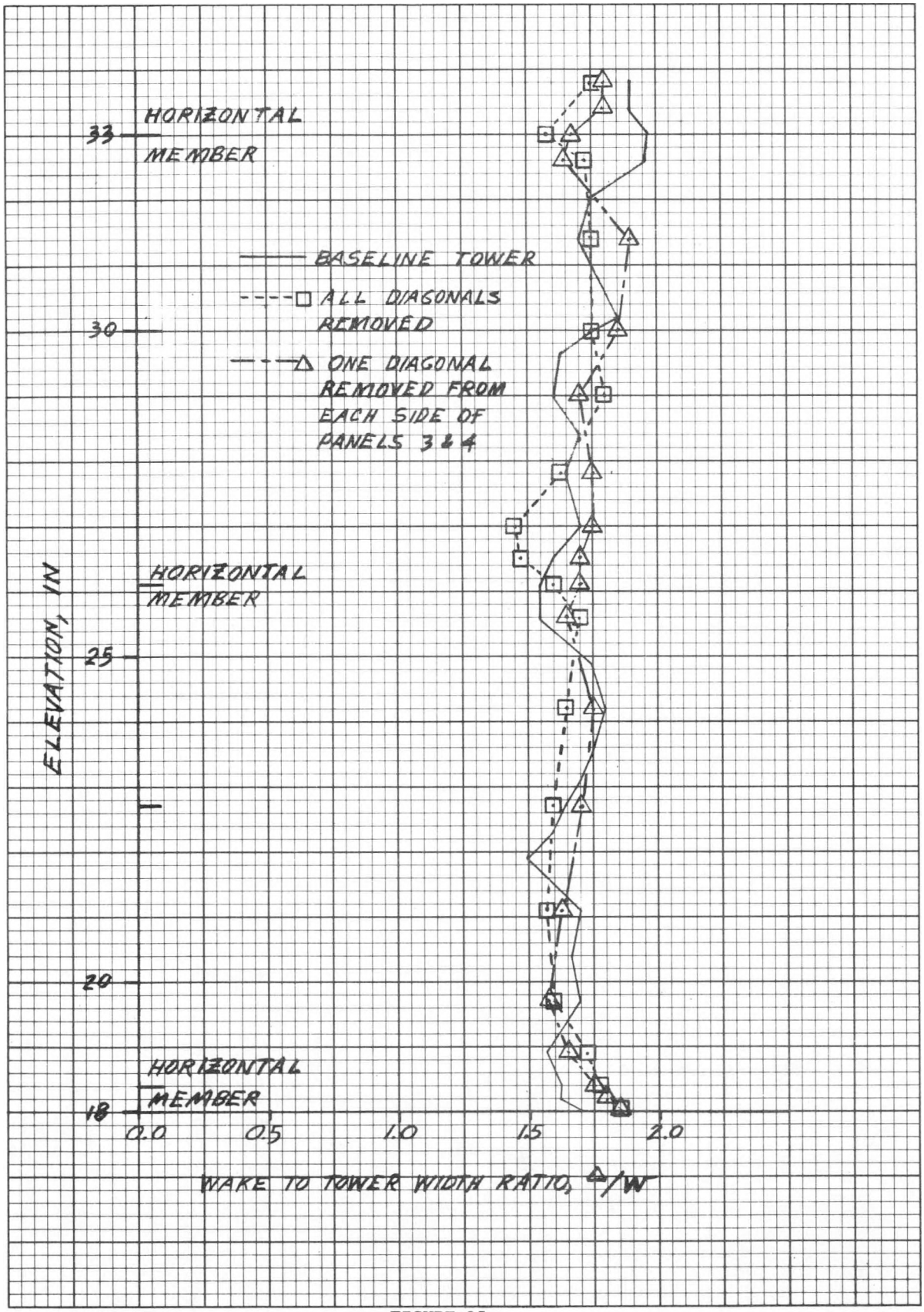

FIGURE 35a

Comparison of Variation of Wake-to-Tower Width Ratio with Elevation for Baseline Tower and Tower with Diagonals Removed (Wind Direction 0^{o})

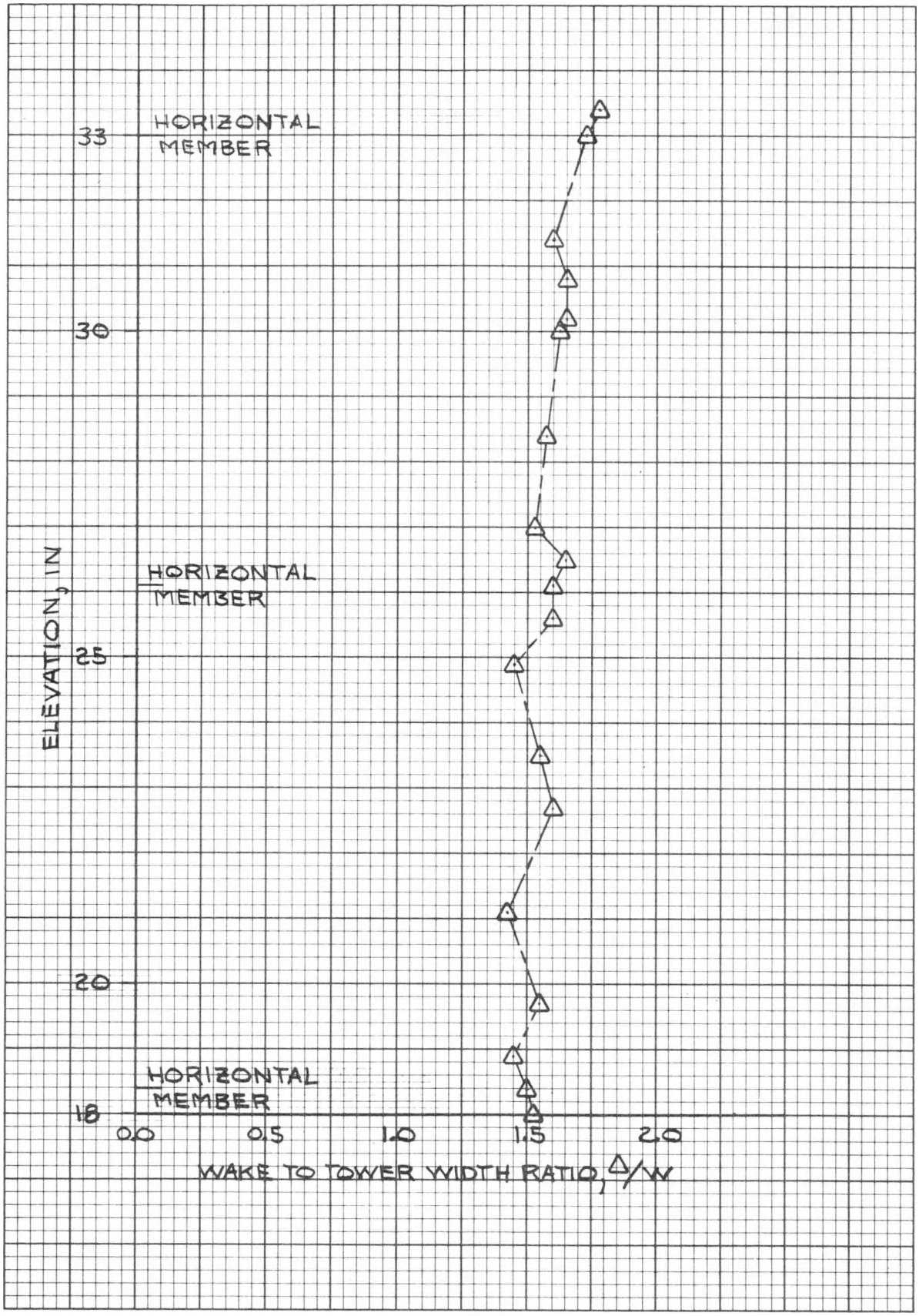

FIGURE 35b

Variation of Wake-to-Tower Width Ratio with Elevation for Tower with One Diagonal Removed from Each Side of Panels 3 and 4 (Wind Direction of 10^{o})

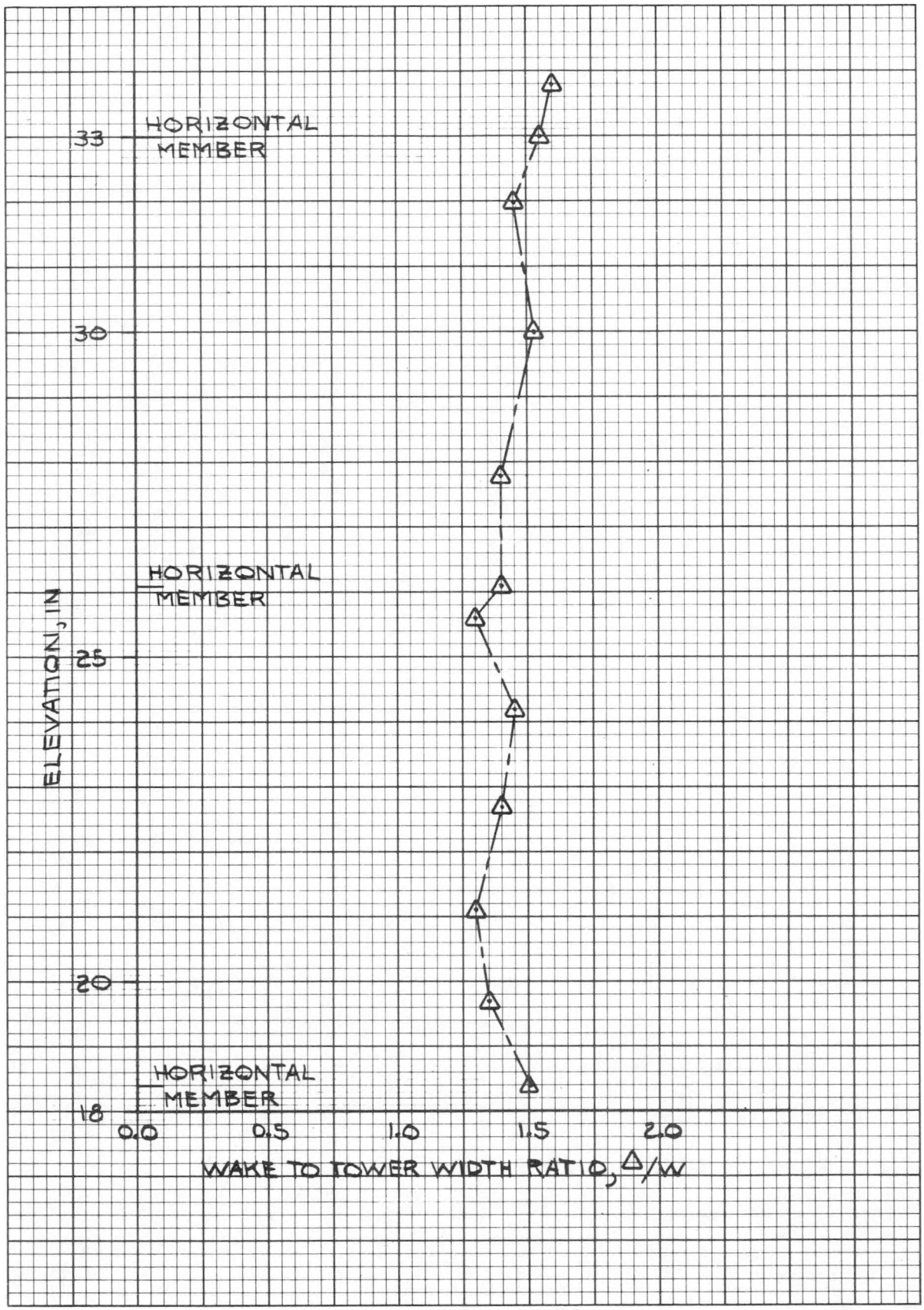

FIGURE 35c

Variation of Wake-to-Tower Width Ratio with Elevation for Tower with One Diagonal Removed from Each Side of Panels 3 and 4 (Wind Direction of 35°)

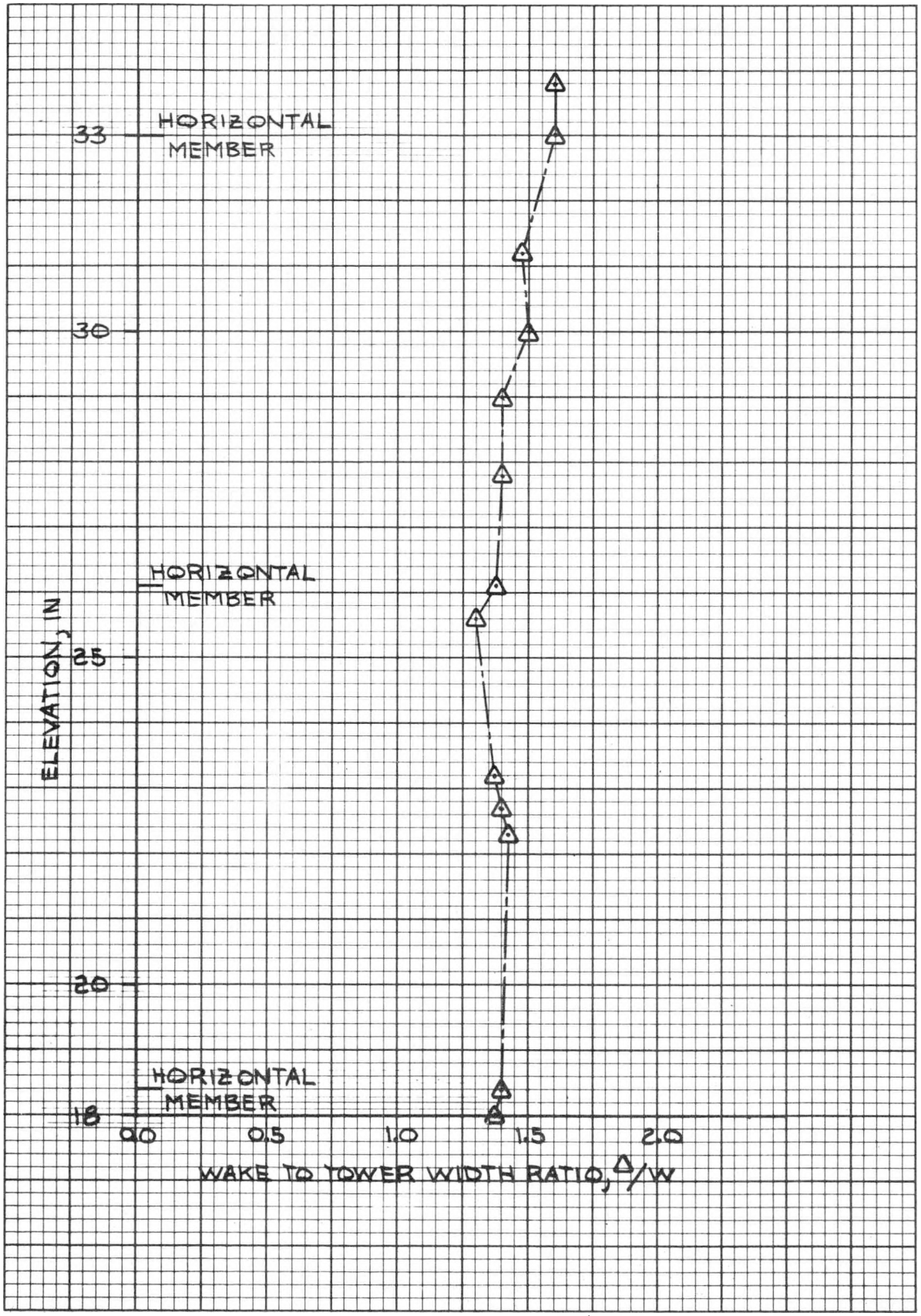

FIGURE 35d
Variation of Wake-to-Tower Width Ratio with Elevation for Tower with One Diagonal Removed from Each Side of Panels 3 and 4 (Wind Direction of 40°)

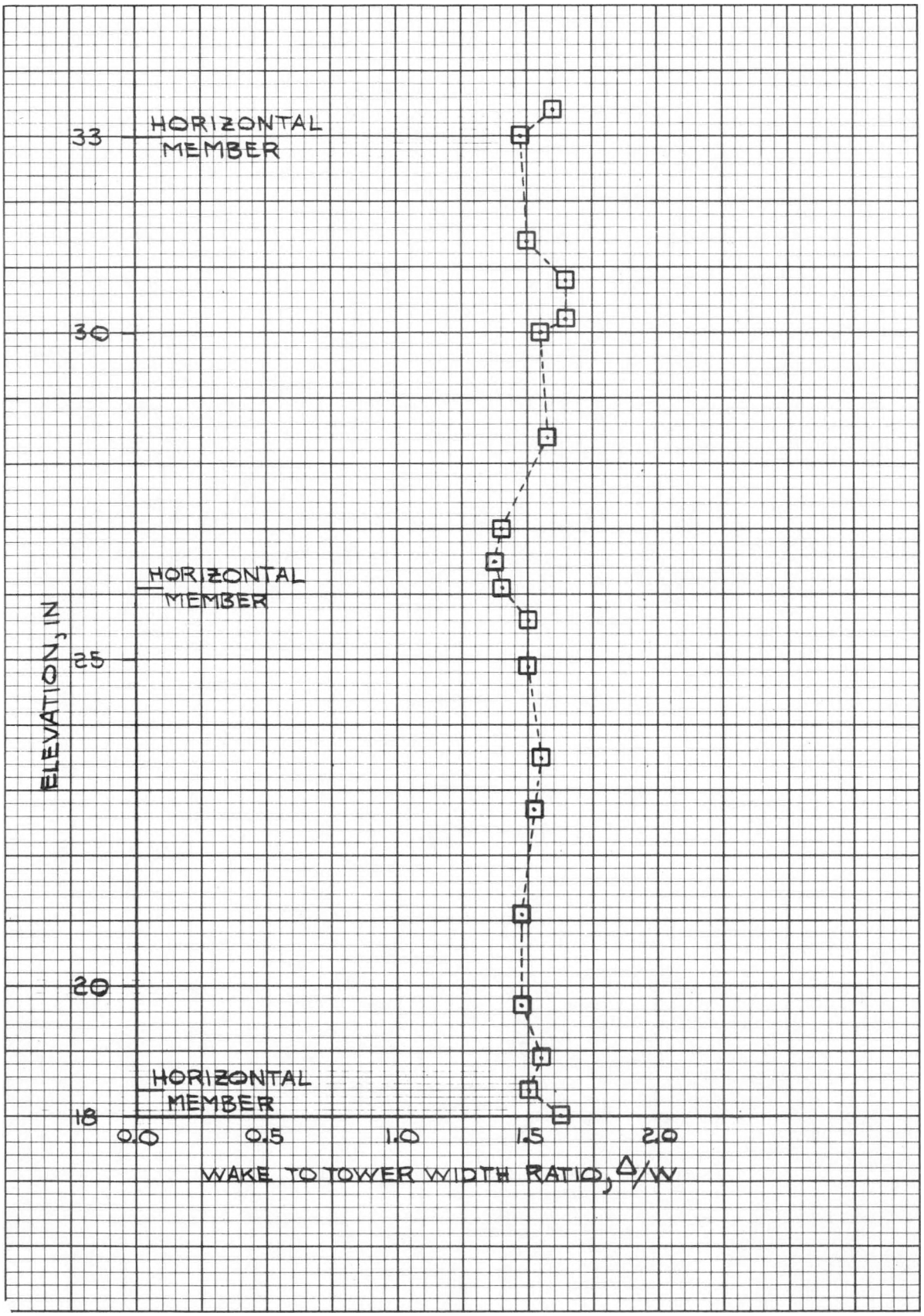

FIGURE 36a

Variation of Wake-to-Tower Width Ratio with Elevation for Tower With All Diagonals Removed from Panels 3 and 4 (Wind Direction of 10^{o})

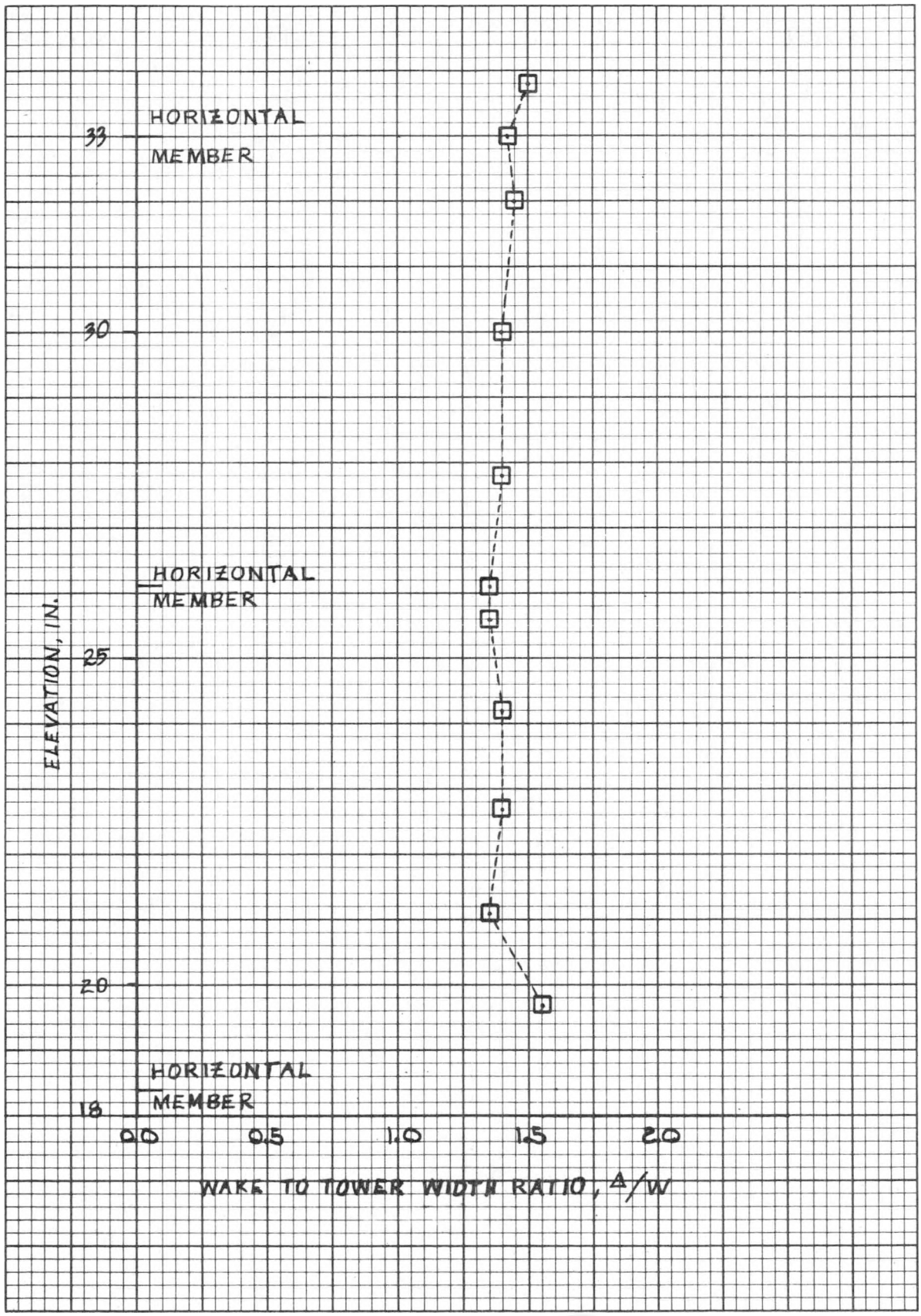

FIGURE 36b

Variation of Wake-to-Tower Width Ratio with Elevation for Tower With All Diagonals Removed from Panels 3 and 4 (Wind Direction of 35^{o})

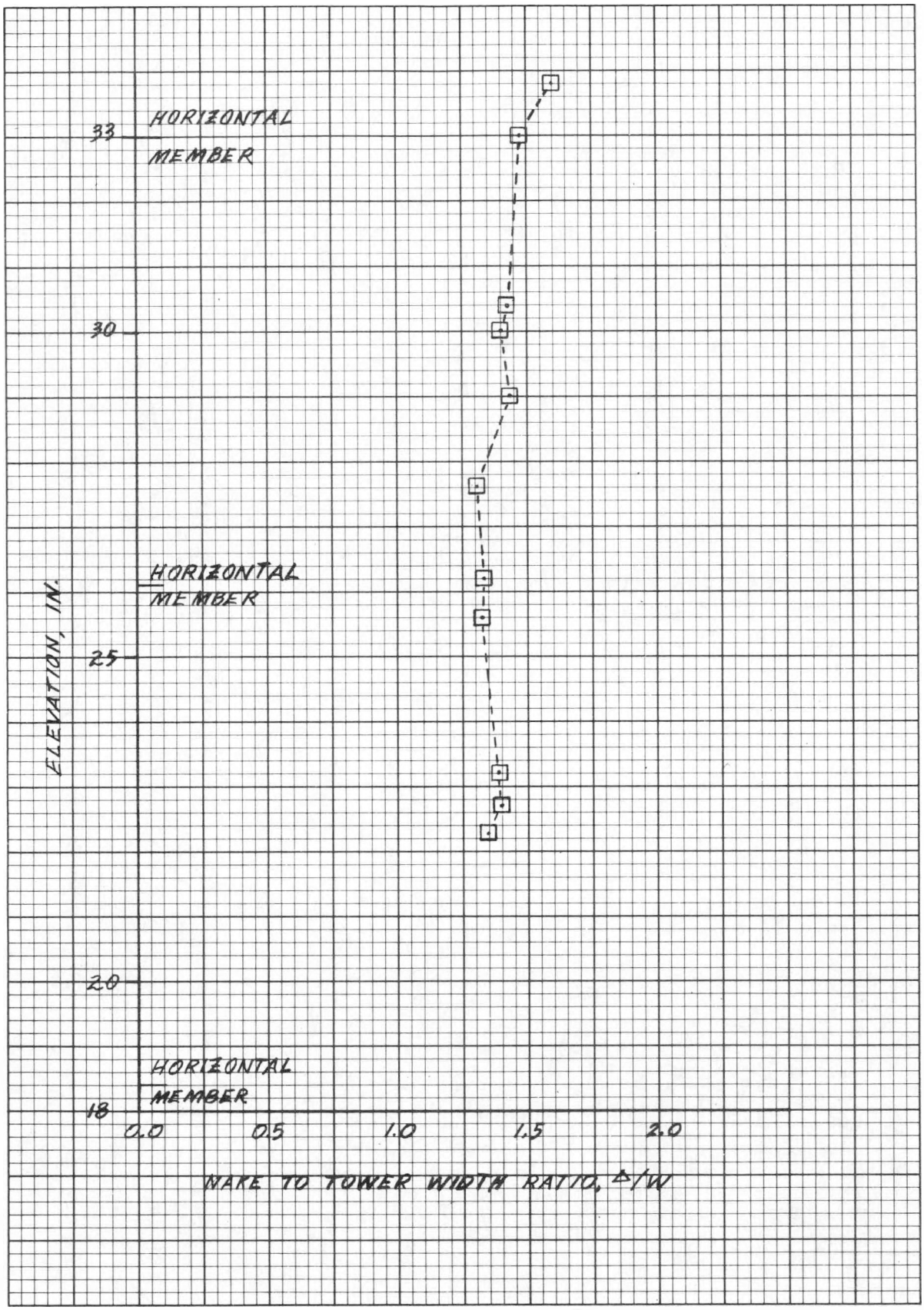

FIGURE 36c
Variation of Wake-to-Tower Width Ratio with Elevation for Tower With All Diagonals Removed from Panels 3 and 4 (Wind Direction of 40°)

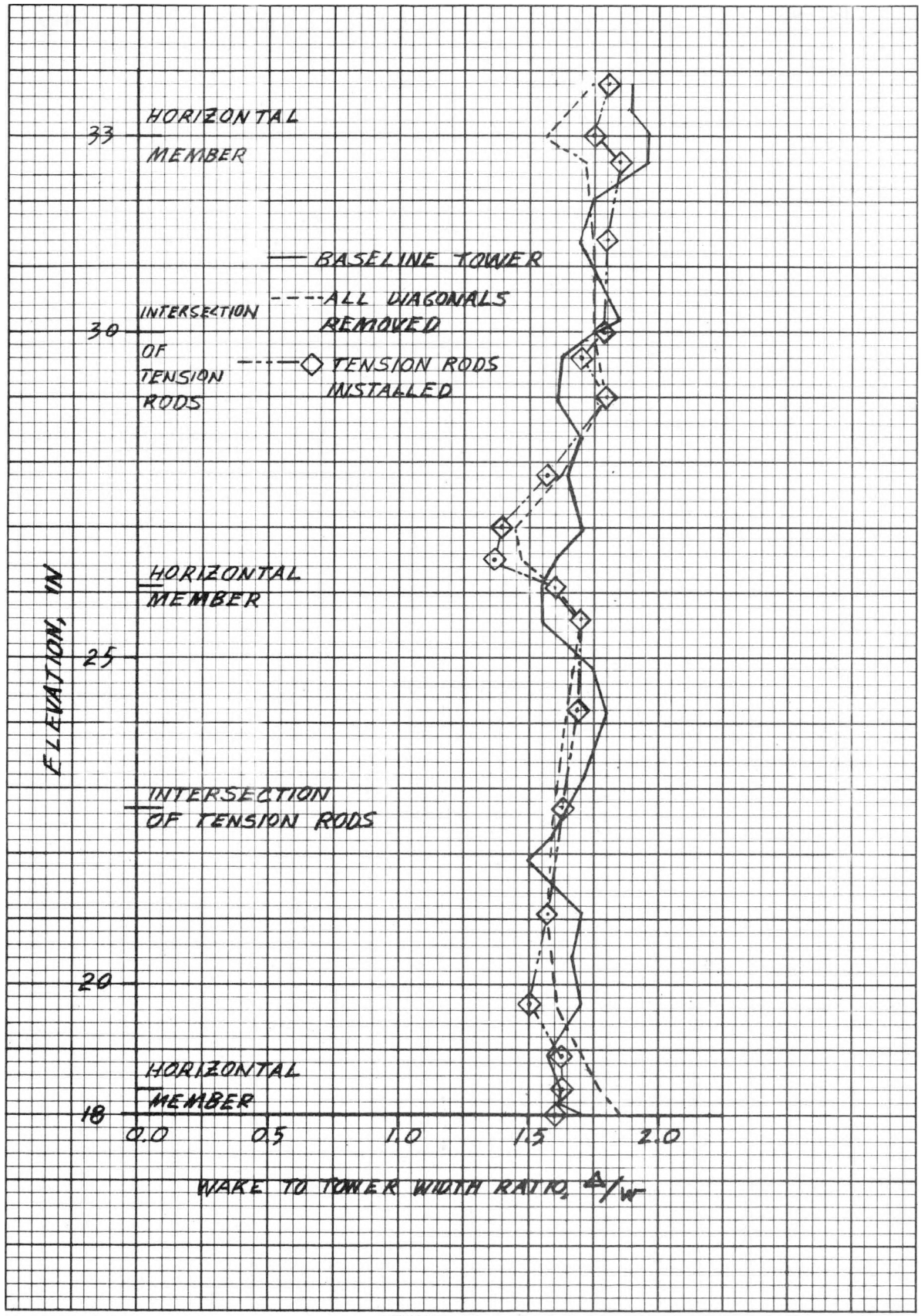

FIGURE 37a

Comparison of Variation of Wake-to-Tower Width Ratio with Elevation for Baseline Tower, Tower with All Diagonals Removed, and Tower with Tension Rods (Wind Direction 0°)

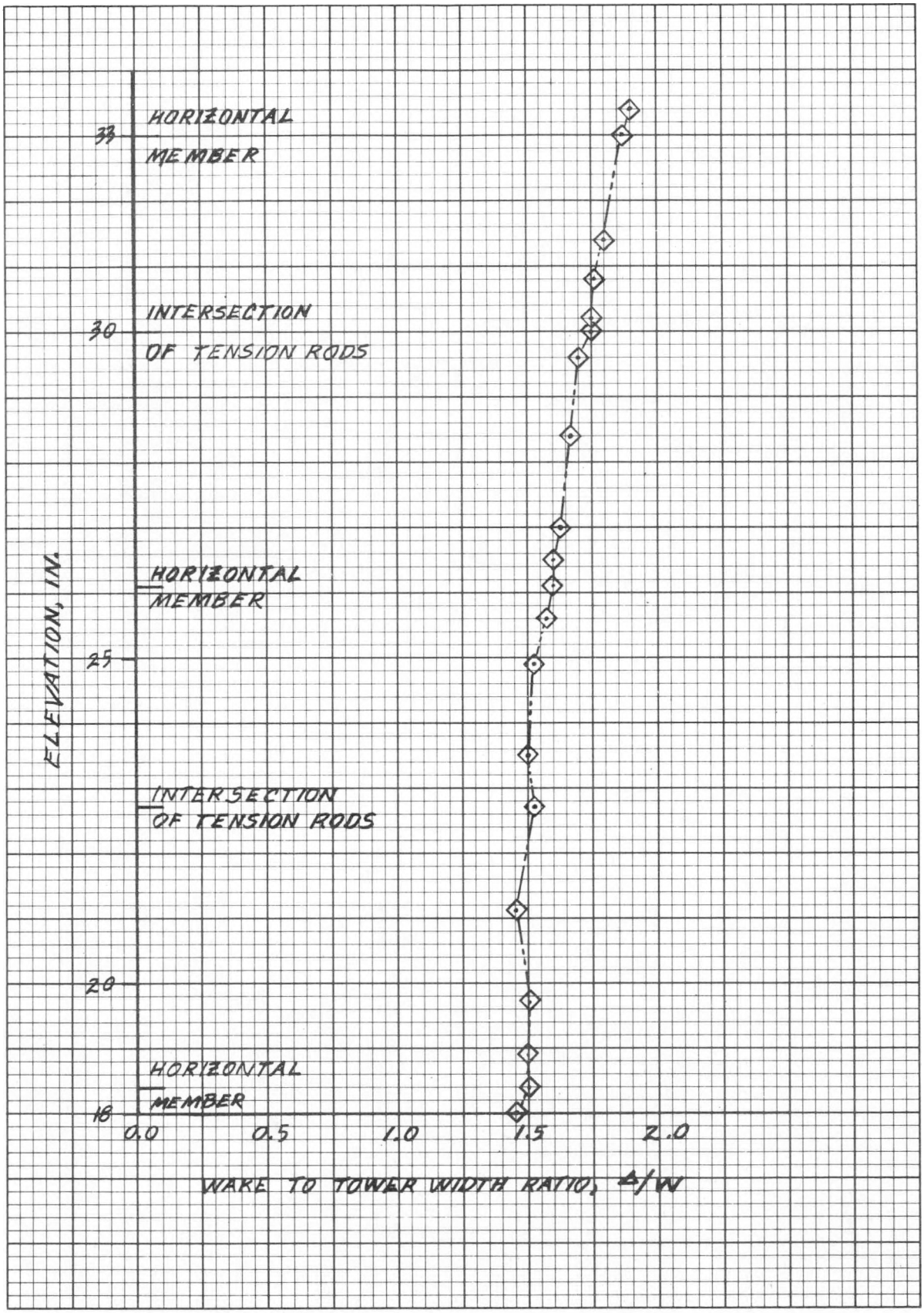

FIGURE 37b
Variation of Wake-to-Tower Width Ratio with Elevation for Tower with Tension Rods Installed as Diagonals in Panels 3 and 4 (Wind Direction of 10°)

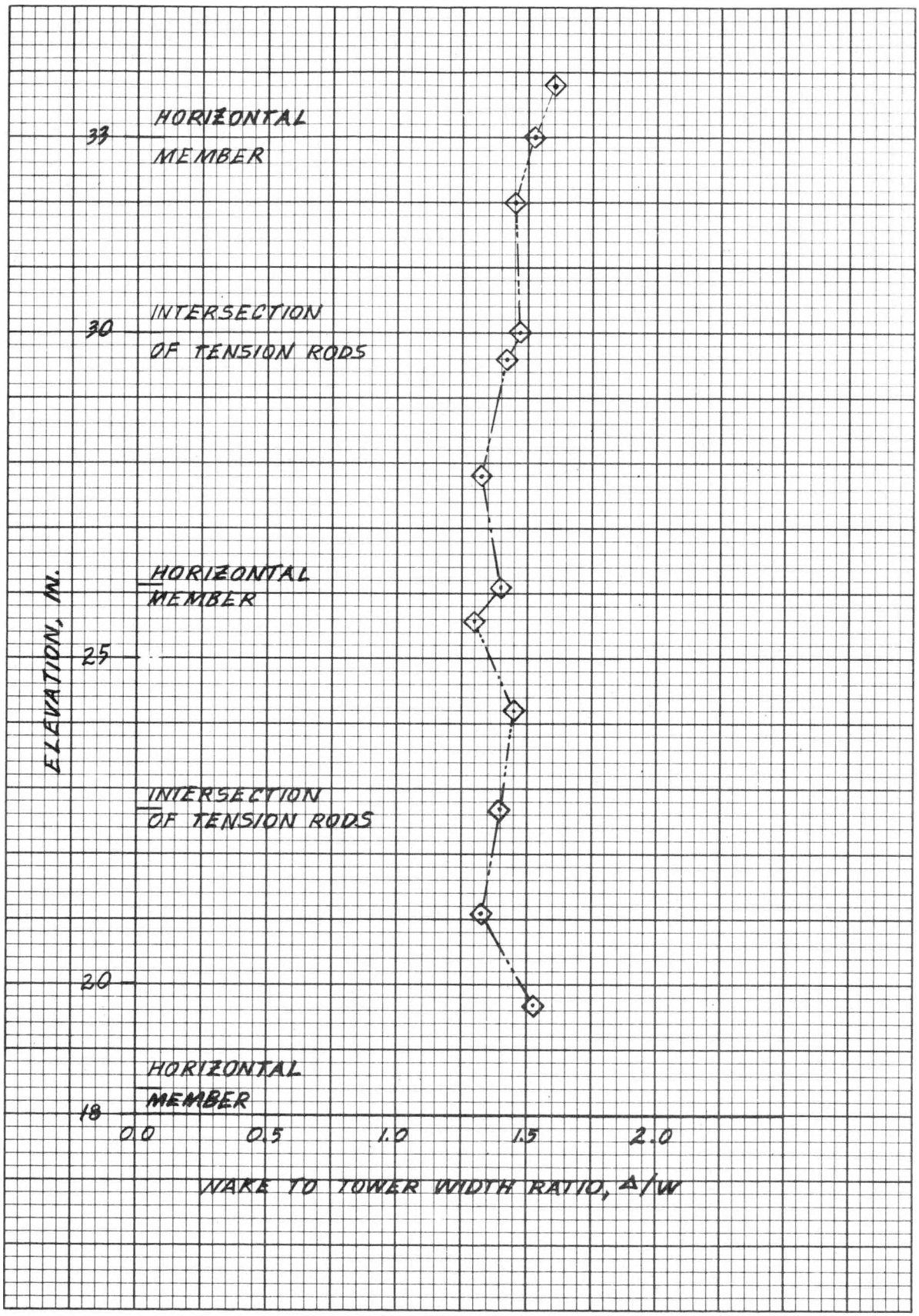

FIGURE 37c
Variation of Wake-to-Tower Width Ratio with Elevation for Tower with Tension Rods Installed as Diagonals in Panels 3 and 4 (Wind Direction of 35^{o})

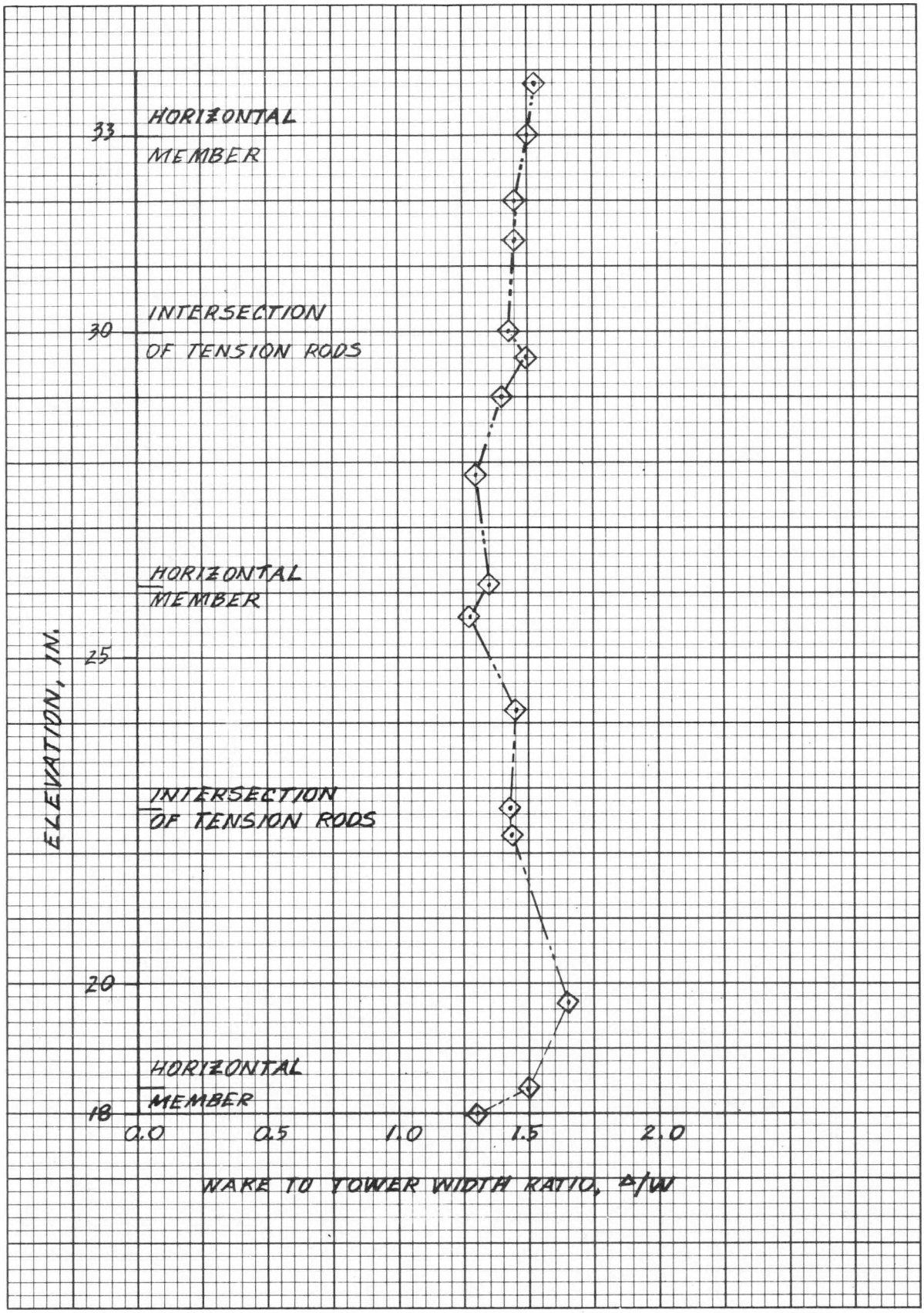

FIGURE 37d
Variation of Wake-to-Tower Width Ratio with Elevation for Tower with Tension Rods Installed as Diagonals in Panels 3 and 4 (Wind Direction of 40°)

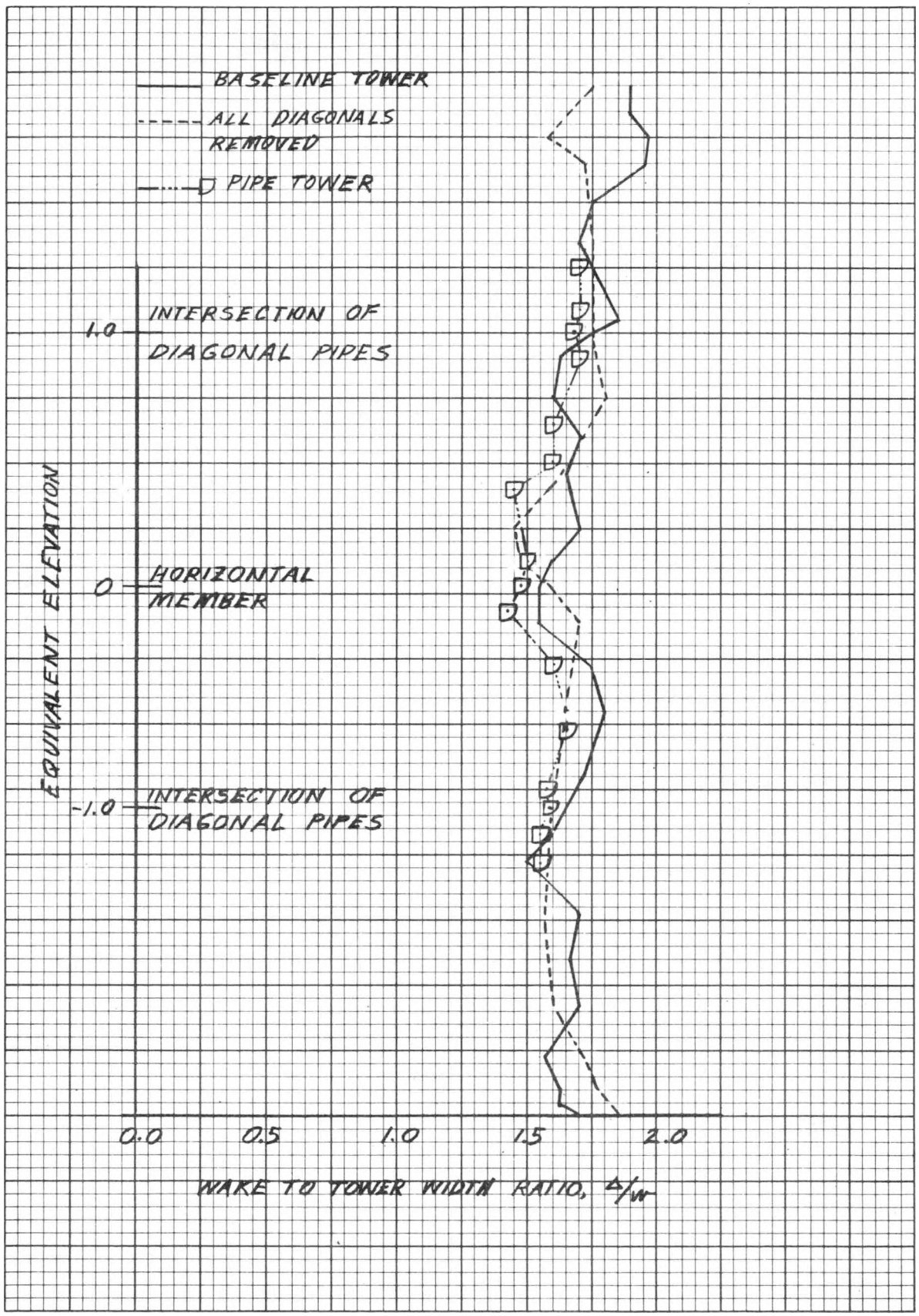

FIGURE 38a
Comparison of Variation of Wake-to-Tower Width Ratio with Elevation for Baseline Tower, Tower with All Diagonals Removed, and All-Pipe Tower (Wind Direction 0^{o})

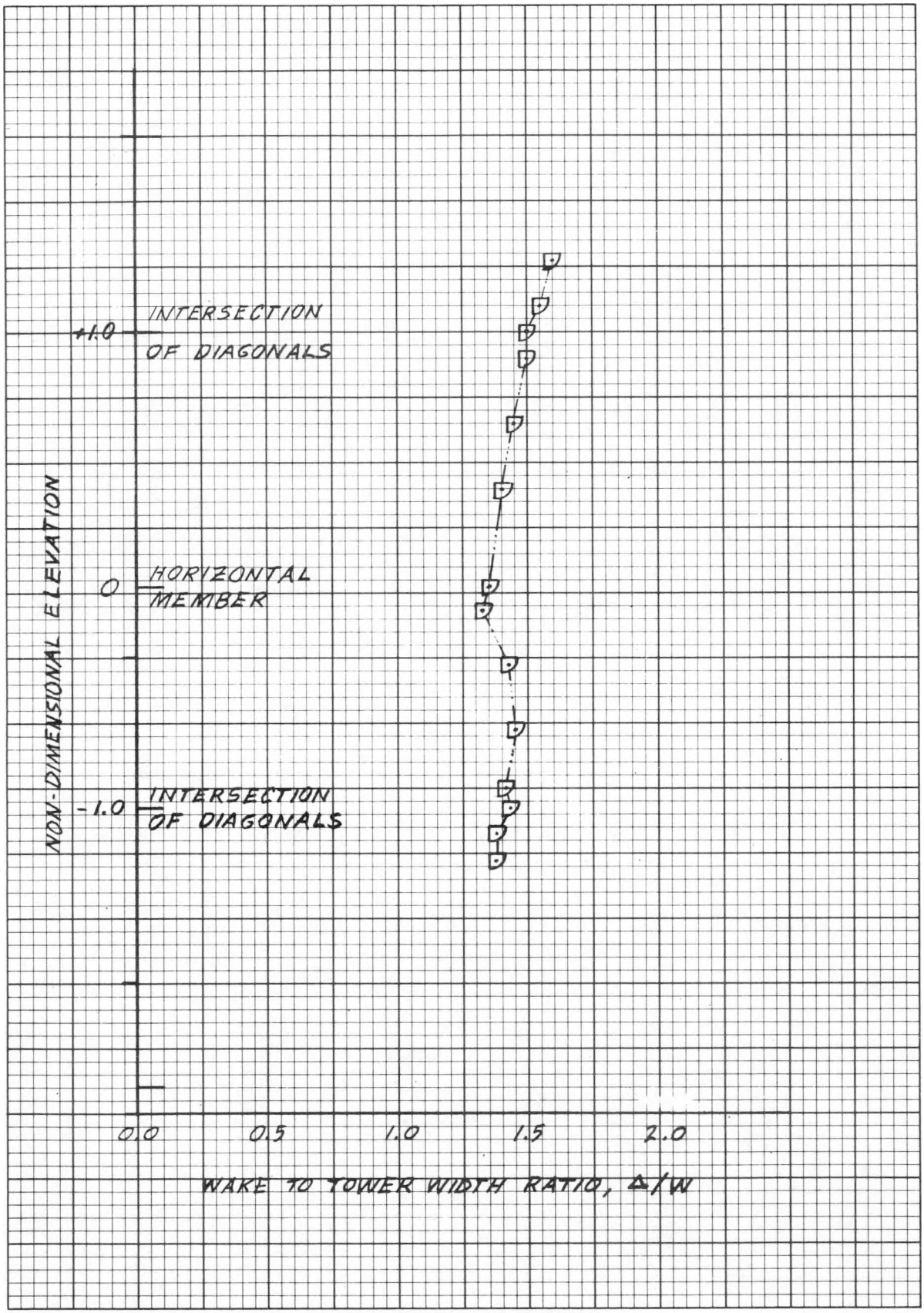

FIGURE 38b
Variation of Wake-to-Tower Width Ratio with Elevation for All-Pipe Tower
(Wind Direction 10^{o})

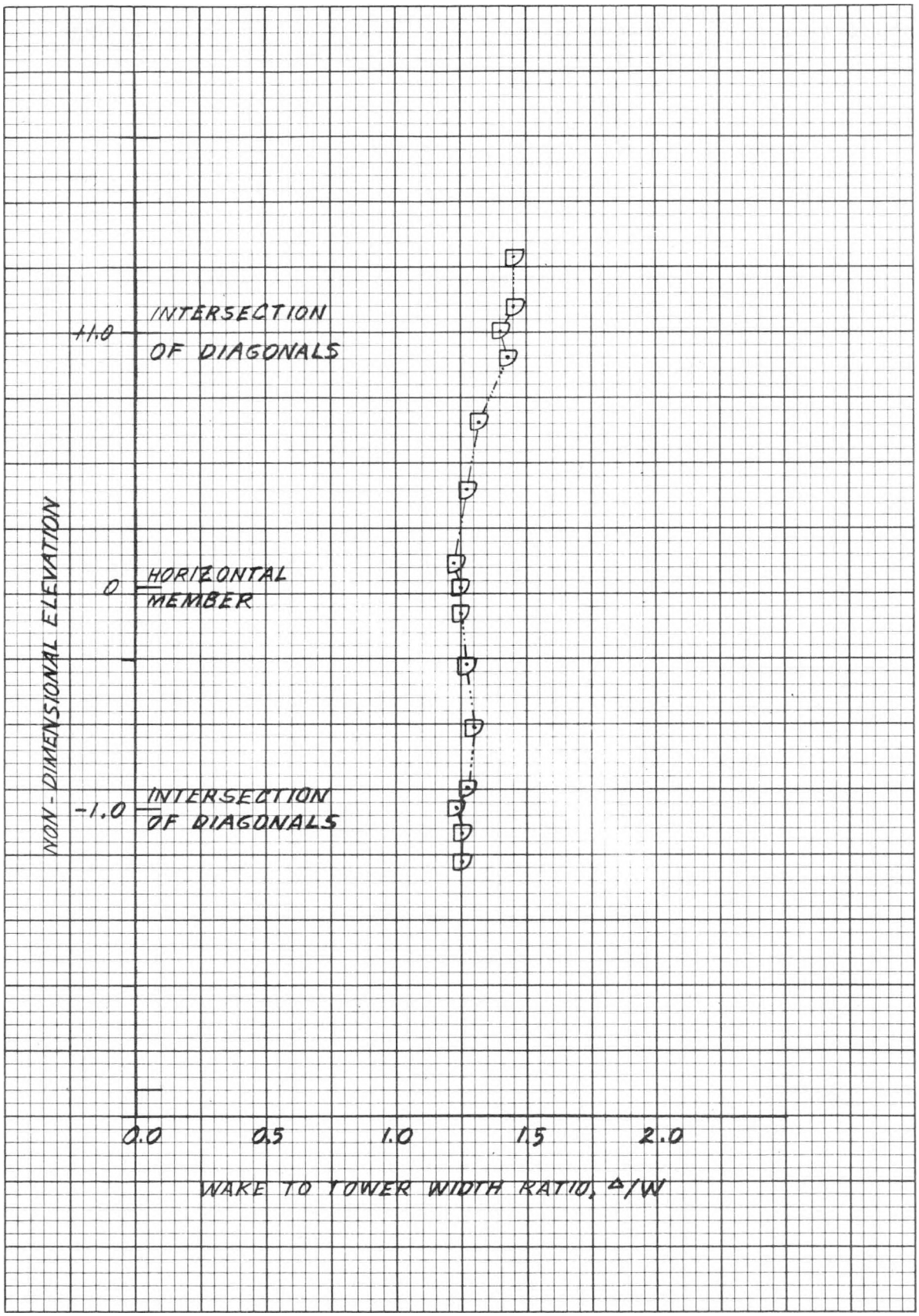

FIGURE 38c
Variation of Wake-to-Tower Width Ratio with Elevation for All-Pipe Tower
(Wind Direction 35^{o})

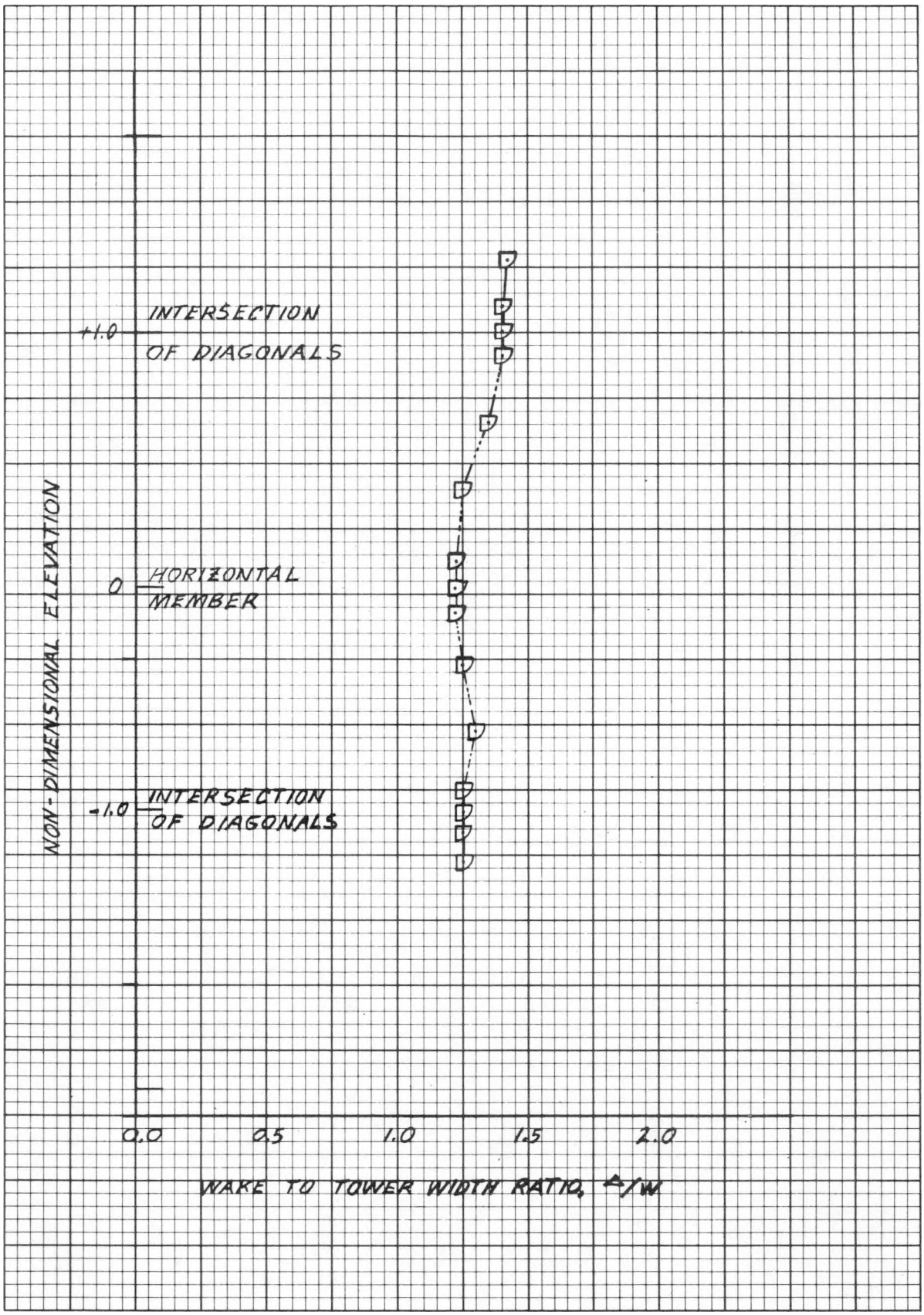

FIGURE 38d
Variation of Wake-to-Tower Width Ratio with Elevation for All-Pipe Tower
(Wind Direction 40^{o})

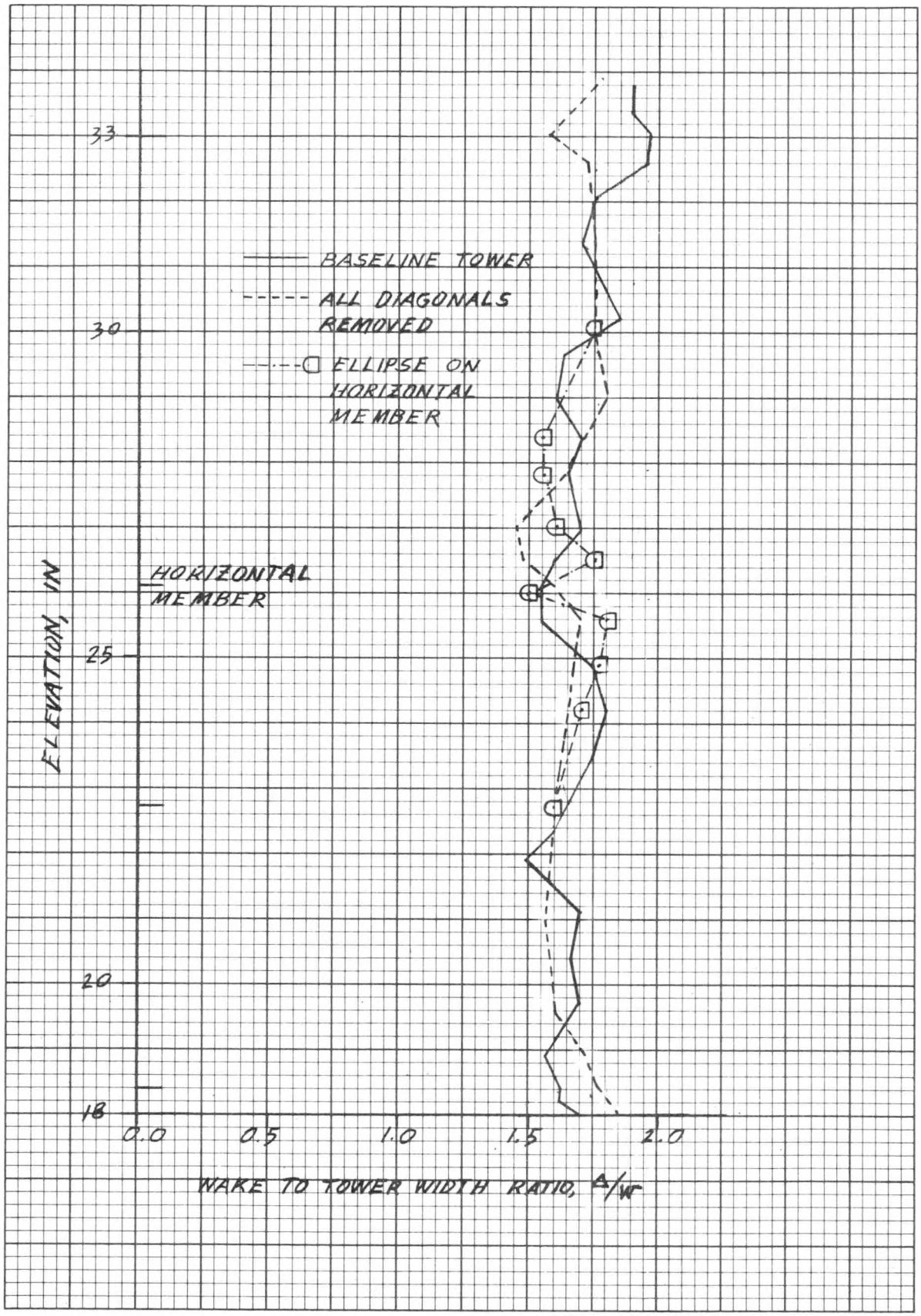

FIGURE 39a

Comparison of Variation of Wake-to-Tower Width Ratio with Elevation for Baseline Tower and for Tower With and Without Ellipses Installed on Horizontal Member (Wind Direction 0°)

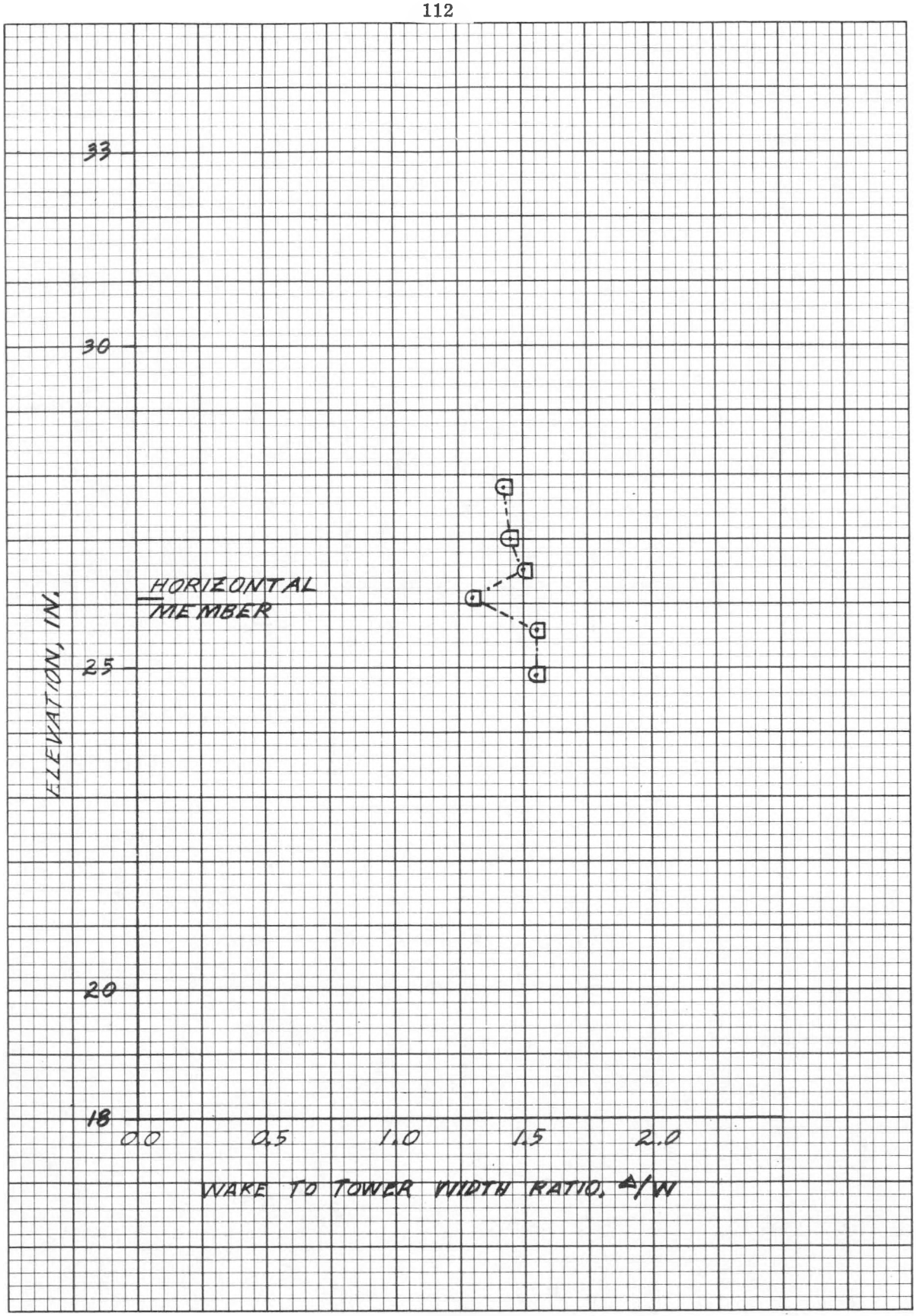

FIGURE 39b

Variation of Wake-to-Tower Width Ratio with Elevation for Tower with Ellipses Installed on Horizontal Member with All Diagonals Removed (Wind Direction of 10^{o})

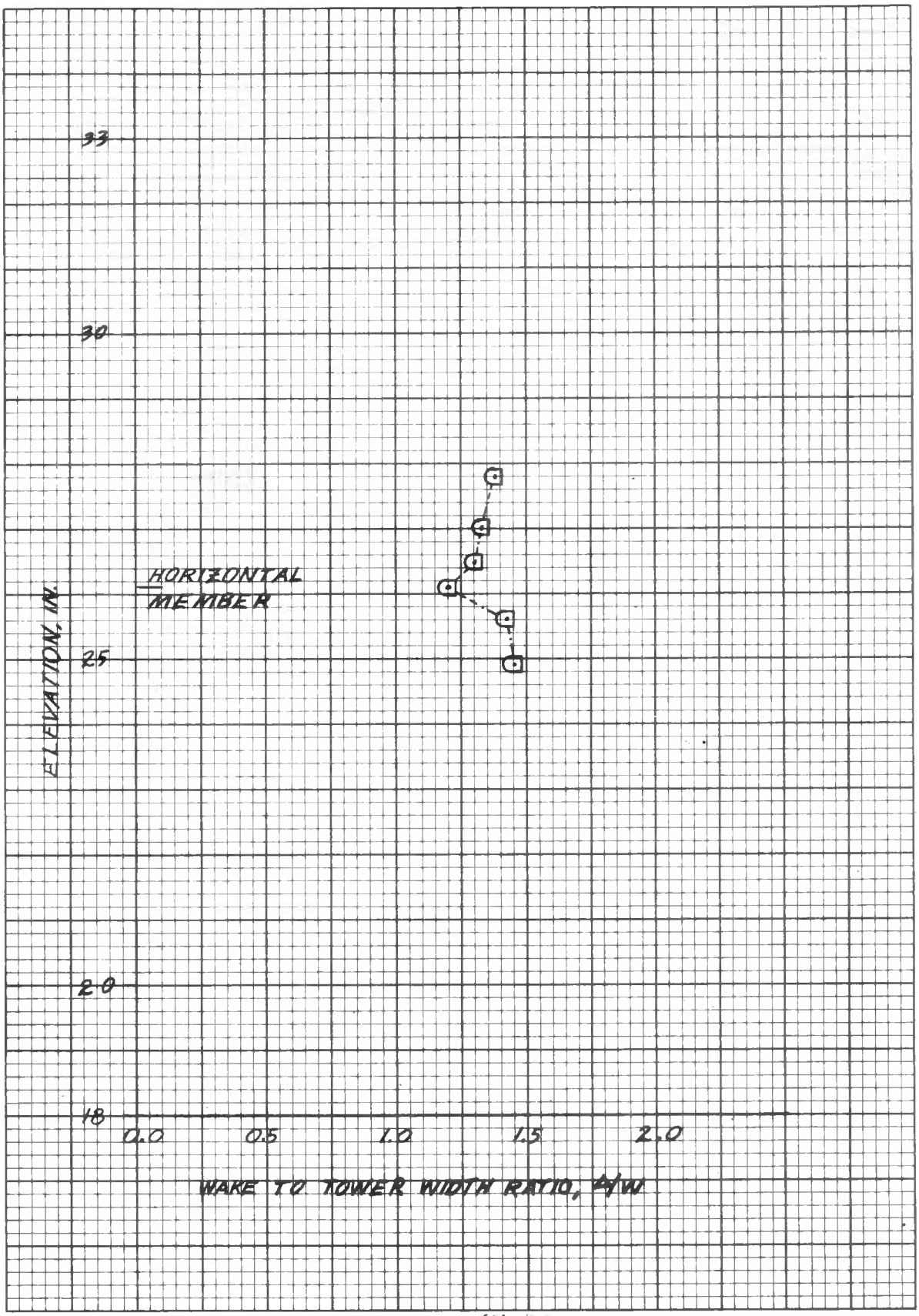

FIGURE 39c

Variation of Wake-to-Tower Width Ratio with Elevation for Tower with Ellipses Installed on Horizontal Member with All Diagonals Removed (Wind Direction of 35°)

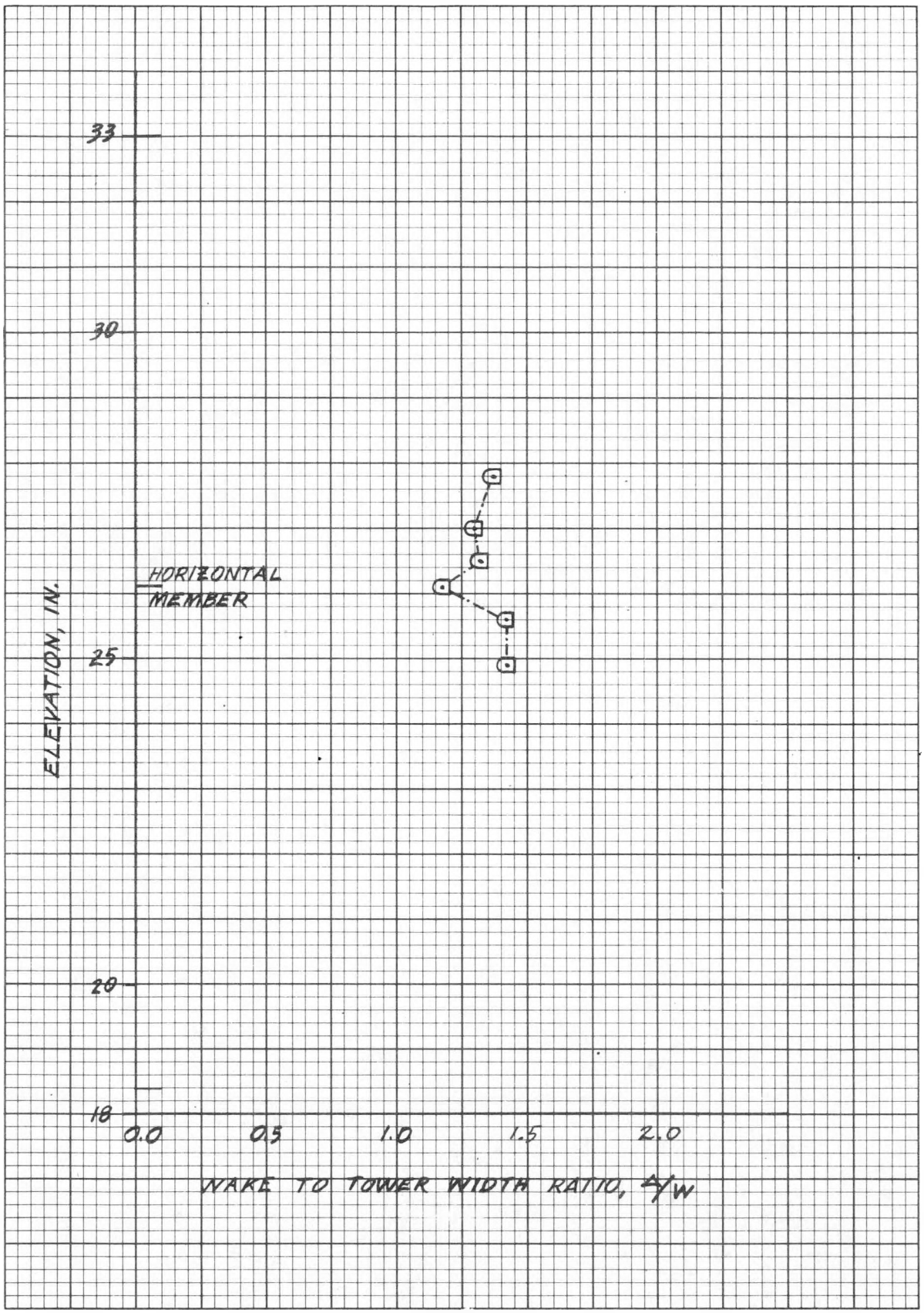

FIGURE 39d

Variation of Wake-to-Tower Width Ratio with Elevation for Tower with Ellipses Installed on Horizontal Member with All Diagonals Removed (Wind Direction of 40^{o})

APPENDIX D

Variation of Average Velocity Ratio with Wind Approach Angle for Selected Elevations.

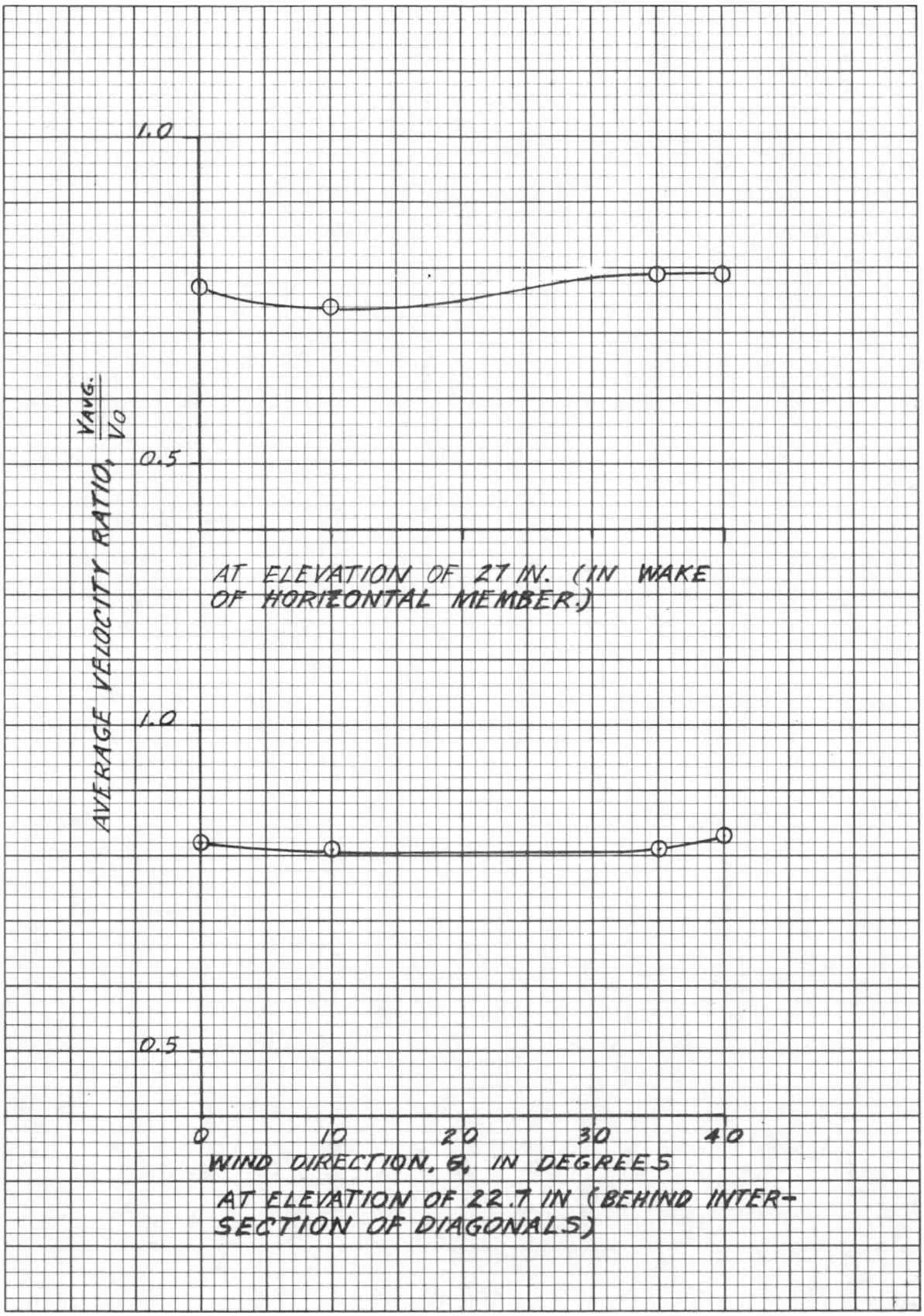

FIGURE 40a
Effect of Wind Direction on Average Velocity Ratio for Baseline Tower

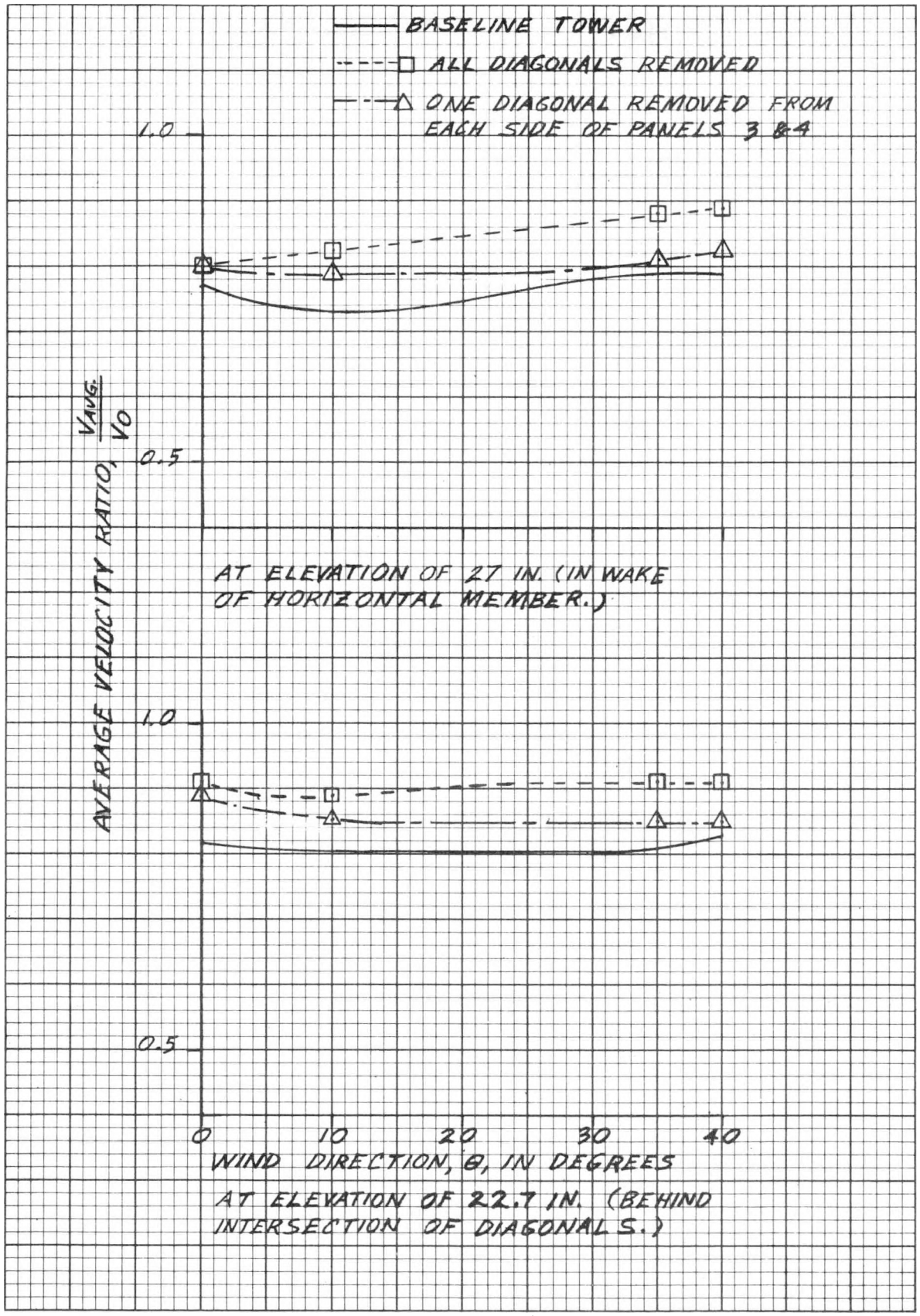

FIGURE 40b
Comparison of Effect of Wind Direction on Average Velocity Ratio for Baseline Tower and Tower with Diagonals Removed

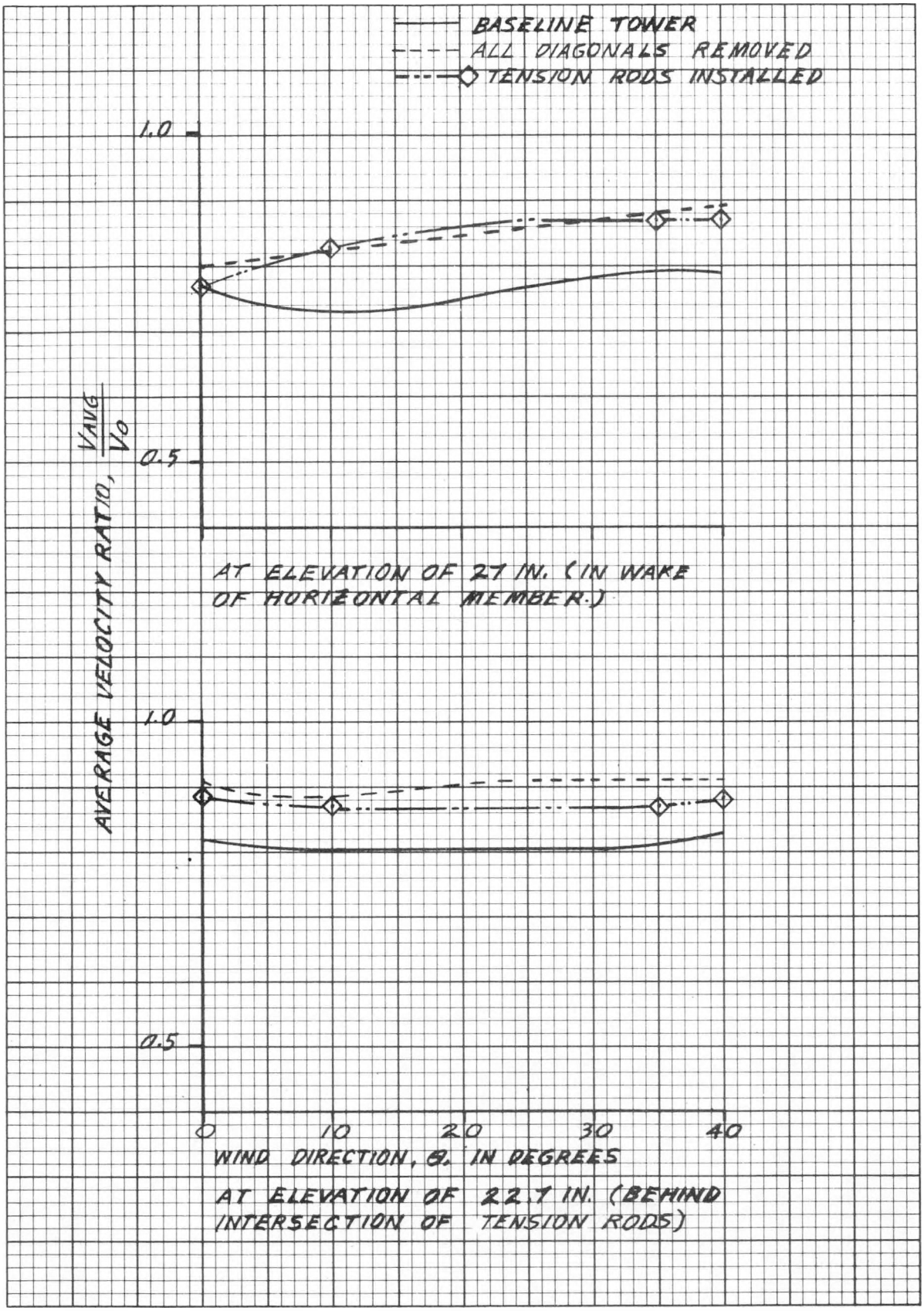

FIGURE 40c
Comparison of Effect of Wind Direction on Average Velocity Ratio for Baseline Tower, Tower with All Diagonals Removed, and Tower with Tension Rods

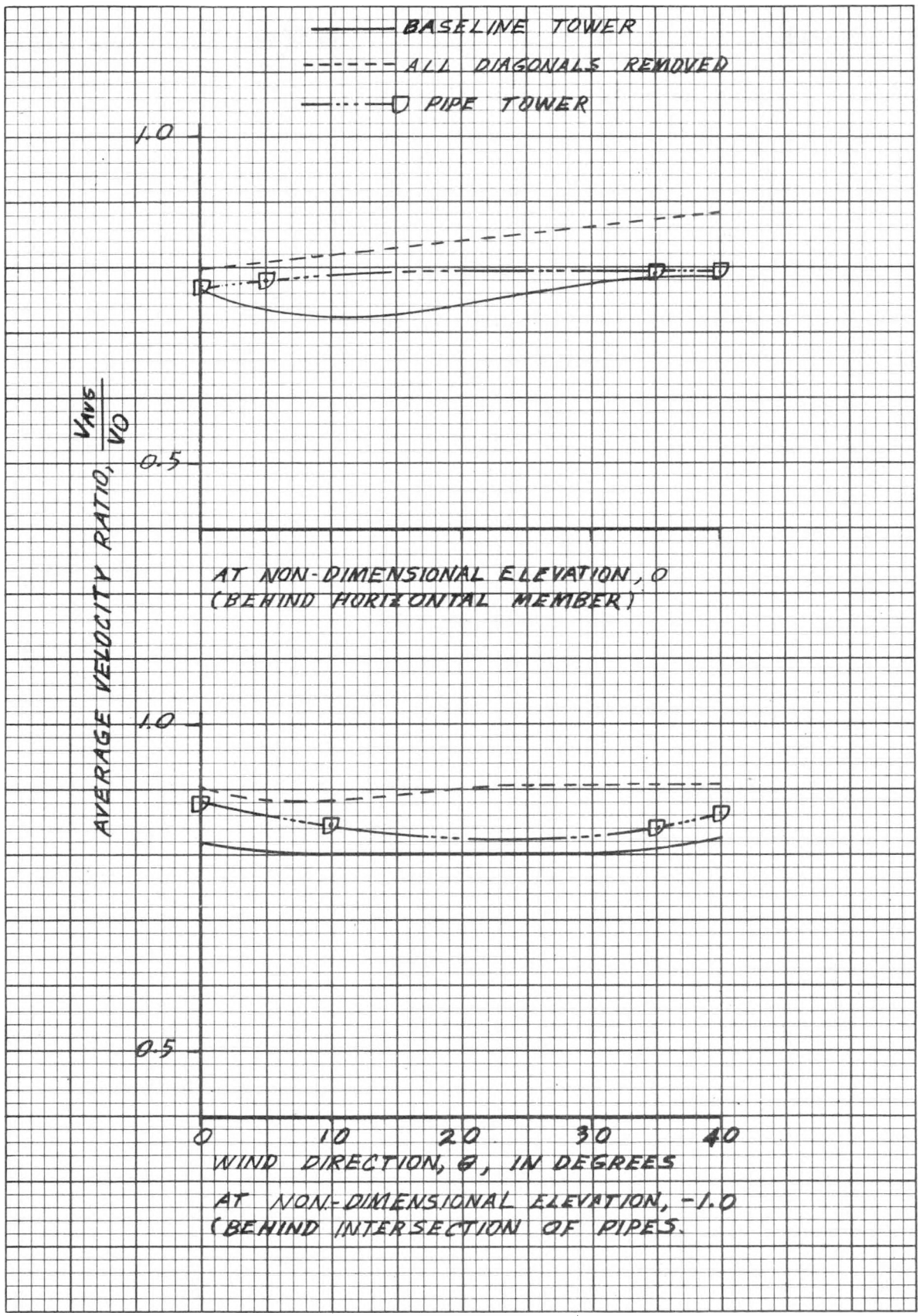

FIGURE 40d
Comparison of Effect of Wind Direction on Average Velocity Ratio
for Baseline Tower, Tower with All Diagonals Removed, and All-Pipe Tower

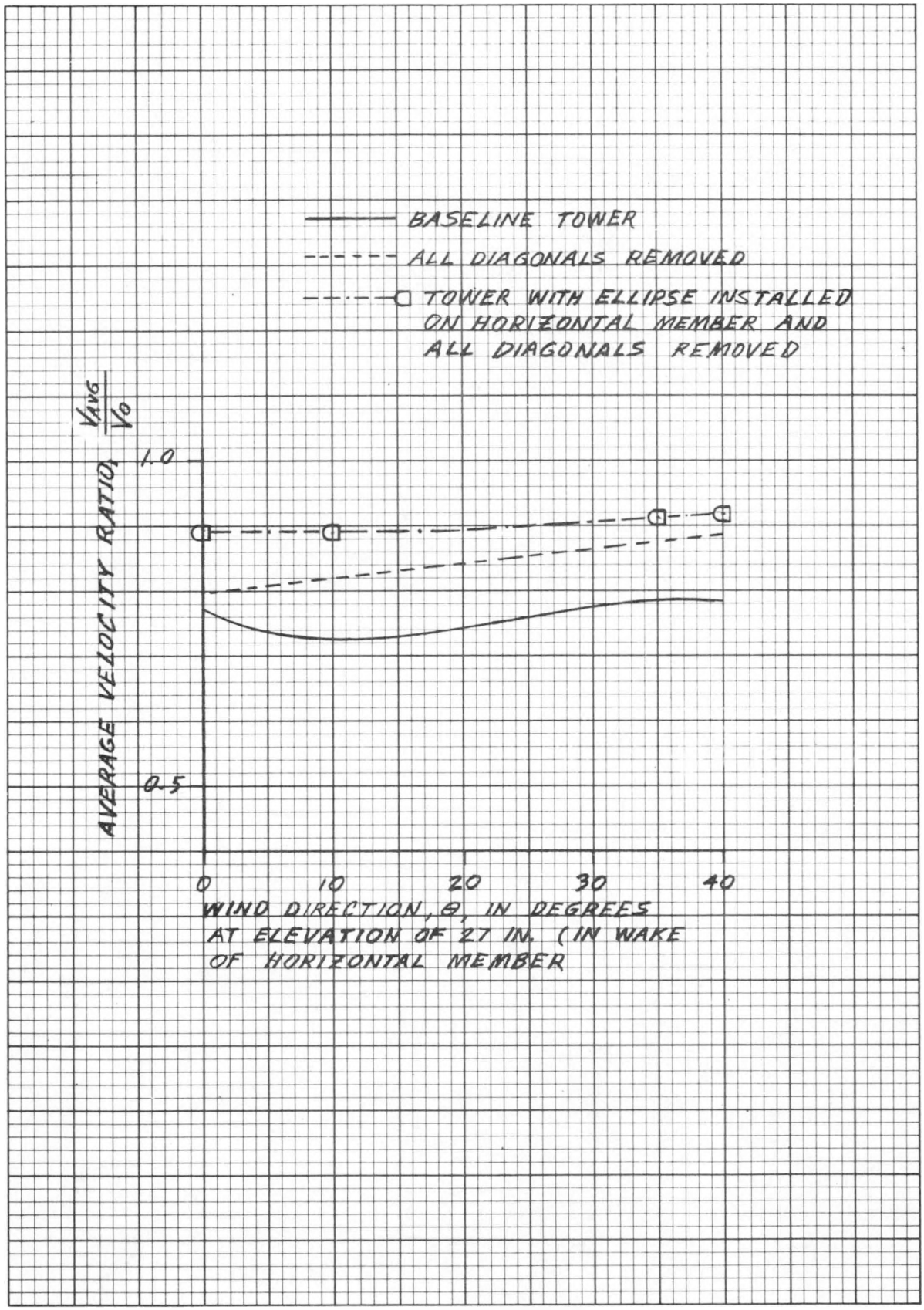

FIGURE 40e

Comparison of Effect of Wind Direction on Average Velocity Ratio for Baseline Tower and for Tower With and Without Ellipses Installed on Horizontal Member (Wind Direction 0^{o})

APPENDIX E

Wake Characteristics of Ellipses, Airfoils and Roughened Cylinders

The profiles measured in the wake of isolated ellipses, airfoils, and roughened cylinders are presented in Figures 45, 46, 47, and 48. These profiles were measured for the purpose of determining the wake characteristics of these elements prior to testing them on the tower model.

A comparison of the profile in the wake of the horizontals with ellipses on them with the profile in the wake of an isolated ellipse, show that the V_{min}/V_o are nearly the same. This suggests that the wake from the forward ellipse had little effect on wake of the downstream ellipse.

The tests with in-line airfoils showed that there is a Reynolds Number effect that has an influence on the wake width and depth. The Reynolds Number of the airfoils on the tower model legs, 0.72×10^5, was much lower than the value (3.45×10^5) for airfoils on the legs of the full size Mod-0 tower. At the lower Reynolds Number the airfoils on the model would produce a lower V_{min}/V_o than in the wake of the full scale in-line airfoils. This was verified by measurements of V/V_o profiles that were made at both high and low Reynolds Numbers. These are shown in Figure 45.

An investigation was conducted to evaluate levels of surface roughness and to define effectiveness because caution must be exercised when applying this concept. A particular surface roughness is effective in wake reduction only over a very narrow range of wind velocity or Reynolds Number. This is illustrated in Figure 46. The drag coefficient for circular cylinders of varying degrees of roughness is presented as a function of Reynolds Number. The drag coefficient is directly related to wake width, so that a low drag coefficient implies a small wake behind the cylinder. The value of the Reynolds Number is directly proportional to wind velocity for a given diameter circular cylinder, low speed (incompressible) flow, and the viscosity of the air. For a given surface roughness, the range of Reynolds Numbers, i.e., the range of wind velocities, over which the low drag and, hence, small wake width exists is very small. This range is much smaller than the range of Reynolds Numbers over which the wind turbine is designed to operate. For example, the Mod-0 wind turbine is designed to operate over a Reynolds Number range from 1.5×10^5 to 5×10^5, wind speeds from 8 mph to 60 mph. From Figure 46, no single surface roughness is effective over nearly this wide a range of Reynolds Numbers. To be practical, therefore, the following factors must be evaluated:

1. Range of wind speeds
2. Ease of fabrication
3. Weathering

Six different degrees of surface roughness were investigated for reducing the wake behind a round cross-section vertical member. The tunnel wind speed was reduced to 64 mph for these tests in order to obtain a Reynolds Number comparable to the full scale tower value. The rough surfaces were obtained by

carefully wrapping a 3-inch diameter cylinder with various grades of garnet paper. The effect of surface roughness on the wake is presented in Figure 47 in terms of velocity profiles for the tunnel orientation shown in Figure 16. The degree of roughness is expressed in terms of the ratio of the diameter of the roughness particles to the diameter of the vertical member. The Reynolds Number is constant at a value of 1.5×10^5, which is the full scale value at the design wind speed of 8 mph. As shown in Figure 47, the most effective value of surface roughness was 0.0024 (k/D) for this application. This was to be expected from an examination of the curves of Figure 46. The velocity ratio profile for the most effective surface roughness (k/D = 0.0024) is plotted in Figure 48, together with the profiles for a smooth cylinder and for the full scale airfoil. The wake velocity for this roughness condition is 93% of the free stream value, essentially the same value as was obtained using the airfoils. Thus roughening the surface of a vertical member can be as effective in reducing its wake as installing airfoils. Furthermore, the effectiveness of a roughened vertical member would be independent of wind direction without requiring moving parts.

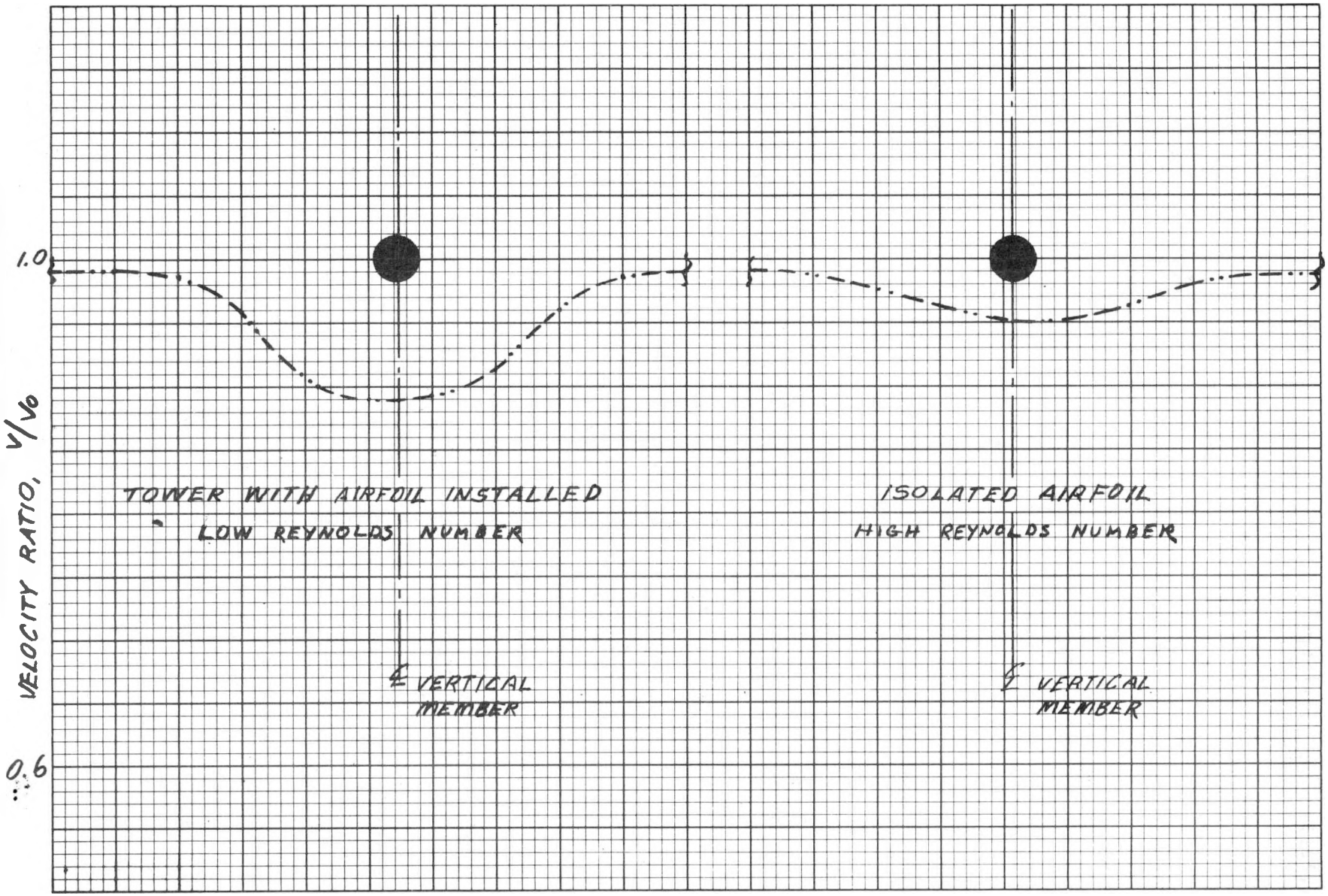

FIGURE 41

Comparison of Velocity Ratio Profile Behind Vertical Member for Tower With Airfoils Installed on Vertical Member With All Diagonals Removed and for Full Size Isolated Airfoils (Wind Direction 0^{o})

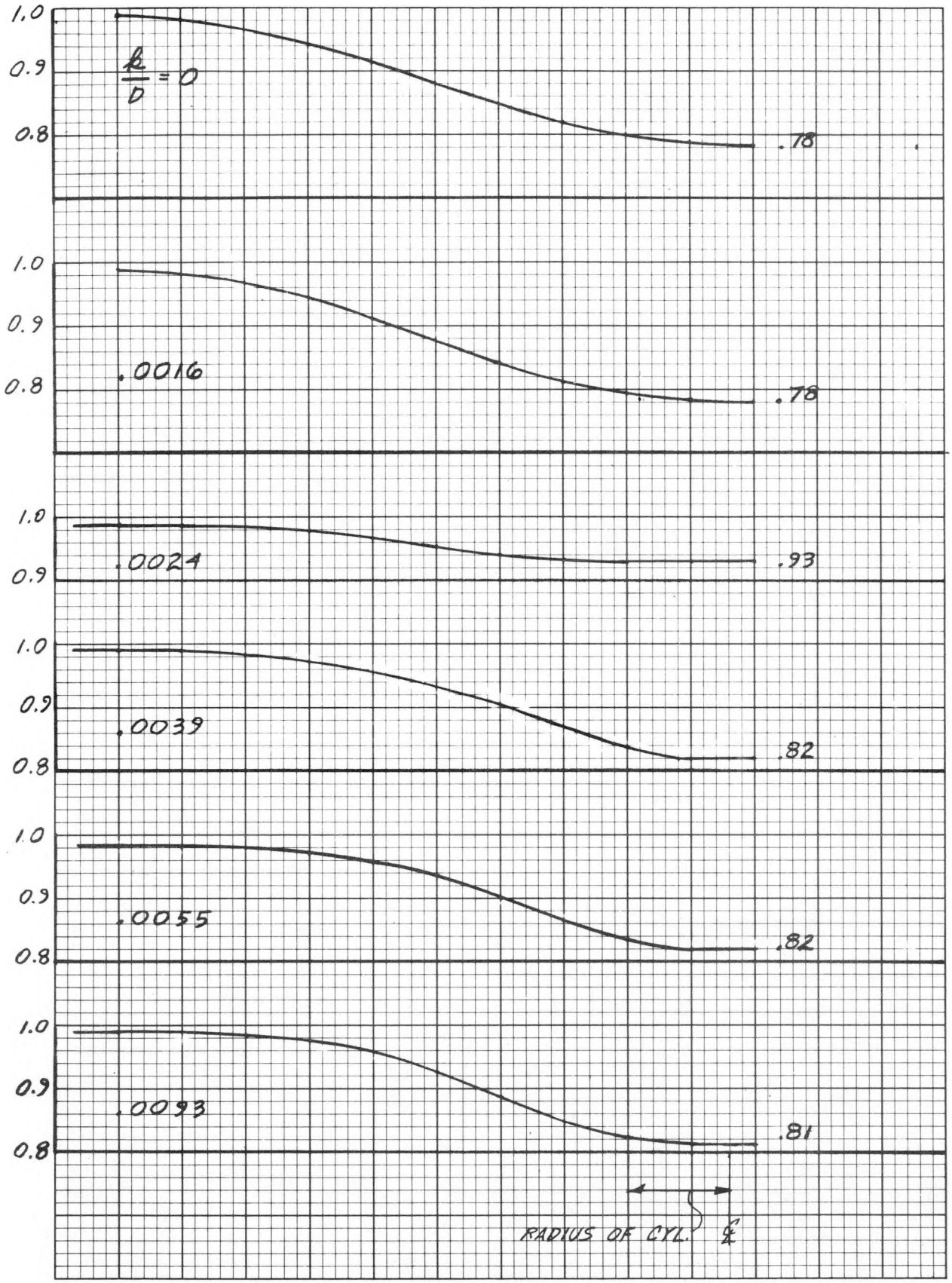

FIGURE 42
Effect of Surface Roughness on Wake Behind Vertical Circular Column
(Reynolds Number = 1.5×10^5)

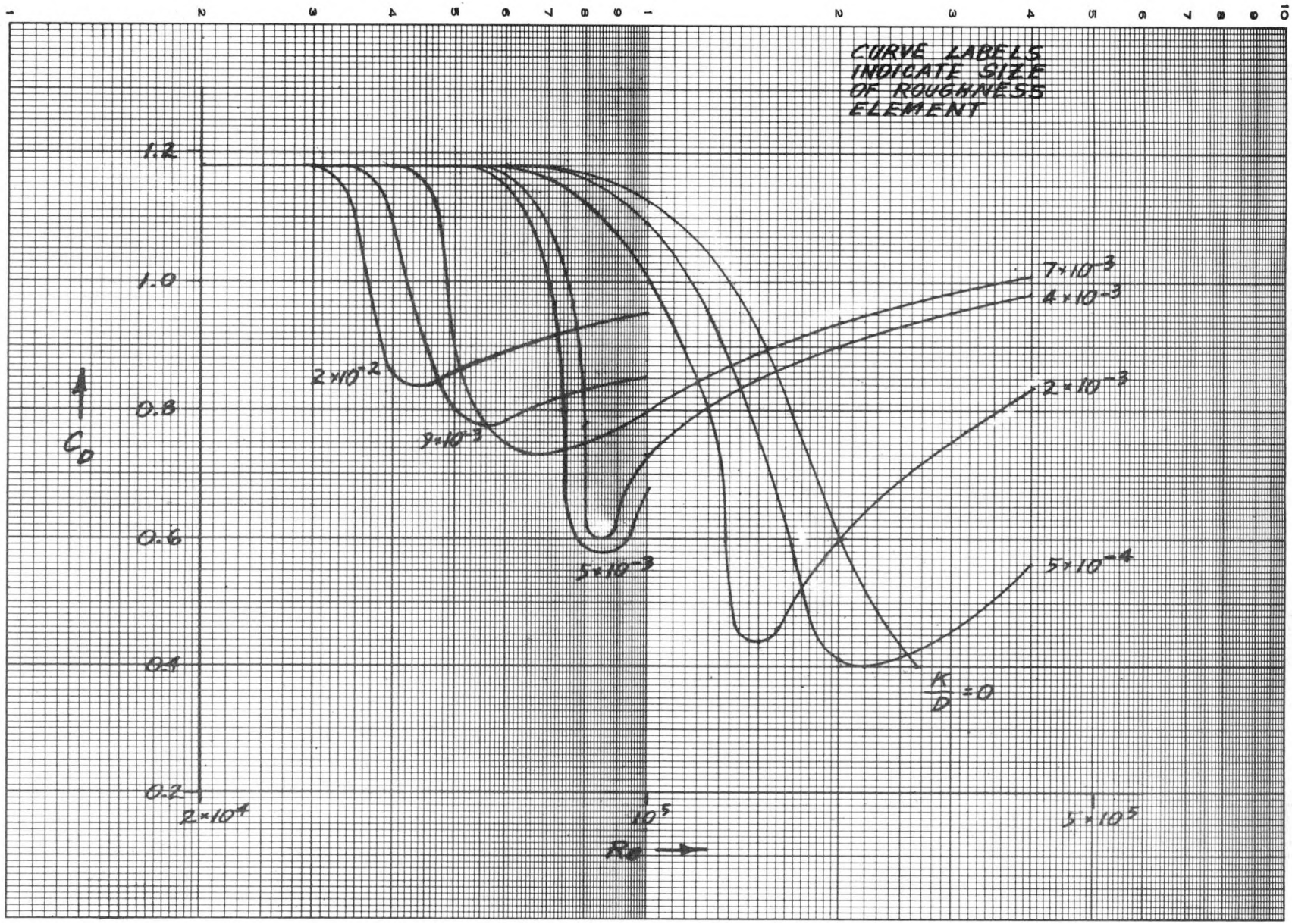

FIGURE 43
Drag on Circular Cylinders of Varying Roughness (Ref. 4)

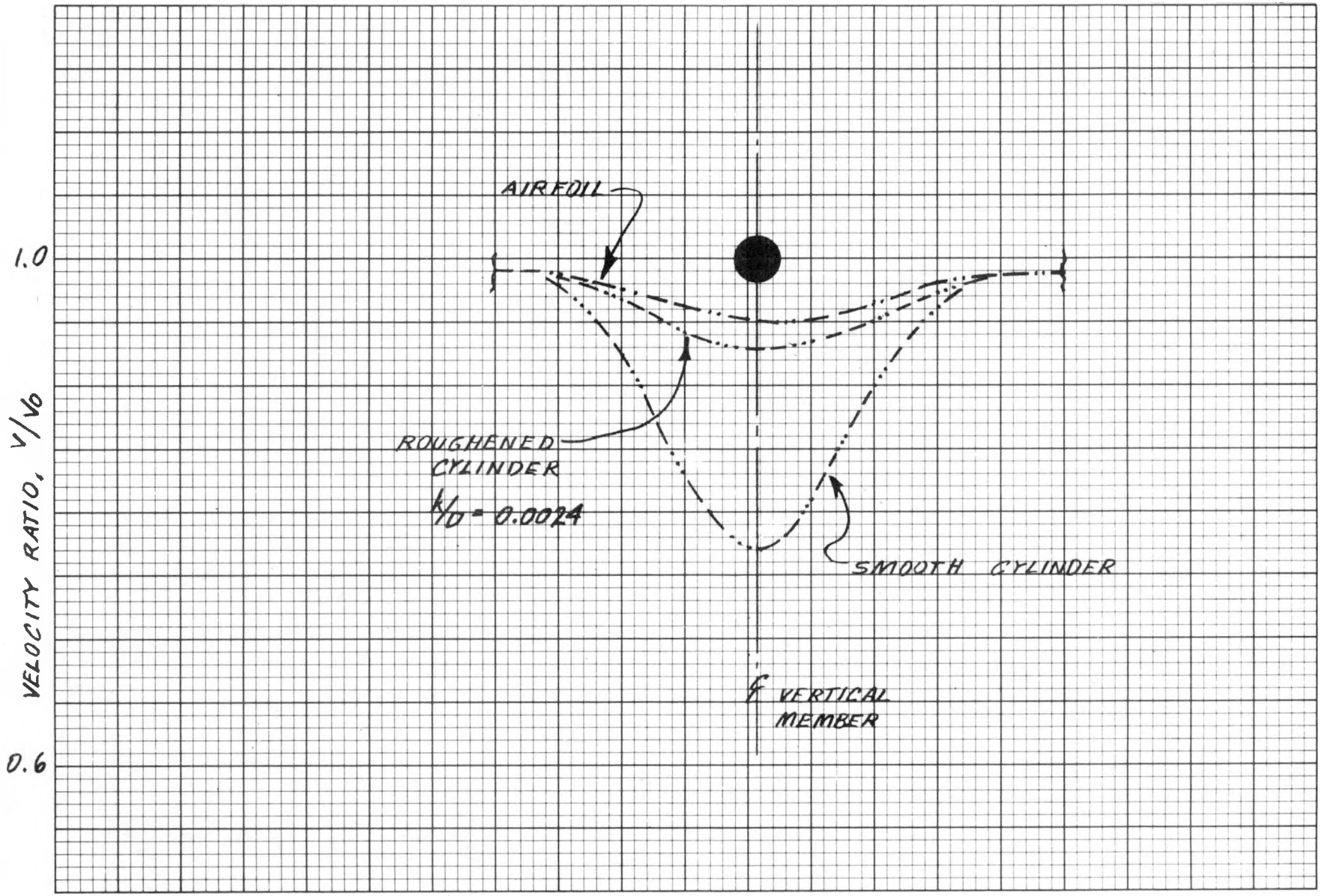

FIGURE 44
Comparison of Velocity Ratio Profile Behind Vertical Member for Smooth and Roughened Cylinder and for Isolated Airfoil (Wind Direction 0°)